RATIONAL DESIGN OF METAL-ORGANIC FRAMEWORK (MOF)-BASED SUPERCAPACITOR ELECTRODES FOR ENHANCED ENERGY STORAGE

by

OTUN KABIR OPEYEMI

submitted in accordance with the requirements for the degree of

DOCTOR OF PHILOSOPHY

in Chemistry

at the

UNIVERSITY OF SOUTH AFRICA

SUPERVISOR: Prof. Xinying Liu

CO-SUPERVISOR: Prof. Diane Hildebrandt

November 2021

DECLARATION

Name: Otun Kabir Opeyemi

Student number: 61061999

Degree: PhD Chemistry

Title: Rational Design of Metal-Organic Framework (MOF)-based Supercapacitor Electrodes for Enhanced Energy Storage

I declare that the above thesis is my own work and that all the sources that I have used or quoted have been indicated and acknowledged by means of complete references.

I further declare that I submitted the thesis to originality checking software and it falls within the accepted requirements for originality.

I further declare that I have not previously submitted this work, or part of it, for examination at Unisa for another qualification or at any other higher education institution.

02/02/2022

_____ _____

SIGNATURE DATE

ABSTRACT

Metal-organic frameworks (MOFs) are gaining popularity as a new electrode material for supercapacitor applications, due to their large specific surface area, excellent tunability and unique pore characteristics. Yet, the poor structural stability and low electrical conductivity of MOFs usually limit their performance. In this study, the supercapacitor performance of MOF-based materials was enhanced using several approaches, including the template strategy, binder-free/metal doping and in situ growth with carbon-based materials. Prior to applying these methods, pristine MOFs and their composite electrodes were prepared using the solvothermal method and then characterized by XRD, SEM/EDX, TEM, BET, TGA, Raman and FTIR. The template strategy transformed double-linker Ni-MOF into NiO and NiO/Ni composite electrodes after annealing in air under different conditions.

The electrochemical analysis results measured by CV, GCD and EIS showed that MOF calcined at 400 ^{o}C (NiO/Ni-400) delivered the highest capacitance (753 Fg^{-1} at 1 Ag^{-1}) and a high energy/power density. Additionally, NiO/Ni-400 exhibited good cyclic stability, with 90% retention after 1000 cycles. Electrochemical kinetics analysis confirmed the pseudocapacitive behavior of the electrode materials at all scan rates. Zn-doped Ni-MOFs grown directly on nickel foam and used as binder-free electrodes exhibited flower-decorated ball-shaped microstructures, in addition to high surface areas and excellent pore characteristics. The composite containing Zn/Ni (1:2) exhibited the highest specific capacitance (391 Fg^{-1} at 1 Ag^{-1}), with superior rate capability and good cycling stability. This electrode delivered maximum energy and power densities of 12 Wh kg^{-1} and 2500 Wkg^{-1}, respectively. The charge storage mechanism was predominantly controlled by the diffusion process, indicating a promising battery-type supercapacitor electrode.

In situ growth of ZIF-8-derived ZnO/C on functionalized MWCNT produced a new ZnO/C@MWCNT nanocomposite, which exhibited better storage performance compared to ZnO/C. The remarkable performance of the MOF-based electrodes in this study was attributed to the synergistic effects of the compositing materials, low charge transfer resistance and optimum dopant concentration. Aside from expanding the applicability of MOFs, this research may help to create a new path to bridge the performance gap between supercapacitors and batteries.

Keywords

Metal-organic frameworks

Supercapacitors

Ni-MOF

ZIF-8

Energy storage

MWCNT

Nanocomposites

ZnO/C

Energy density

Kinetics

RESEARCH OUTPUT

(i) List of publications

- **Otun, K.O.,** Xaba, M.S., Zong, S., Liu, X., Hildebrandt, D., El-Bahy, S.M. and El-Bahy, Z.M., (2022) Double linker MOF-derived NiO and NiO/Ni supercapacitor electrodes for enhanced energy storage. Colloids and Surfaces A: Physicochemical and Engineering Aspects, 634, p.128019.
- **Otun, K.O.,** Xaba, M.S., Zong, S., Liu, X., Hildebrandt, D., El-Bahy, S.M. Alotaibi, M.T. and El-Bahy, Z.M., (2022) ZIF-8-derived ZnO/C decorated hydroxyl-functionalized multi-walled carbon nanotubes as a new composite electrode for supercapacitor application. Colloid and Interface Science Communications**,** 47, p. 100589
- **Otun, K.O**., M.S. Xaba, Liu X., Hildebrandt, D. (2021) Design of zinc and nickel-based MOFs and composites as electrode materials for supercapacitor application, Nova Sci. Publisher Press. ISBN:978-53619-5262-2.
- **Otun, K.O.,** Morena S.X., Zong S., Liu X., Chen A. (2021) Flexible supercapacitors based on nancomposites of MOFs, Elsevier, ISBN: 978-0-323-91179-5. (**Accepted for publication**)
- **Otun, K.O**., 2020. Temperature-controlled activation and characterization of iron-based metal-organic frameworks. Inorganica Chimica Acta, 507, p.119563.
- **Otun, K.O.**, Liu, X. and Hildebrandt, D. (2020) Metal-organic framework (MOF)-derived catalysts for Fischer-Tropsch synthesis: Recent progress and future perspectives, **Journal of Energy Chemistry**, 51, pp.230-245.
- **Otun, K.O**., Y. Yali, Liu, X, Hildebrandt, D. (2020). Synthesis, structure and perfromance of iron carbide in Fischer-Tropsch Synthesis: A critical review, **FUEL,** 296**,** pp.120689.
- **Otun, K.O.,** Morena S.X, Zong S., Liu X., Hildebrandt D. (2022) Self-assembled Zn-functionalized Ni-MOF for high electrochemical energy storage performance. (**Draft**)

(ii) Conferences attended/Acceptance

- **Otun, K.O.,** Morena S. Xaba, S. Zong, Liu X., Hildebrandt D. ZIF-8-drived ZnO/C decorated by functionalized multiwalled carbon nanotubem, F&R Energy, Houston Texas, USA, Feb 15-17 2022 (Accepted for oral presentation and registration done).

- **Otun, K.O**., Y. Yali, Liu, X. and Hildebrandt, D. Advances in MOFs for energy applications. Poster Presentation at Catalysis Society of South Africa CATSA, Pilanesberg, South Africa, 19-22 November, 2017.
- **Otun, K.O**., Y. Yali, Liu, X. and Hildebrandt, D. Activation and characterization of MOFs. Poster Presentation at Catalysis Society of South Africa (CATSA) Conference, Cape Town, South Africa, 8-11 November, 2019.

ACKNOWLEDGMENTS

First and foremost, I want to thank Almighty Allah, The First and the Last, who bestowed on me sound health, tenacity and the requisite knowledge to successfully complete this research. Alhamdulillah Robil Aalameen.

I would also like to sincerely thank my supervisors, Prof. Xinying Liu and Prof. Diane Hildebrandt, for their constant support, constructive criticism, invaluable suggestions and incredible motivation in making this feat a reality. Prof. Liu's open-door policy and constant words of encouragement ('You can do it' and 'You can have a try', as he always says), in particular, ensured that, as a PhD candidate, I was not struggling with the challenges alone, as I could seek his scholarly advice at any time throughout this journey. The inestimable contributions of Prof. Yali and Dr Moyo from the FT group are also kindly appreciated.

I also want to acknowledge the non-academic staff at IDEAS, who ensured that I enjoyed full access to the research facilities and approved all the procurement items, including the chemicals and reagents. Humphrey, Katu, Dolly, Alicia, Genevieve, Mandla and others from neighboring departments are all appreciated in this regard.

To my friends, lab mates, colleagues and those who crossed paths with me during this PhD adventure and touched my life positively, I am falling short of words to say thank you. Dr Morena, Dr George, Chitalu, Trevor, Dr Shahid Ansari, Dr Leonard, Trevor, Dr. Majid, Dr. Shiba, Charles, Amusat Olaitan, Bello, Wale, Dr Success, Balopy, Clinton, Dr Dauda, Dr Vic, Dr Adio, Prof. Ahmed, Prof. James, Dr Lukman, Abdulwasiu, Safurat, Dr. Adeleke, Atkins, Mr Jimoh, Saheed, Ayipo, Jaji, Abdullahi, BJ, Ridwan, to mention but a few - you are all cherished.

Furthermore, I want to thank my employer, the Kwara State University, Nigeria, for granting me leave of absence to undertake this PhD study in South Africa. My profound gratitude also goes to my academic mentors, Prof. Muibat Bello and Prof. Kazeem Gbolagade, whose constant motivation, prayers and encouragement served as catalysts to push this research over the finishing line.

Achieving this milestone would not have been possible without the support of my parent, siblings, and beloved wife, Waliyah Arike, and my beautiful daughter, Nusaybah Ayomide, who stood like rock with me and celebrated every success I achieved.

Last, but not least, the financial support and bursary from IDEAS, National Research Foundation (Grant IDs: UID 113648 and 132152), and the University of South Africa are gratefully acknowledged.

Dedication

I dedicate this thesis to my late father, teacher and mentor, Mr K.A. Otun, who died a year after I embarked on this PhD program. (May the Lord have mercy on him.)

List of abbreviations

AC	Activated carbon
APD	Arc plasma deposition
ASC	Asymmetric supercapacitor
BDC	1,4-benzenedicarboxylate
BET	Brunaer-Emmett-Teller
BJH	Barrett-Joyner-Halenda
BTC	1,3,5-benzenetricarboxylic acid
CC	Carbon cloth
CF	Carbon fiber
CNF	Carbon nanofiber
CNT	Carbon nanotube
CV	Cyclic voltammetry
CVD	Chemical vapor deposition
DABCO	1,4-diazabicyclo[2.2.2] octane
DHTP	2,5-dihydroxyterephthalic acid
EDLC	Electric double layer capacitor
EDS	Energy dispersive spectroscopy
EDX	Energy dispersive X-ray
EIS	Electrochemical impedance spectroscopy
FESEM	Field emission scanning electron microscope
FTIR	Fourier transform infra-red

GCD	Galvanostatic charge discharge
GO	Graphene oxide
HC	Hybrid capacitor
HCF	honeycomb-type carbon framework
HCI	Hydrochloric acid
HHCF	Hierarchical honeycomb-type carbon frameworks
HKUST	Hong Kong University of Science and Technology
HR-TEM	High-resolution transmission electron microscopy
HSC	Hybrid supercapacitor
Ina	Isonicotinate
IRMOF	Isoreticular metal-organic frameworks
JUC-155	MOFs developed by Jilin University China
LDH	Layered double hydroxide
LED	Light emitting diode
LIB	Lithium-ion battery
MIL	Material Institute Lavoisier
MMOF	Mixed-metal metal-organic framework
MOF	Metal-organic framework
MWCNT	Multi-walled carbon nanotube
NF	Nickel foam
NP	Nanoparticle
PANI	Polyaniline
PC	Pseudocapacitor

PEDOT	Poly(3,4-ethylenedioxythiophene)
POM	Polyoxometalates (POM)
PPy	Polypyrrole
PTFE	Polytetrafluoroethylene
PVP	Polyvinyl pyrrolidine
RGO	Reduced graphene oxide
SC	Supercapacitor
SCE	Saturated calomel electrode
SEM	Scanning electron microscopy
SSC	Solid state supercapacitor
TEM	Transmission electron microscopy
TGA	Thermal gravimetric analysis
XRD	X-ray diffraction
ZIF	Zeolitic imidazolate framework
ZNN	Zinc-doped nickel MOF

Table of Contents

List of Figures

List of Tables

Chapter 1: Introduction

1.1 Short background

One of the major problems facing humanity, which requires urgent attention, is how to secure our energy for future use, as the depletion of fossil fuels continues, while energy demands continue to grow [1-2]. This challenge is even more pressing, given the recent surge in the global market for portable and wearable electronic devices and environmental upheaval of climate change caused by non-renewable fuels [3].

Renewable energy is considered a promising green solution because it is eco-friendly and sustainable [4]. At present, most renewable energy resources are stored and conveyed in the form of electricity [5]. Therefore, technology that can enhance energy efficiency while not harming the environment (such as energy storage devices) remains the hope of the future. Lithium-ion batteries (LIBs) and supercapacitors are the leading candidates in this regard [6]. However, LIBs are limited by low power density and poor cycle life, despite their high energy density [7]. Supercapacitors can deliver high power density and have remarkable cycling stability, but are plagued by low energy density [8]. Therefore, neither of the two storage devices can satisfy the requirements of high energy density, high-power density and good cycle life. The Ragone diagram provided in Figure 1.1. shows the energy and power densities of different storage devices.

Supercapacitors have aroused research attention and become a popular topic of research because of their fast charge-discharge rate, long cycle life, high power density and eco-friendly characteristics [9-10]. Supercapacitors store energy by means of two distinct mechanisms. The first is by physical adsorption of ions demonstrated by electric double layer capacitor (EDLC) materials. Examples include carbon-based materials such as graphene and carbon nanotubes (CNTs). The second mechanism stores energy via an electron transfer reaction, which is characteristic of pseudocapacitive materials such as metal oxide, metal hydroxides and metal sulfides. The EDLC-type materials are more stable and conductive than pseudocapacitors, but they are plagued by low capacitance [11-12].

The key components of a supercapacitor are the electrode, an electrolyte (which could be aqueous or organic) and a separator (which restricts short circuiting between two electrodes) [13]. The role played by the electrodes cannot be over-estimated and good electrode materials for supercapacitor

applications have a high surface area, good pore characteristics, high conductivity and a minimal cost [14]. Consequently, the judicial choice of suitable electrode materials and their rational design for supercapacitor electrodes are the most appropriate way to make supercapacitors better than LIBs with respect to storage performance. The variety of fields in which supercapacitors are being used continues to grow, including recent use in the exit doors of the Airbus 380 airplane, while they continue to be used in electronic consumer gadgets, backup systems and various other power and energy maintenance devices [15-16].

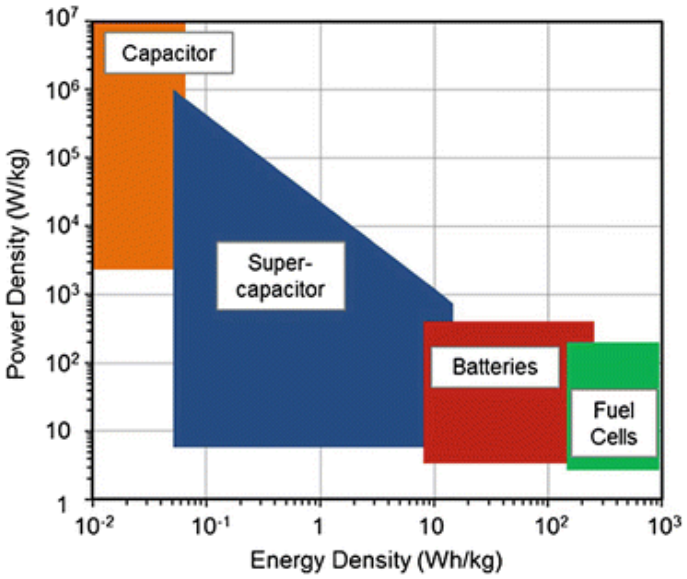

Figure 1.1 Ragone plot of the energy and power density of different devices [17].

1.2 Performance parameters of a supercapacitor

The main parameters used to test the performance of an electrode for supercapacitor applications are the specific capacitance (C, F/g), energy density (E, Wh/kg), power density (P, W/kg), rate capability and cycling stability [18-19]. The specific capacitance of a supercapacitor indicates the charge storage ability of a supercapacitor and is expressed as per equation (1.1). The energy density typifies how much energy can be stored, which is calculated using equation (1.2). The power density is an estimate of the mass unit of power that can be delivered, as expressed in equation (1.3) [20].

$$C = \frac{I \times \Delta t}{m \times \Delta V} \quad (1.1)$$

$$E = \frac{C \times (\Delta V)^2}{7.2} \quad (1.2)$$

$$P = \frac{3600E}{\Delta t} \quad (1.3)$$

Where: I(A) is the discharge current; Δt (s) is the discharge time; m(g) designates the mass of active material; ΔV (V) is the discharge potential window.

Another key performance testing parameter is cycling stability, which measures the stability of a supercapacitor over a given charge-discharge cycle. A good supercapacitor will lose a minimal amount of its capacitance over an extended number of cycles [21].

The rate capability of a supercapacitor electrode is its ability to retain its capacitance value over an extended range of current density or scan rates [22]. The cycle life and rate capability are calculated using equation (1.4) and (1.5).

$$Cycling\ stability\ (\%) = \frac{Capacitance\ value\ after\ cycling}{\text{Capacitance value before cycling}}\ x\ 100 \quad (1.4)$$

$$Rate\ capability\ (\%) = \frac{Initial\ Specfic\ capacitance - final\ specific\ capacitance}{\text{Initial specific capacitance}}\ x\ 100 \quad (1.5)$$

1.3 Electrochemical supercapacitor evaluation

The basic tools employed to evaluate the electrochemical performance of a supercapacitor are cyclic voltammetry (CV), galvanostatic charge-discharge (GCD) and electrochemical impedance spectroscopy (EIS) analyses [23]. The active material is optimized in a three-electrode system configuration - comprising the active material as the working electrode, the reference electrode (e.g. Ag/AgCl or Hg/HgO) and the counter electrode (e.g. platinum wire) - before it is tested in a two-electrode system, where necessary.

1.3.1 Cyclic Voltammetry

The CV analysis probes the relationship between the applied voltage and the response of the working electrode to the current applied [24]. The shape taken by the CV curve is largely determined by the energy storage mechanism of the supercapacitor used, which can be an EDLC, a pseudocapacitor or a hybrid of the two. (See Figure 1.2.) The CV curve is also useful for

calculating the specific capacitance of a supercapacitor electrode at different scan rates, and is instrumental in electrochemical kinetic analysis [25].

1.3.2 Galvanostatic charge discharge

The galvanostatic charge discharge (GCD) test shows the potential response of a working electrode with respect to time [26]. The linearity or non-linearity of a supercapacitor electrode depends on the storage mechanism used. While the EDLC-type usually takes a linear form, the pseudocapacitor or battery-type is usually non-linear, as shown in Figure 1.2. The energy, power density and cycling stability can be calculated from the GCD curves using equations (1.1 – 1.3) provided earlier.

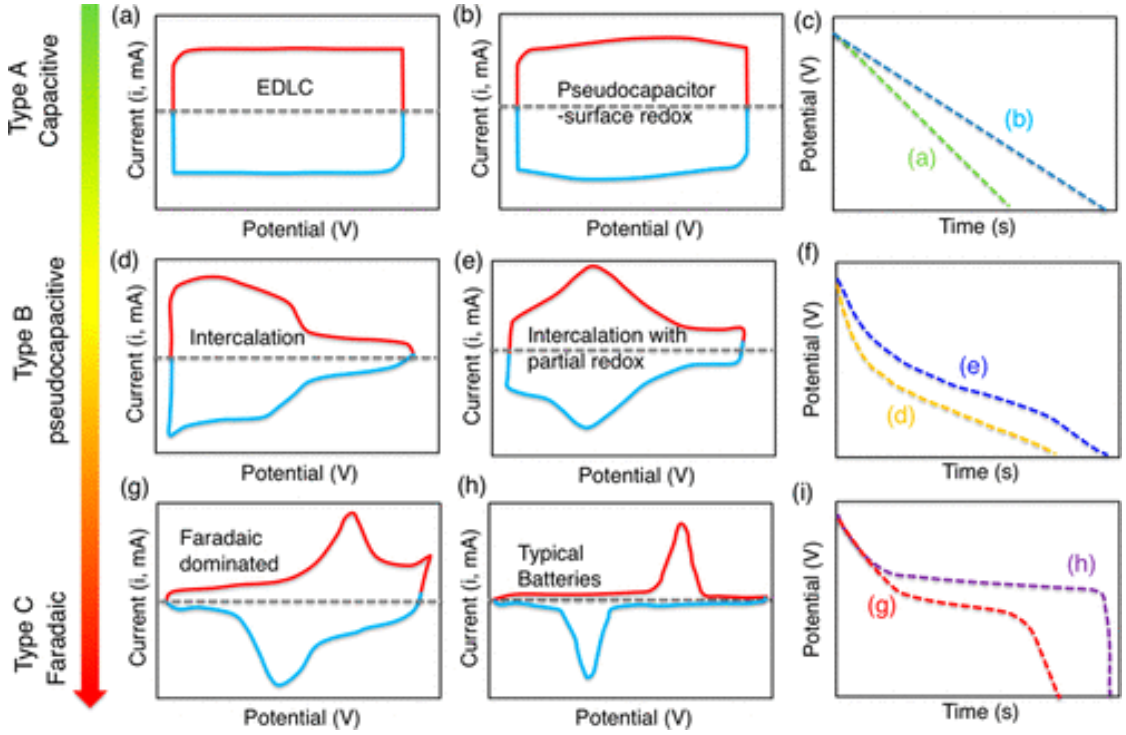

Figure 1.2 CV and GCD curves of different electrode materials.
Source: Ref. [27]

1.3.3 Electrochemical impedance spectroscopy

Electrochemical impedance spectroscopy (EIS) is a multi-frequency electrochemical technique used to estimate the electrical resistance of active materials in a solution over an extended range of frequencies (usually from 1 mHz to 10 kHz) [28]. The Nqyuist plot obtained from the EIS measurement reflects the impedance spectra over a known range of frequencies [29]. (See Figure

1.3.) An electrochemical circuit is usually drawn to fit the EIS spectra and different fitting parameters, including internal resistance to the solution (Rs), charge transfer resistance (Rct) and Waburg impedance (W). The parameters can be used to measure the conductivity of the electrode material and (by extension) the overall capacitive performance.

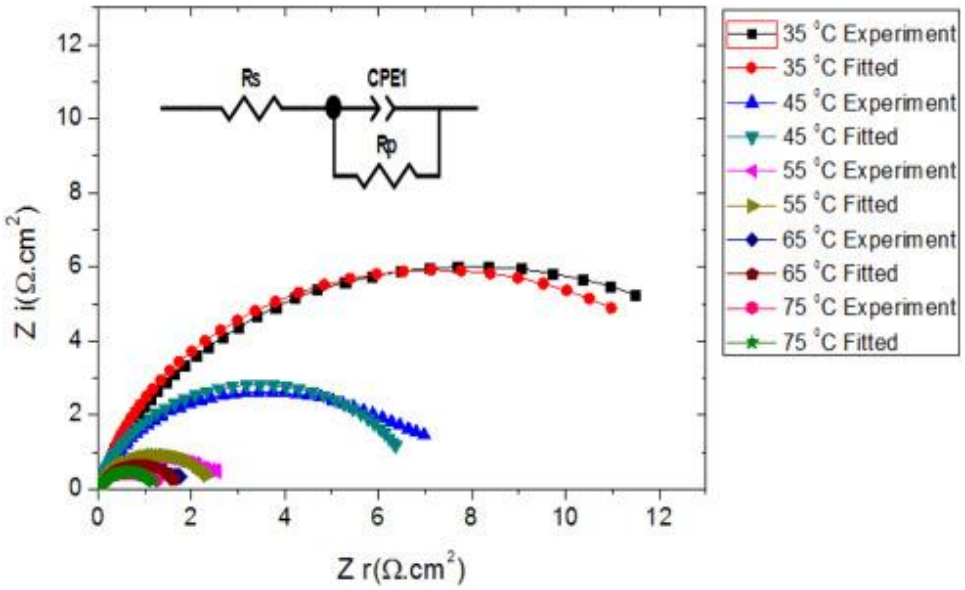

Figure 1.3 Typical Nyquist plot of silver oxide thin film electrodes, with the inset showing the equivalent circuit.
Source: Ref. [29]

1.4 MOFs for supercapacitors

Metal-organic frameworks (MOFs) are novel coordinated porous materials constructed from metal secondary building units and organic linkers [30]. MOFs have a unique 3D structure, which means that their pore characteristics can easily be tuned by changing the bridging linkers. As a result, MOFs have proved to be useful functional porous materials in various fields, including catalysis, drug delivery, gas storage and separation [31-33]. Furthermore, their large specific surface area and tunable pore properties are the main reasons why they can also be used as electrochemical supercapacitor electrodes [34]. MOFs comprising both the metal clusters and carbon sources (from the organic linker) ensure that they can be employed as templates or precursors for advanced electrode materials.

The latest research on MOFs for supercapacitor applications can be grouped into three categories, namely: [35-38]

- Controlling the physicochemical properties of MOFs by using them as precursors or templates to produce MOF-based materials, including porous carbon, metal oxides, metal hydroxides, metal sulfides and a host of other derivatives. In this category, the synthetic protocol adopted for the synthesis of precursor electrodes will go a long way in fine-tuning the morphology, size and chemical composition of the derived electrode materials compared to pristine MOFs.
- Forming nanocomposites by combining MOFs with conductive polymers (such as polyaniline (PANI) or polypyrrole (Ppy)) or carbon materials (such as activated carbon (AC), graphene and CNTs). This approach is key to improving the structural stability, conductivity and cycling stability of MOF-derived electrodes.
- The third category involves fabricating novel MOFs used exclusively as supercapacitor electrodes. The stability and conductivity are important considerations for pristine MOFs, even if new, to be employed directly as supercapacitor electrodes [39-40].

1.5 Problem statement and justification

Electrode materials play a key role in the performance of a supercapacitor, including in terms of specific capacitance, energy/power density and cycling stability. Only electrode materials with remarkable conductivity, excellent energy density and stable storage performance are suitable for use in supercapacitor applications. To date, designing an ideal supercapacitor electrode with high energy density has remained a challenge, with the conventional EDLC-type and the pseudocapacitive materials limited by poor conductivity, limited cycle life, low energy density and low capacitance.

Recently, MOFs have come to be considered ideal electrodes for supercapacitors because of their well-coordinated structure, remarkable porosity, high surface area and ease of tunability/functionality. However, poor electronic conductivity and low stability are serious drawbacks that limit them being used to produce supercapacitors on a commercial scale. To overcome this challenge, MOFs are either used as sacrificial templates or they are composited with conductive substrates, such as carbon-based materials and conductive polymers, while preserving the structural integrity of the parent MOFs. The synergistic effects of these composite electrodes

offer new physicochemical properties and improve the electrochemical performance of the electrode.

In recent years, noteworthy breakthroughs have been recorded in the use of MOF-derived electrodes for supercapacitors. Nonetheless, more improvements should be made, especially in terms of energy density and cycling stability. In this study, a rational and multi-faceted approach towards boosting the performance of MOF-derived electrodes in terms of energy density and stable performance was taken to probe the storage mechanism using detailed electrochemical kinetics analysis. The aim was to gain a better understanding of the structure-performance relationship and further improve on it.

1.6 Research aim and objectives

This study was aimed at: developing new electrode materials and a unique strategy for enhanced energy storage applications using MOFs as the template: and gaining a deeper understanding of the improved performance. The intention was to develop a solution to overcome the low performance of pristine MOFs in supercapacitors, which are usually plagued by low conductivity and poor stability.

The following detailed objectives enabled the aims of the study to be achieved:

- To employ MOFs as sacrificial templates or precursors to obtain new electrode materials.
- To introduce unique strategies to obtain composite electrodes for supercapacitor applications.
- To study the electrochemical supercapacitor performance of the as-prepared electrodes using CV, GCD and EIS.
- To study the effects of varying parameters and conditions on the electrochemical performance of MOF-based electrodes.
- To appraise the electrochemical kinetics analysis of the electrodes using different models.
  To gain in-depth understanding of the energy storage mechanism of the fabricated electrodes.

1.7 Thesis structure

This study report is organized into seven (7) chapters, i.e.:

Chapter 1: Introduction

This chapter gives a brief background on supercapacitors, MOFs, performance parameters and evaluation indices. It also details the research problem, the justification for the research, its aims and objectives and the structure of the thesis.

Chapter 2: Literature review

Chapter 2 provides a review of the literature on the use of MOF-derived Zn and Ni-based electrodes for supercapacitor applications. Recent progress made and the challenges in this area are discussed, while areas that require further investigation are noted. Consequently, this chapter provides a template for a proper discussion of the research work that has been done in subsequent chapters.

Chapter 3: Flexible supercapacitors based on nanocomposites of MOFs

This chapter provides an extended review of the literature that deals with advances made with nanocomposites of MOF-derived electrodes beyond Zn and Ni. The supercapacitors could meet the growing demand if they are flexible and deliver high performance. Hence, this chapter focuses on the prospects in terms of the electrode materials prepared in this study and provides various suggestions for future research.

Chapter 4: Dual ligand MOF-derived composite electrodes for elevated supercapacitor performance

This chapter describes a new double-ligand MOF strategy to fabricate NiO and NiO/C composite electrodes for supercapacitor applications, and the results are presented and discussed. Characterization of the electrodes was done with the aid of XRD, TGA, BET, Raman, SEM/TEM and FTIR. The electrochemical energy storage performance using CV, GCD and EIS established the proof of concept, while the charge storage mechanism of the electrodes was evaluated using electrochemical kinetics analysis.

Chapter 5: Self-assembled Zn-doped Ni-MOF as free-standing electrodes for supercapacitor applications.

Chapter 5 provides a discussion of the different concentrations of Zn ions used to dope pristine MOFs, which are used as binder-free electrodes for supercapacitor applications. The electrochemical performance of the various doped samples and a comparison with the relevant literature data is provided. The electrochemical performance of the highest performing electrode - which is measured in terms of specific capacitance, energy/power density, cycling stability and rate capability - was justified by studying its storage mechanism.

Chapter 6: Multi-walled carbon nanotube (MWCNT)-modified ZnO/C as a new composite electrode for improved energy storage

In an attempt to enhance the performance of the MOF-derived supercapacitor electrodes, which are plagued by low conductivity, hydroxyl functionalized MWCNT was used to modify ZnO/C. The resultant ZnO/CMWCNT composite electrode was applied in supercapacitor applications for the first time. This study also involved a comparison of the electrochemical performance of the as-prepared electrodes to relevant materials in the literature.

Chapter 7: Conclusion and recommendations

This chapter completes the thesis, gives an overview of the key findings in this study and provides useful suggestions for future research directions.

In summary, this thesis provides vital information regarding different strategies to improve the performance of MOF-based electrodes in electrochemical energy storage application. The practicality of this is geared towards developing new and fascinating electrode materials for supercapacitors. A list of references are provided at the end of each chapter, while the thesis ends with recommendations for further research output and the appendices.

References

1. Kalair, A., Abas, N., Saleem, M.S., Kalair, A.R. and Khan, N., 2021. Role of energy storage systems in energy transition from fossil fuels to renewables. *Energy Storage*, *3*(1), p.e135.
2. Schlögl, R., 2021. Chemical energy storage enables the transformation of fossil energy systems to sustainability. *Green Chemistry*, *23*(4), pp.1584-1593.

3. Goodenough, J.B., 2015. Energy storage materials: A perspective. *Energy Storage Materials*, *1*, pp.158-161.
4. Leonard, M.D., Michaelides, E.E. and Michaelides, D.N., 2020. Energy storage needs for the substitution of fossil fuel power plants with renewables. *Renewable Energy*, *145*, pp.951-962.
5. Argyrou, M.C., Christodoulides, P. and Kalogirou, S.A., 2018. Energy storage for electricity generation and related processes: Technologies appraisal and grid scale applications. *Renewable and Sustainable Energy Reviews*, *94*, pp.804-821.
6. Liu, J., Wang, J., Xu, C., Jiang, H., Li, C., Zhang, L., Lin, J. and Shen, Z.X., 2018. Advanced energy storage devices: Basic principles, analytical methods, and rational materials design. *Advanced Science*, *5*(1), p.1700322.
7. Nyholm, L., Nyström, G., Mihranyan, A. And Strømme, M., 2011. Toward flexible polymer and paper-based energy storage devices. *Advanced Materials*, *23*(33), pp.3751-3769.
8. Gwon, H., Kim, H.S., Lee, K.U., Seo, D.H., Park, Y.C., Lee, Y.S., Ahn, B.T. and Kang, K., 2011. Flexible energy storage devices based on graphene paper. *Energy & Environmental Science*, *4*(4), pp.1277-1283.
9. Yang, M. and Zhou, Z., 2017. Recent breakthroughs in supercapacitors boosted by nitrogen-rich porous carbon materials. *Advanced Science*, *4*(8), p.1600408.
10. Senthilkumar, S.T., Wang, Y. and Huang, H., 2015. Advances and prospects of fiber supercapacitors. *Journal of Materials Chemistry A*, *3*(42), pp.20863-20879.
11. Shao, Y., El-Kady, M.F., Sun, J., Li, Y., Zhang, Q., Zhu, M., Wang, H., Dunn, B. and Kaner, R.B., 2018. Design and mechanisms of asymmetric supercapacitors. *Chemical Reviews*, *118*(18), pp.9233-9280.
12. Zhang, S. and Pan, N., 2015. Supercapacitors performance evaluation. *Advanced Energy Materials*, *5*(6), p.1401401.
13. Borchardt, L., Oschatz, M. and Kaskel, S., 2014. Tailoring porosity in carbon materials for supercapacitor applications. *Materials Horizons*, *1*(2), pp.157-168.
14. Kim, S.Y., Gopi, C.V.M., Reddy, A.E. and Kim, H.J., 2018. Facile synthesis of a NiO/NiS hybrid and its use as an efficient electrode material for supercapacitor applications. *New Journal of Chemistry*, *42*(7), pp.5309-5313.

15. Wang, Y. and Xia, Y., 2013. Recent progress in supercapacitors: From materials design to system construction. *Advanced Materials*, *25*(37), pp.5336-5342.
16. Deng, Y., Xie, Y., Zou, K. and Ji, X., 2016. Review on recent advances in nitrogen-doped carbons: Preparations and applications in supercapacitors. *Journal of Materials Chemistry A*, *4*(4), pp.1144-1173.
17. Marichi, R.B., Sahu, V., Sharma, R.K. and Singh, G., 2017. Efficient, sustainable, and clean energy storage in supercapacitors using biomass-derived carbon materials. *Handbook of Ecomaterials*, pp.1-26.
18. Eddahech, A., Ayadi, M., Briat, O. and Vinassa, J.M., 2013. Online parameter identification for real-time supercapacitor performance estimation in automotive applications. *International Journal of Electrical Power & Energy Systems*, *51*, pp.162-167.
19. Xia, G.T., Li, C., Wang, K. and Li, L.W., 2019. Structural design and electrochemical performance of PANI/CNTs and MnO2/CNTs supercapacitor. *Science of Advanced Materials*, *11*(8), pp.1079-1086.
20. Roberts, M.E., Wheeler, D.R., McKenzie, B.B. and Bunker, B.C., 2009. High specific capacitance conducting polymer supercapacitor electrodes based on poly (tris (thiophenylphenyl) amine). *Journal of Materials Chemistry*, *19*(38), pp.6977-6979.
21. Dougal, R.A., Liu, S. and White, R.E., 2002. Power and life extension of battery-ultracapacitor hybrids. *IEEE Transactions on Components and Packaging Technologies*, *25*(1), pp.120-131.
22. Wang, G., Wang, H., Lu, X., Ling, Y., Yu, M., Zhai, T., Tong, Y. and Li, Y., 2014. Solid-state supercapacitor based on activated carbon cloths exhibits excellent rate capability. *Advanced Materials*, *26*(17), pp.2676-2682.
23. Wang, R., Ma, Y., Wang, H., Key, J., Brett, D., Ji, S., Yin, S. and Shen, P.K., 2016. A cost effective, highly porous, manganese oxide/carbon supercapacitor material with high rate capability. *Journal of Materials Chemistry A*, *4*(15), pp.5390-5394.
24. Shakir, I., Sarfraz, M., Rana, U.A., Nadeem, M. and Al-Shaikh, M.A., 2013. Synthesis of hierarchical porous spinel nickel cobaltite nanoflakes for high performance electrochemical energy storage supercapacitors. *Rsc Advances*, *3*(44), pp.21386-21389.
25. Xu, P., Zeng, W., Luo, S., Ling, C., Xiao, J., Zhou, A., Sun, Y. and Liao, K., 2017. 3D Ni-Co selenide nanorod array grown on carbon fiber paper: Towards high-performance flexible

supercapacitor electrode with new energy storage mechanism. *Electrochimica Acta*, *241*, pp.41-49.

26. Bala, H., Dymek, M. and Drulis, H., 2014. Development of metal hydride material efficient surface in conditions of galvanostatic charge/discharge cycling. *Materials Chemistry and Physics*, *148*(3), pp.1008-1012.
27. Gogotsi, Y. and Penner, R.M., 2018. Energy storage in nanomaterials–capacitive, pseudocapacitive, or battery-like? *ACS Nano*, pp. 2081-2083.
28. Pajkossy, T. and Jurczakowski, R., 2017. Electrochemical impedance spectroscopy in interfacial studies. *Current Opinion in Electrochemistry*, *1*(1), pp.53-58.
29. Oje, A.I., Ogwu, A.A. and Oje, A.M., 2021. Effect of temperature on the electrochemical performance of silver oxide thin films supercapacitor. *Journal of Electroanalytical Chemistry*, *882*, p.115015.
30. Kitagawa, S., 2014. Metal–organic frameworks (MOFs). *Chemical Society Reviews*, *43*(16), pp.5415-5418.
31. Otun, K.O., Liu, X. and Hildebrandt, D., 2020. Metal-organic framework (MOF)-derived catalysts for Fischer-Tropsch synthesis: Recent progress and future perspectives. *Journal of Energy Chemistry*, *51*, pp.230-245.
32. Otun, K.O., 2020. Temperature-controlled activation and characterization of iron-based metal-organic frameworks. *Inorganica Chimica Acta*, *507*, p.119563.
33. Wang, A., Luo, M., Lü, B., Song, Y., Li, M. and Yang, Z., 2021. Effect of Na, Cu and Ru on metal-organic framework-derived porous carbon supported iron catalyst for Fischer-Tropsch synthesis. *Molecular Catalysis*, *509*, p.111601.
34. Du, W., Bai, Y.L., Xu, J., Zhao, H., Zhang, L., Li, X. and Zhang, J., 2018. Advanced metal-organic frameworks (MOFs) and their derived electrode materials for supercapacitors. *Journal of Power Sources*, *402*, pp.281-295.
35. Mohanty, A., Jaihindh, D., Fu, Y.P., Senanayak, S.P., Mende, L.S. and Ramadoss, A., 2021. An extensive review of three dimension architectural metal-organic frameworks towards supercapacitor application. *Journal of Power Sources*, *488*, p.229444.
36. Wang, L., Han, Y., Feng, X., Zhou, J., Qi, P. and Wang, B., 2016. Metal–organic frameworks for energy storage: Batteries and supercapacitors. *Coordination Chemistry Reviews*, *307*, pp.361-381

37. Wang, K., Bi, R., Huang, M., Lv, B., Wang, H., Li, C., Wu, H. and Zhang, Q., 2020. Porous cobalt metal–organic frameworks as active elements in battery–supercapacitor hybrid devices. *Inorganic Chemistry*, *59*(10), pp.6808-6814.
38. Zhao, X., Gong, L., Wang, C., Wang, C., Yu, K. and Zhou, B., 2020. A facile grinding method for the synthesis of 3D Ag metal–organic frameworks (MOFs) containing Ag6Mo7O24 for high-performance supercapacitors. *Chemistry–A European Journal*, *26*(20), pp.4613-4619.
39. Liu, Y., Xu, N., Chen, W., Wang, X., Sun, C. and Su, Z., 2018. Supercapacitor with high cycling stability through electrochemical deposition of metal–organic frameworks/polypyrrole positive electrode. *Dalton Transactions*, *47*(38), pp.13472-13478.
40. Gu, M., Wu, M., Wang, S.C., Chen, C., Xiong, D. and Yi, F.Y., 2020. Morphology control of nanoscale metal-organic frameworks for high-performance supercapacitors. *Electrochimica Acta*, *343*, p.135617

Chapter 2: Literature review

Design of zinc and nickel-based MOFs and composites for supercapacitor applications

Abstract

A sustainable, cost-effective, clean energy storage system is key to meeting growing global energy demands and to solving the problem of over-reliance on fossil fuels. Most existing supercapacitor materials used to store energy are limited by either low energy density or electrolyte leakage. This may be rectified by designing high-performance electrode materials that can balance energy density and power delivery while maintaining superb storage performance. Metal-organic frameworks (MOFs) are promising electrode materials for energy storage applications, because they have well-ordered pores in regular patterns, which can store energy by creating redox sites that enhance faster ion-diffusion. The major impediments to using pristine MOFs as electrode materials for supercapacitors are poor cycle stability and low electrical conductivity. This can be remediated by designing MOF composites with good electrical conductivity and good cycle stability.

This chapter deals with recent advances made in improving the electrochemical energy storage applications of MOFs by exploiting the synergistic benefits of the components that constitute transition metal-based composites. Specifically, attention is given to smart design of composite electrode materials from MOFs containing zinc and nickel-based electrodes and their electrochemical performance. The main obstacles to using transition metal-based MOFs as supercapacitors (SCs), and the key steps to further improving their use in applications are detailed in this chapter. It is expected that this chapter will provide insight into rational design of high-performing electrode materials using Zn and Ni-MOF-based electrodes for enhanced electrochemical energy storage applications.

Keywords: Energy storage, MOFs, supercapacitor, transition metals, energy density

2.1 Background

Sustainable energy storage and conversion systems have seen a spark in research attention due to economic concerns and concern about environmental pollution. Specifically, there are ever-increasing demands for energy and a renewed drive to employ clean, green, efficient energy sources to replace fossil fuels that contribute to global warming, climate change and other environmental-related problems [1].

Of crucial significance are the batteries and supercapacitors used as storage devices in myriad applications, such as in the energy and transportation sectors. Both devices have gained prominence globally and concerted effort is being made to boost their performance, in order to meet the enormous expectations of the world's growing population [2]. Different approaches and techniques have been adopted to improve the electrochemical performance of electrode materials used as energy storage devices [3]. Compared to conventional batteries, supercapacitors (otherwise known as ultracapacitors) possess desirable characteristics, such as a long cycle life, superb power density and a fast charge-discharge rate [4]. They are designed to make up for the deficiencies associated with batteries, such as low power density and a short cycle life [5]. They can swiftly and conveniently store large amounts of energy and discharge it just as quickly. Supercapacitors are increasingly being used in industry these days, and have found use in energy devices, electronics (such as cameras, phones and laptops) and memory backup systems. SCs have also been instrumental in retrieving the braking energy in trains and buses, and, more recently, have been used to open the emergency doors of the Airbus A380 airplane [6-7].

One common disadvantage that limits the use of supercapacitors in large-scale applications is their low energy density [8]. For instance, compared to lithium-ion batteries (LIBs), which can attain an energy density of about 200 Wh/kg, supercapacitors can only deliver energy density below 10 Wh/kg [9]. One of the strategies devised to overcome this performance limitation is the fabrication of novel electrode materials with an enhanced ions/electrons transportation rate [10]. Another approach involves increasing the voltage (V) or capacitance (C) of the cell via optimization of the interface between the electrodes and electrolytes, according to the equation $E=0.5CV^2$ [11]. But in this chapter, more attention is paid to the former approach than to the latter.

The rational fabrication of electrode materials influences the performance of SCs in no small way. Some of the parameters that determine the optimal performance of a good SC include

a substantial specific surface area, high conductivity, excellent pore characteristics, good thermal stability and low cost [12]. Materials appropriate for use as high-performance SCs that perform better than the batteries are carefully chosen and optimized to obtain the desired properties. Examples of SCs include: carbon-based materials such as activated carbon (AC); carbon nanotubes (CNTs) and carbon nanofibers (CNFs); metal oxides/hydroxides such as Co_3O_4, MnO_2 and RuO_2; conductive polymers such as polypyrrole (PPy) and polyaniline (PANI) [13]. These conductive materials have both advantages and disadvantages. For instance, carbon-based materials are characterized by good stability and high conductivity, but feature low energy density. Despite the considerable specific capacitance of metal oxides/hydroxides, they exhibit low conductivity [14].

Based on the storage mechanism that operates, supercapacitors are grouped into three categories, viz: electrical double-layer capacitors (EDLC), pseudocapacitors (PC) and hybrid capacitors (HC) [15]. (See Figure 1.) The third class, a hybrid supercapacitor (HSC), is a combination of the first two storage mechanisms. The EDLC stores the charge (non-Faradaic) electrostatically at the interface of the electrode and electrolyte through the adsorption-desorption process [16]. Carbon-based materials make up this class (EDLC), in the main. Pseudocapacitors store a charge through the redox reaction (Faradaic process), and complexes of transition metals and conducting polymers are composed of PC. HSCs combine the storage mechanisms of EDLC and PC, as the charge is stored by both Faradaic and non-Faradaic processes [17].

The interminable search for high-performance materials that meet the requirements for a good supercapacitor has resulted in the discovery of porous, crystalline coordination compounds called metal-organic frameworks (MOFs). MOF constituents basically contain metal nodes/clusters and organic linkers, and are known for their excellent pore characteristics, tunable functional groups and well-dispersed metal centers [18]. Compared with other porous materials (such as zeolite), MOFs exhibit a high specific surface area and ordered porosity, which facilitates the transportation of ions during electrochemical reactions [19]. Despite the distinct benefits that accompany the use of MOFs for supercapacitor applications, they suffer from low conductivity, which can limit their use in electrical devices. However, their surface area (which can be as high as 6000 m^2/g) means that they are ideal for investigation in terms of electrochemical applications, especially supercapacitor applications [20], as a large surface area is critical to the high activity of a supercapacitor.

Another concern regarding the use of MOFs as supercapacitor electrodes is their low chemical, thermal and mechanical stability [21]. The low chemical stability of MOFs stems from the type of bonding that exists in MOF structures, which is typically formed via a reversible coordination bond, rather than the conventional covalent bond that is common with most materials. To address this challenge, novel new stable MOFs are synthesized via *de novo* synthesis, or different strategies are developed (including in situ and post-synthetic modifications) to enhance the stability of existing MOFs [22].

The advances made in MOF research in terms of energy storage applications has resulted in them being used as a sacrificial template to synthesize various composites of transition metals, such as Ni, Fe, Co, Cu and Zn. Transition metals possess multiple oxidation states, in addition to excellent specific capacitance. MOF composites could be used to incorporate highly conductive materials - such as AC, CNTs, graphene oxide (GO) and conducting polymers - into the parent MOF to enhance their use in electrochemical energy storage applications.

Among the transition metals, Ni and Zn were selected as the focus of this study because of their abundance, eco-friendliness, cost-effectiveness and excellent redox properties [23-25]. This chapter focuses on recent advances made in the use of transition metal-based (Zn and Ni) MOF composites as supercapacitors for electrochemical energy storage. The smart strategies of modifying the structure of Ni and Zn-based MOFs to obtain composite Zn/Ni oxides, hydroxides and mixed Zn-Ni oxides with improved capacity and reasonable cycling stability are discussed. The overall objective of this chapter is to detail the latest research trends in terms of the electrochemical performance and capacitance of Zn and Ni-based MOF composites, and to highlight the areas that require further attention in order to obtain high-performing materials. Finally, an overview of the research directions and prospects is provided, together with the potential downside in the field of Ni and Zn-based MOFs for supercapacitors.

Table 2.1: Comparison of a battery and supercapacitor as energy storage devices.

S/N	Performance	Battery	Supercapacitor
1	Charge time	1-5 h	0.3-30 s
2	Discharge time	0.3-3 h	0.3-30 s
3	Power density (W/kg)	5-200	Up to 1000

4	Energy density (Wh/kg)	1-100	1-10
5	Charge-discharge efficiency	0.7-0.85	0.85-0.98
6	Cycle life	500-2000	> 100000

Source: Ref. [26]

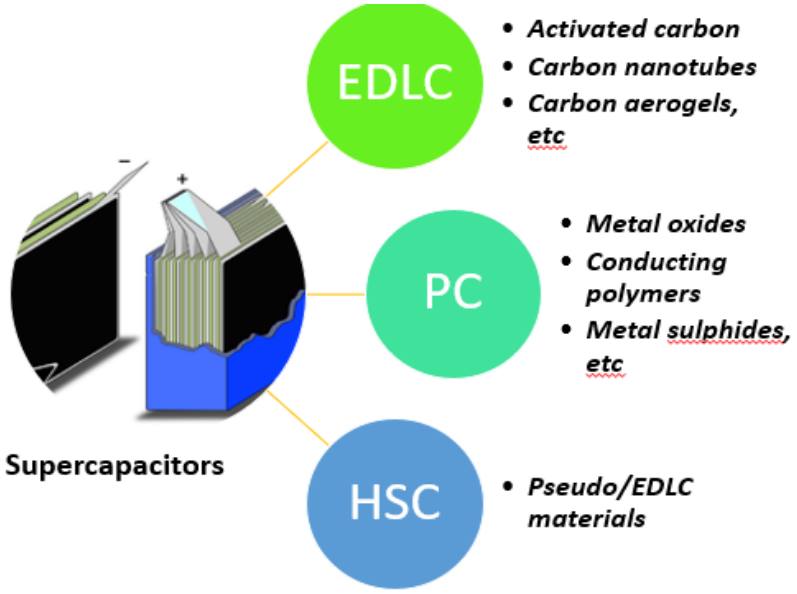

Figure 2.1 Different types of supercapacitors and some examples: EDLC; PC; HSC.

2.2 Potential of Ni and Zn-based MOFs for supercapacitors

The research done on coordinating transition metal ions such as Ni and Zn with organic linkers has led to breakthroughs in the research on synthesizing MOFs and investigating their performance in different applications, including energy storage [27]. However, when pristine MOFs are employed as electrode materials for supercapacitors, they suffer from low conductivity and short cycling stability, which limit their rate performance and, by extension, their use in practical applications [28]. However, a large number of porous Ni and Zn-based nanostructures and their composites have been fabricated via several strategies that will be expounded on in the next section [29]. These strategies aim to improve the electrochemical performance of the parent MOF while also preserving its properties. Additionally, these modifications can also deliver the target level of conductivity and the other requirements needed to enhance the overall performance of an electrode.

Ni-based compounds and derivatives have mainly been used as electrode materials for energy storage because of their excellent redox potential and their ability to facilitate rapid ion diffusion and electron transfer [30]. For instance, Zhao et al. used pristine Ni-MOF as a template to synthesize Ni nanoparticles in a matrix of N-doped porous carbon (Ni/N-PC), which was then used as the electrode material for supercapacitors [31]. The results obtained demonstrated that the material displayed a high-rate performance (2002 Fg^{-1} at a current density of 1 Ag^{-1}) and outstanding cycling stability (about 92% after 5000 cycles at 10 Ag^{-1}). In another study, Qu and co-workers designed an Ni-ADC-DABCO MOF that displayed considerable pseudo-capacitive performance with a specific capacitance of 522 Fg^{-1} at 1 Ag^{-1} [32].

Zn-based MOFs are another promising material that can serve as a template for the design and synthesis of a large number of high-performance composite materials, to make up for the challenges associated with pristine MOFs [33]. In particular, zinc helps to promote electrical conductivity and enhance redox reactions. Some of the pristine MOFs from which derivates are obtained are MOF-177, MOF-5, IRMOF-1, ZIF-8, $[Zn_2(bdc)_2dabco]_n$ [34-35]. These MOF materials differ in their organic functionality, textural properties and electrochemical performance. Unlike Ni-MOFs, pristine Zn-MOFs have rarely been reported in the literature as potential supercapacitor electrodes. Even with Ni-MOFs, their low cycling stability at a high current density still poses some problems. Hence, there is a need to develop composite materials that will possess high cycling stability at a high current density.

2.3 Smart design of composite electrode materials from Ni and Zn-based MOF templates

Composite materials with sufficient conductivity and stability are required to produce the next generation of electrode materials with good electrochemical performance [36]. Zn and Ni-based composites are used due to their superior conductivity, strong redox reaction and superior mechanical strength. The transition metal-based electrode materials are made using three main strategies, i.e. the etching, annealing and template processes [37-40]. Only a small percentage of Ni and Zn-based MOFs are commonly used to produce MOF derivatives. These are elucidated on in the next section.

2.3.1 Annealing approach

MOFs can be used as a template for direct synthesis of MOF composites by preserving the structural integrity of the parent MOF. Annealing MOFs into Ni and Zn-based electrodes is a convenient and effective approach [41], as the organic linker in Ni and Zn-based parent MOFs converts to volatiles to produce Ni and Zn-based electrodes. However, the structural integrity of MOFs may be threatened at a high temperature, which may have a strong effect on the textural properties of the resulting nanostructures [42]. Even when the temperature is lowered, some drawbacks may limit the practical use of the obtained derivatives, including low electrical conductivity of the derived carbon materials, which may result from poor crystallinity [43]. Therefore, it is critical to incorporate strategies that will help create pores and stabilize the framework during the pyrolysis process. Several studies have adopted this approach, including the study done by Park and co-workers [44], who synthesized flower-like (NMF-1) and hollow spherical (NMF-2) NiO from Ni-MOFs containing 2-methylimidazole and terephthalic acid, respectively. The parent MOF was annealed for 4 h at 400 ^{o}C in air. Electrochemical testing of the electrodes showed that the hollow sphere NiO performed better than the flower-like NiO, with the former having a specific capacitance of 1058 Fg^{-1} at a current density of 2 Ag^{-1} compared to the 857 Fg^{-1} shown by the latter at the same current density. The hollow spherical NiO also possesses great capacity retention, i.e. above 93% after 5000 cycles. The authors attributed the enhanced performance to adequate active sites and transport ports that are large enough for electroactive species [44].

In order to enhance the performance of single metal electrodes, Wang and co-workers fabricated oxides of $ZnCo_2O4$ supported on Ni foam from Co/Zn-MOF for a supercapacitor application [45]. The bimetallic oxides were formed when the precursor MOF was annealed at different temperatures for stabilization prior to oxidation. The resulting crystalline bimetallic oxides possessed nanosheet morphology, while the incorporation of Zn influenced the size and thickness dramatically. When tested for supercapacitor applications in a 3 M electrolyte (KOH) solution, $ZnCo_2O_4$ annealed at 200 ^{o}C and showed a very high areal capacitance of 3.19 F cm^{-2} at a current density of 2 mA cm^{-2}. Additionally, at an elevated current density of 2 mA cm^{2}, about 84% of the initial capacitance value was retained.

In summary, annealing has been noted as a facile strategy to produce the derivative Zn and Ni-based compounds for high-performance storage capability. However, the annealing temperature must be selected carefully, and must preferably be below the decomposition temperature of the framework under inert temperature. If not, the framework collapse can lead to clustering of the particles, which affects the textural properties of the derivatives and the resultant electrochemical performance.

2.3.2 Etching approach

The etching process is a smart way to prepare Ni and Zn composite electrode materials with an open architecture and doped heteroatoms from MOF precursors [46]. Several organic molecules are used as etching agents, including inorganic and organic acids. This strategy is simple, and the structural features of the resulting materials can be tuned by altering the transformation parameters [47]. Liu and co-workers [48] adopted this strategy to obtain a transition metal-based electrode. A mesoporous silica layer was employed to wrap ZIF-8 and so guard against the agglomeration of the resulting porous carbon during pyrolysis. (See Figure 2.2.) The silica layer was removed by etching to produce well dispersed porous carbon nanospheres with a particle size below 100 nm.

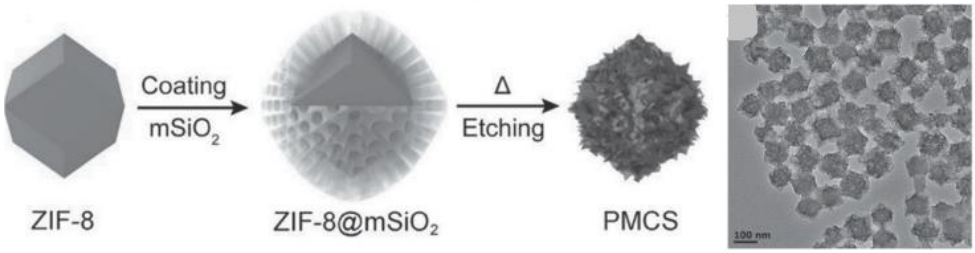

Figure 2.2: Scheme for the fabrication of a porphyrin-like carbon sphere from ZIF-MOF using the etching process.
Source: Ref. [48]

Similarly, in 2019, Ma et al. [49] used Zn-ZIF (ZIF-8) and the etching method to produce "hierarchical porous honeycomb-type carbon frameworks (HHCF)" for use in supercapacitor applications. (See Figure 2.3.) The honeycomb-type carbon framework (HCF) was initially obtained during high-temperature calcination of the ZIF-8 precursor, coupled with PVP as an additional carbon source. Acid was then used to etch the Zn metal and the HHCF is produced when various micropores appear on the HCF framework. The HHCF showed extraordinary

electrochemical performance when tested with a specific capacitance of 361 Fg^{-1} at a current density of 1 Ag^{-1} in 6M KOH and 182 Fg^{-1} when the current density was increased to 100 Ag^{-1}. (See Figure 2.3.) The HHCF also exhibited a considerable current density of 74 $WhKg^{-1}$ in ionic liquid. The HHCF was also used as the electrode material for a flexible solid-state supercapacitor and showed high energy density, great flexibility and remarkable specific capacitance [49].

Thus, the etching method is a promising strategy for transforming MOF templates into Zn and Ni composite electrodes. Its efficiency can be enhanced by optimizing the etching parameters and the morphological conditions of MOFs, which will leave an abundance of active sites on the resulting nanostructures for easy access to electrolyte ions and ensure enhanced energy storage performance. However, the high cost of MOF precursors may limit their use in practical applications.

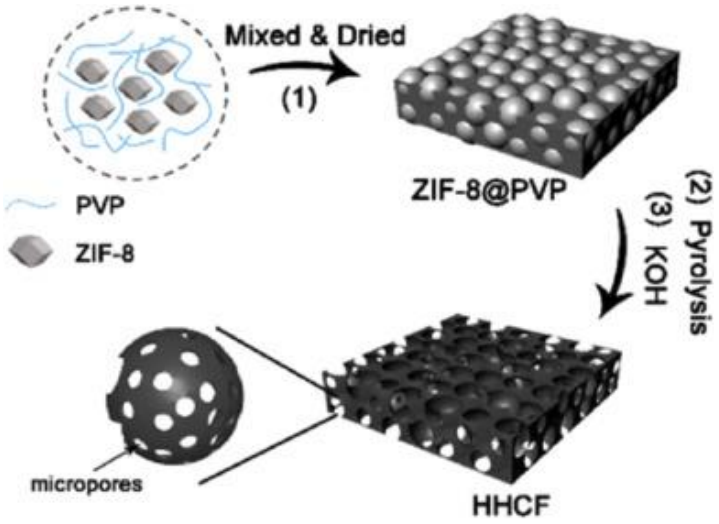

Figure 2.3 Representation of the synthesis of HHCF.
(1) Self-growth of ZIF-8 nanostructures laced with PVP to produce ZIF-8@PVP. 2) Synthesis of HHCF by pyrolysis of ZIF-8@PVP at 800 ºC in Argon. 3) Activation process involving etching of KOH and the removal of Zn.)
Source: Ref. [49].

2.3.3 Hydrolyzing approach

The commonly used annealing strategy often requires a high temperature to obtain MOF derivatives, which leads to the aggregation of nanoparticles. The MOF-hydrolyzing approach can be used instead for controlled transformation of MOF templates into transition metal hydroxides with textural properties that are appropriate for use in supercapacitor applications [50]. Interestingly, this method allows for recycling expensive organic linkers and the commercialization of electrode materials. During hydrolysis of MOFs into the transition metal hydroxides of interest, the bond coordinating the transition metal and the linker breaks up, which allows the organic ligand to be hydrolyzed [51]. The precipitated ligand can then be recovered by neutralizing the aqueous solution to fabricate more MOF materials and composites. Additionally, the hydrolyzing conditions need to be optimized to maintain the porosity and morphology of the parent MOFs.

One example of this strategy is seen in the work of Zhou et al., where controlled alkaline hydrolysis of MOFs yielded a hierarchical Ni-based layered double hydroxide (LDH) via the pseudomorphic conversion approach, while the structural integrity of the MOF template was preserved. [52]. A Ni-based MOF, $N[Ni_3(OH)(Ina)_3(BDC)_{1.5}]$, was employed as the template, as it contains the $Ni_3(\mu_3\text{-}OH)$ building unit that conforms with LDH. Using isotopic tracing analysis, it was shown that the μ_3-OH cluster in the template was instrumental in preserving the structural integrity of the resulting particles during hydrolysis. This is possible by preventing leaching of the Ni^{2+}. The cluster can also help with the judicious selection of MOF templates. Benefitting from the fact that MOFs are easily adjustable, the Ni^{2+} in the parent MOFs was partly substituted with Co^{2+} during MOF synthesis to afford Ni/Co-LDH microspheres with varying ratios. This conversion was monitored by scanning electron microscopy (SEM) and transmission electron microscopy (TEM), as shown in Figure 2.4. The results obtained revealed that Ni/Co-MOF-7:3 has uniform microspheres with particle sizes up to 1.5 μm (Figure 2.4a), which remained constant after soaking in a 1 M KOH solution (Figure 2.4b). The pseudomorphic conversion process was also established, with the TEM images (Figure 2.4c) showing the same size particles (1.5 μm). The homogeneous distribution of Co and Ni in Ni/Co-LDH-7:3 was shown by EDS elemental mapping. (See Figure 2.4d.) When applied as a supercapacitor electrode, Ni/Co-LDH-7:3 exhibited a superior capacitance of 1652 Fg^{-1} at a current density of 1 Ag^{-1} and outstanding cycling stability,

even after 2000 cycles. When the electrode was employed as an all-solid-state asymmetric supercapacitor at a power density of 74.3 W/kg, it possessed a high energy density of 32.9 Wh/kg [52].

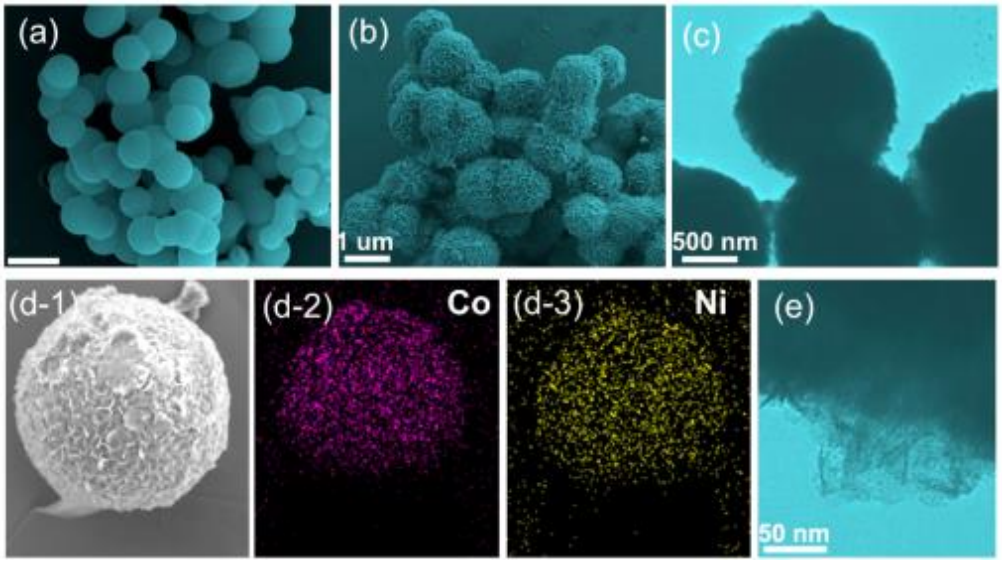

Figure 2.4 Characterization results showing (a) SEM image of the MOF template - Ni/Co-MOF-7:3. (b) SEM image of the fabricated electrode - Ni/Co-LDH-7:3. c and e) TEM images at different magnifications of the Ni/CoLDH-7:3. d 1 to 3) Mapping of the Ni/Co-LDH-7:3 using SEM.
Source: Ref. [52]

Although hydrolysis of MOFs is a well-organized and cost-effective strategy for the design of transition metal hydroxides, the partial transformation of MOF residuals can limit the charge storage capability, as a result of the 'outside-in' process. The MOF residuals may also interact with the electrolyte and impede the charge/discharge cycles - and therefore the cycle stability of the electrode material. To this end, Sun et al. undertook the first-ever study on complete hydrolysis of Ni-MOF-74, $Ni_2(dhtp)(H_2O)_2.8H_2O$. The result of which possesses regular 1D pores in hierarchical nickel hydroxide, $Ni(OH)_2$ for supercapacitor application [53]. This complete transformation can occur concurrently inside and outside the MOF template, based on the reaction temperature. This is critical to ensure high performance of the supercapacitor, because the organics within $Ni(OH)_2$ help to prevent the transportation of OH^- and elongate the diffusion paths. When tested for electrochemical activity, the MOF-derived $Ni(OH)_2$ obtained at 75 ^oC displayed a specific capacitance of 713 C/g at 1 Ag^{-1}; this dropped to about 58.2% of the original value at 25 A g^{-1} [53]. In addition, an all-solid asymmetric supercapacitor electrode was fabricated using

$Ni(OH)_2$ and active carbon, which revealed an energy density of 36.2 Wh/kg at 436.1 W/kg power density [53].

It is also evident from most studies involving transition metal-based electrodes for supercapacitors that they are always accompanied by low cycle stability, because of the exacting volume effects and low reaction kinetics during the charge-/discharge step. To remediate this, Zhang et al. used a hot alkaline hydrolysis strategy to synthesize a core-shell $Ni_{0.7}Co_{0.3}(OH)_2$ microsphere from an Ni-Co-MOF precursor that was hydrolyzed in KOH and heated at different temperatures [54]. Transformation of the template into hydroxides is a two-step reaction process, viz. MOF hydrolysis and hydroxide crystallization. The two reactions first occurred outside the MOF sphere, and there is a chance that the inner spheres were wrapped by crystallized MOF-derived $Ni_{0.7}Co_{0.3}(OH)_2$. So, the rate of the two reactions must be equal to achieve complete hydrolysis. Complete hydrolysis occurred at a temperature of 120 ^oC at a KOH concentration of 0.2 M. This material showed outstanding performance when tested for electrochemical supercapacitor application. At a current density of 0.2 Ag^{-1}, the $Ni_{0.7}Co_{0.3}(OH)_2$ electrode prepared at 0.2 M KOH showed a high specific capacity of 945 C/g, and retained this even after 10000 cycles. When fabricated for an asymmetric supercapacitor device, it exhibited an outstanding current density of about 40 Wh/kg at a power density close to 401 W/kg and retained this performance even after 20,000 cycles [54].

In summary, hydrolysis of MOFs is a promising route to obtain hydroxides from Zn and Ni-based electrode materials, which can lead to good electrochemical performance. This strategy allows the expensive organic ligands to be recovered, and it can also be applied for large-scale synthesis of transition metal-based electrodes for supercapacitor applications. However, limitations such as incomplete hydrolysis and low cycle stability may affect storage capability, if the reaction conditions are not well optimized.

2.4 Applications of MOF-derived Zn and Ni-based electrodes in SCs

Supercapacitors (SCs) that are classified as pseudocapacitors, based on the charge storage mechanism, usually exhibit good storage ability [55]. These pseudocapacitors use transition metal oxides (such as ZnO and NiO) as their working electrodes. They can be fabricated either by conventional means or via pristine MOFs when they are annealed in specific environments [56]. Compared with traditional methods, MOF-derived ZnO and NiO possess considerably higher

porosity, with an excellent specific surface area that can facilitate rapid diffusion of electrolyte ions for enhanced electrochemical storage performance [57]. Despite these advantages, MOF-derived transition metal oxides may not always deliver optimum performance, especially if certain electrical conductivity enhancing factors are lacking. Therefore, ZnO and NiO are incorporated with polymers and carbonaceous materials, and are sometimes doped with other transition metals, in order to make up for the deficiencies. The final composite electrode materials usually exhibit good electrical conductivity, a large specific surface area, excellent porosity and considerable stability, which translates into high capacitive retention and stable performance [58].

2.5 MOF-derived Zn and Ni oxides composite electrodes in SCs

Because of its outstanding thermal/chemical stability and great mechanical flexibility, ZnO is regarded as a material of interest in terms of high-performance supercapacitor applications among the different known transition metal oxides [59]. ZnO is frequently combined with a hybrid material to boost its electrochemical performance in order to maximize its potential as an electrode material [60]. Because of the additional benefits inherited from both the MOF and the zeolite, such as adjustable porosity, ease of functionalization, and strong chemical and thermal stability of MOFs, ZIF is commonly used as the ZnO precursor [61]. The resultant hybrid materials made from parent MOF materials have a high conductivity, high porosity, and a large specific surface area [62], demonstrating the advantages of the constituent components. MOF-74(Zn) was investigated as a template for zinc composite ZnO-carbon (ZnO-C) by Gan and colleagues [63]. The capacitive performance of porous ZnO-C (obtained via pyrolysis of the parent MOFs at various temperatures) increased with increasing temperature. Using a 1 M H_2SO_4 electrolyte solution, the composite material that was pyrolyzed at 900 ^oC demonstrated the greatest capacitive performance, with a specific capacitance of 197.84 Fg^{-1} at 0.1 Ag^{-1}. However, increasing the pyrolysis temperature (up to 1000 ^oC) caused the specific capacitance value to drop. This might be due to the fact that at higher temperatures, the pore size distribution constricted. Surprisingly, after 1000 cycles, nearly 98 percent of the capacitance was preserved at 1 Ag-1, demonstrating the composite material's exceptional cycling stability [63].

Rooting metal oxides (including ZnO) on a substrate to build a bridge, which decreases mechanical shedding and improves electrical conductivity between the substrate and the active material, is another efficient technique to increase their electrochemical performance. Han et al., for example,

used a root-etch-wrap technique to produce a hollow-core shell-structured electrode that integrates the structural composition and synergistic qualities of the different elements that make up the electrode [64]. PANI/ZnO@ZIF-8-CC, the manufactured electrode, has good conductivity and mechanical strength, resulting in a fantastic areal capacitance of 4839 mF cm-2 at 5 mA cm-2, a high rate capability, and high cycling stability (87 percent for 10,000 cycles at 5 mAcm-2) [64]. (For further information, see Figure 2.5.) The synergistic raised surface area and porosity of the MOF precursors, ZIF-8 and ZnO, along with the pseudocapacitance advantages of PANI, resulted in an improved capacitance of this electrode. When compared to the capacitance performance of PANI-ZIF-67 without ZnO (2146 mF cm-2 at 10 Vs-1) [64], the former demonstrated a greater capacitance performance.

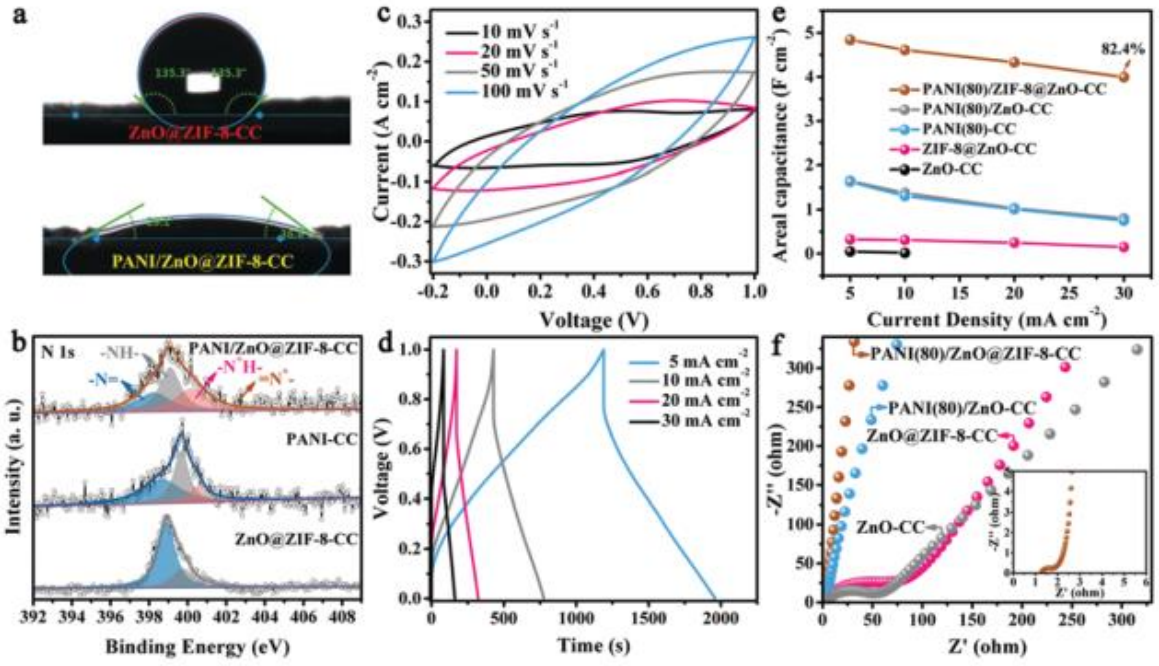

Figure 2.5 Electrochemical performance of the composite.
a) Contact angles of electrodes without PANI (ZnO@ZIF-8-CC) and with PANI, PANI/ZnO@ZIF-8-CC. b) N 1s spectrum of both electrodes. c) CV. d) GCD plots of PANI-incorporated electrodes. e) Capacitance. f) Nyquist plots PANI-incorporated electrodes.
Source: Ref. [64]

Because of its inexpensive cost, great abundance, outstanding thermal/chemical stability, and remarkable theoretical specific capacitance (3750 F g-1) [65], NiO is regarded one of the most promising electrode materials for supercapacitor applications. However, because NiO's specific

capacitance is much lower than its theoretical value, various adjustments are necessary to improve its electrochemical supercapacitor performance [66]. In other cases, such as in the work of Wu and co-workers [67], who reported NiO nanocubes with a specific capacitance of 1012 mF cm^{-2}, attempts were made to change the form and structure of NiO. NiO in various forms, such as hollow structures, nanoplates, nanoslices, nanospheres, and nanocolumns, has been described in other research [68-69]. In other circumstances, incorporating conducting elements such as carbon materials (including graphene, CNTs, and reduced graphene oxides) to improve their electrical conductivity might improve the performance of the NiO structure for supercapacitor applications [68]. Because of the powder nature of composite electrodes, insulated binders are used in these circumstances [69].

A NiO nanostructure was employed as a template and precursor for smart synthesis of a well-distributed porous MOF-based nickel oxide-composite electrode by Chen et al. in 2020 [70]. A two-step hydrothermal procedure was used, in which NiO was grafted onto CNF as a self-sacrificing template and precursor, and subsequently Ni-MOF was created by adding an organic linker (H3BTC). Under optimal reaction circumstances, the final electrode was made using a separate hydrothermal process. The NiO@Ni-MOF/NF electrode produced has a capacitive performance of 1853 C cm^{-2} at 1 m A cm^{-2}. The NiO@Ni-MOF/NF positive electrode and CNT negative electrode of the asymmetric supercapacitor produced energy and power densities of 39.2 W h kg^{-1} and 700 W kg^{-1}, respectively. Furthermore, after 3000 cycles, the electrode preserved a capacitance of 94 percent. This composition improved the electrode's conductivity and gave the MOF precursor a moderate orientation, which helped to shorten the transport channel and increase ion storage [70].

Shin et al. produced a new nickel oxide/carbon composite as a stand-alone electrode for a supercapacitor use in 2021 [71]. In that work, a Ni-MOF with a 1D structure was constructed on CNF and shown outstanding conductivity. As shown in Figure 2.6a, this was followed by direct heating at 400 oC for 1 hour in a N2 environment. The produced materials' surface morphology (as determined by FESEM and HRTEM) revealed that Ni-MOF was effectively developed on the CNF surface [71]. (See Figures 2.6b and 2.6c for further information.) It was also discovered that carbonizing the MOF precursor produced a nickel oxide-based electrode while maintaining the integrity of the MOF, with the exception of minor fissures in the electrode caused by evaporation

of the stacking solvent and framework disintegration [71]. (See Figure 2.6d for further information.) Fabrication of NiOs via the carbonization process was indicated when compared to the electrode without NiO (Figure 2.6f) and without pyrolysis (Figure 6g). With a specific capacitance of 742.2 Fg-1 and 67.1 Fg-1 at current densities of 1 and 10 Ag-1, respectively, the NiO/C@CNF electrode produced in 3 M KOH demonstrated exceptional rate capability. Furthermore, the asymmetric supercapacitor made from the electrode and AC had a high specific energy density of 58.43 Wh kg-1 and a high energy density of 1947 W kg-1, respectively, as well as good cycle stability [71]. The synergistic impact of NiO, which is well-distributed in the carbon matrix, together with the superior electrical conductivity of the CNF film, was contributed to the high performance of the constructed supercapacitor [71].

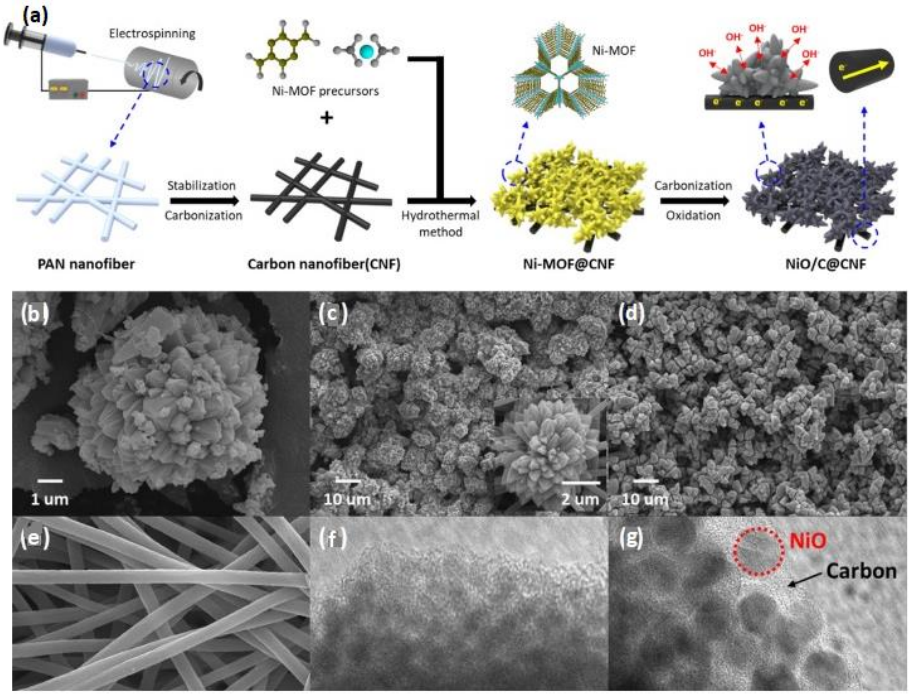

Figure 2.6 Preparation of NiO/C@CNF.
(a) Scheme showing the synthesis of NiO/C@CNF. FE-SEM images of: b) MOF precursor (Ni-MOF); c) NiMOF@CNF; d) NiO/C@CNF; e) CNF HRTEM images of f) MOF precursor @CNF; g) NiO/C@CNF.)
Source: Ref [71]

To ensure closeness between the transition metal oxide nanoparticle and the carbon-based material, it is critical to design a composite electrode in which the particle size of the zinc and nickel oxide microstructure stays tiny while enclosed in the carbon matrix. This will result in an

increase in conductivity, allowing the active areas of the electrode materials to be more easily exposed. Huo and his colleagues' work [72] is an example of this. They observed high electrochemical performance of NiO/C/rGO, which was dependent on pyrolysis of the MOF template on GO for size-control synthesis of NiO (2-3 nm) in a spherical carbon matrix supported by rGO [72]. The nickel oxide and carbon/electrolyte were able to make intimate contact because of the tiny particle size. The resulting carbon/rGO complex, on the other hand, can significantly improve the composite's cycle stability. Furthermore, although the composite electrode had great capacitive performance of about 496.0 Cg-1 at 1 Ag-1, the NiO/C/rGO/SCC HSC demonstrated exceptional energy and power density of 35.9 Wh kg1 and 749.1 W kg1, respectively [72]. After 3000 cycles, the specific capacitance remained around 120 percent of its initial value [72].

To conclude, the research findings discussed in this section have demonstrated that Zn and Ni-MOF are effective precursors for the fabrication of zinc and nickel oxide-composite materials, indicating that they are suitable electrodes for supercapacitor applications.

2.5.1 MOF-based zinc and nickel hydroxides

Even though the MOF hydrolyzing strategy may be limited by incomplete hydrolyzing - which can prevent the optimal performance of the composite electrode as a result of the residual MOFs - it is considered one of the best approaches for preparing transition metal hydroxide (otherwise known as binary metal oxide). It involves hydrolysis of MOFs and crystallization of the KOH solution. Other methods include hydrothermal synthesis [52]. While MOF-based $Ni(OH)_2$ composite electrodes have been reported on extensively, $Zn(OH)_2$ has rarely been used as the electrode material in HSCs. However, in one example, Yang et al. fabricated a $MoS_2/Ni(OH)_2$ composite by treating the MoS_2@Ni-MOF precursor with an alkali [73]. MoS_2 has a high sulfur content, onto which the $Ni(OH)_2$ from the MOF precursor was supported [73]. The composite electrodes have a sufficient amount of active sites, which facilitates the rapid transfer of electrons and redox to create room for efficient charge storage. Figure 2.7 shows that the composite electrode delivered good capacitive performance of close to 2192 Fg^{-1} at 1 Ag^{-1} [73]. The HSC fabricated with it displayed a high energy density of 50.58 $Wh.kg^{-1}$ at a power density of 800 W kg^{-1v} [73].

The morphology of nickel oxide electrodes can also impact the performance of electrochemical supercapacitors. Tang and his team investigated this by exploring the influence of

the different morphologies of $Ni(OH)_2$ fabricated from pristine MOF on the capacitive performance, and compared them using CV, GCD and EIS tests [74]. Sphere-like and sheet-like Ni-MOFs were synthesized via hydrothermal synthesis and used as self-sacrificing templates in the presence of KOH, in order to obtain $Ni(OH)_2$ with different morphologies. Electrochemical testing showed that the sphere-like nickel hydroxide exhibited a more significant energy storage capability, excellent rate stability and comparatively low resistance compared to the pristine material [74]. This was credited to the sphere morphology and the low crystallization structure, which produces more accessible areas and pores for electron transport within the electrolyte [74].

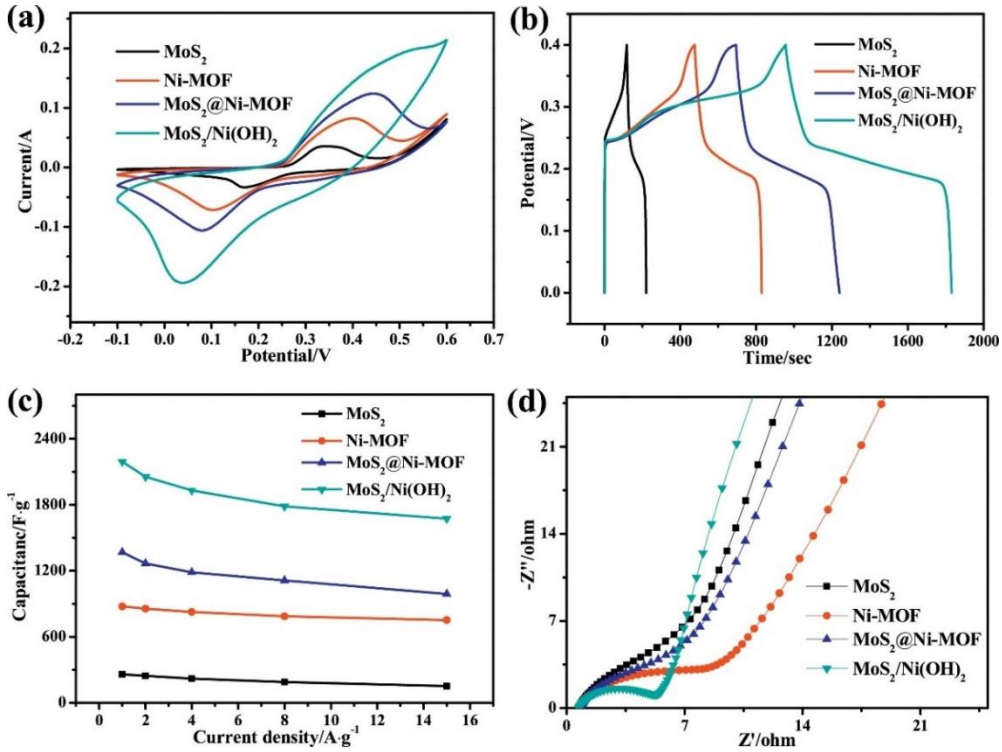

Figure 2.7 Supercapacitor performance of $MoS_2/Ni(OH)_2$ in an electrolyte solution (3M KOH). (a) CV curves at 50 mVs^{-1} scan rate; b) GCD curves at 1 Ag^{-1}; c) specific capacitance measured at different current densities; d) Nyquist plot between 0.01 Hz and 100 kHz.)

In summary, supercapacitor electrodes composed of transition metal hydroxides usually have poor cycling stability because of the intense volume effect during the charge-discharge cycle.

2.5.2 MOF-based mixed metallic Zn and Ni electrodes

Advancements with the mixed-metal approach for MOFs makes it possible for two dissimilar metal ions to be fused into an identical framework to deliver mixed-metal MOFs [75].

This confers structural stability on the resulting MOF-based electrodes and ultimately improves their electrochemical performance [75]. As the name implies, mixed metal MOFs consist of at least two different central metal ions. They are usually fabricated by incorporating the metal of interest into the ligand solution under moderate annealing conditions. However, they can also be prepared using the post-synthetic modification system. With this method, metal ions in single-metal MOFs are replaced with different, but suitable, metal ions when immersed in a concentrated solution of the target metal [76]. [77]. For instance, Wang and co-workers prepared a Ni-containing mixed metal oxide, $NiCo_2O_4$ nano/microstructures for supercapacitor application [78]. The hybrid metal oxide electrode with a flower-like shape delivered a specific capacitance of some 350 Cg^{-1} at 9 mg cm^{-2} and retained about 94% of its original value after 5000 cycles. This performance could be attributed to the unique structure that enhances the Faradaic reaction and ion transfer, while multiple metal oxides can narrow the bandgap and ultimately increase the conductivity [78].

In another example, Qiu and his team developed a new approach to synthesize Ni_xCo_3-xO_4, using MOF-74 as a template [79]. Five isostructural MOFs containing Ni, Co and a combination of both (in different ratios) were converted to derivative mixed metal oxides by calcination at 400 ^oC,, in order to investigate the impact of Ni and Co in the parent MOFs on overall capacitive performance. While the PXRD results validated the successful synthesis of all five oxides - Co_3O_4, NiO, $Ni_xCo_{3-x}O_4$ (1, 2 and 4) - the TEM images showed that they have a porous, coarse morphology and that the surface area (measured by N_2 adsorption-desorption isotherm at 77K) falls within the range of 64-117 m^2/g, which is higher than that seen with conventional metal oxides. Interestingly, the electrochemical performance (measured in terms of capacitance and cyclic stability) of the mixed metal oxides ($Ni_xCo_{3-x}O_4$) was higher than that of the monometallic oxides (NiO and Co_3O_4) derived from the same parent MOF. (See Figure 2.8.) Overall, the mixed metal oxide with Ni and Co in the ratio 1:1 displayed the best performance, with a specific capacitance of 797 F g^{-1} at a current density of 1 A g^{-1}. It is also evident that the M-MOFs exhibit a higher energy density than the monometallic electrode, as a result of their exceptional capacitance and lower resistance [79]. (See Figure 2.8.)

Similarly, zinc-containing mixed metal oxide, especially zinc cobaltite ($ZnCo_2O_4$), is also regarded as one of the best materials for supercapacitor applications, because of its superior electrical conductivity and richer redox, compared to a single metal oxide. For instance, in another

study done by the Qiu group, JCU-155 ($ZnCo_2O(BTC)_2(DMF).H_2O$) was employed as a template to fabricate $ZnCo_2O_4$ by calcining the pristine MOF at different temperatures (400, 450 and 500) [24]. The surface area of the fabricated electrode material decreased with an increase in the thermolysis temperature: 55.0, 45.9 and 20.4 cm^2, respectively, for the materials prepared at 400, 450 and 500 ^oC. The electrochemical performance of the $ZnCo_2O_4$ electrode (as measured by CV), revealed that the surface area has an impact on the capacitance behavior as the electrode material with the highest surface area exhibiting a specific capacitance of 451 Fg^{-1} at a scan rate of 5 mVs^{-1} and stability of 97.9% after 1500 cycles. The performance of selected Ni and Zn-based MOF electrode materials for supercapacitors is summarized in Table 2.2.

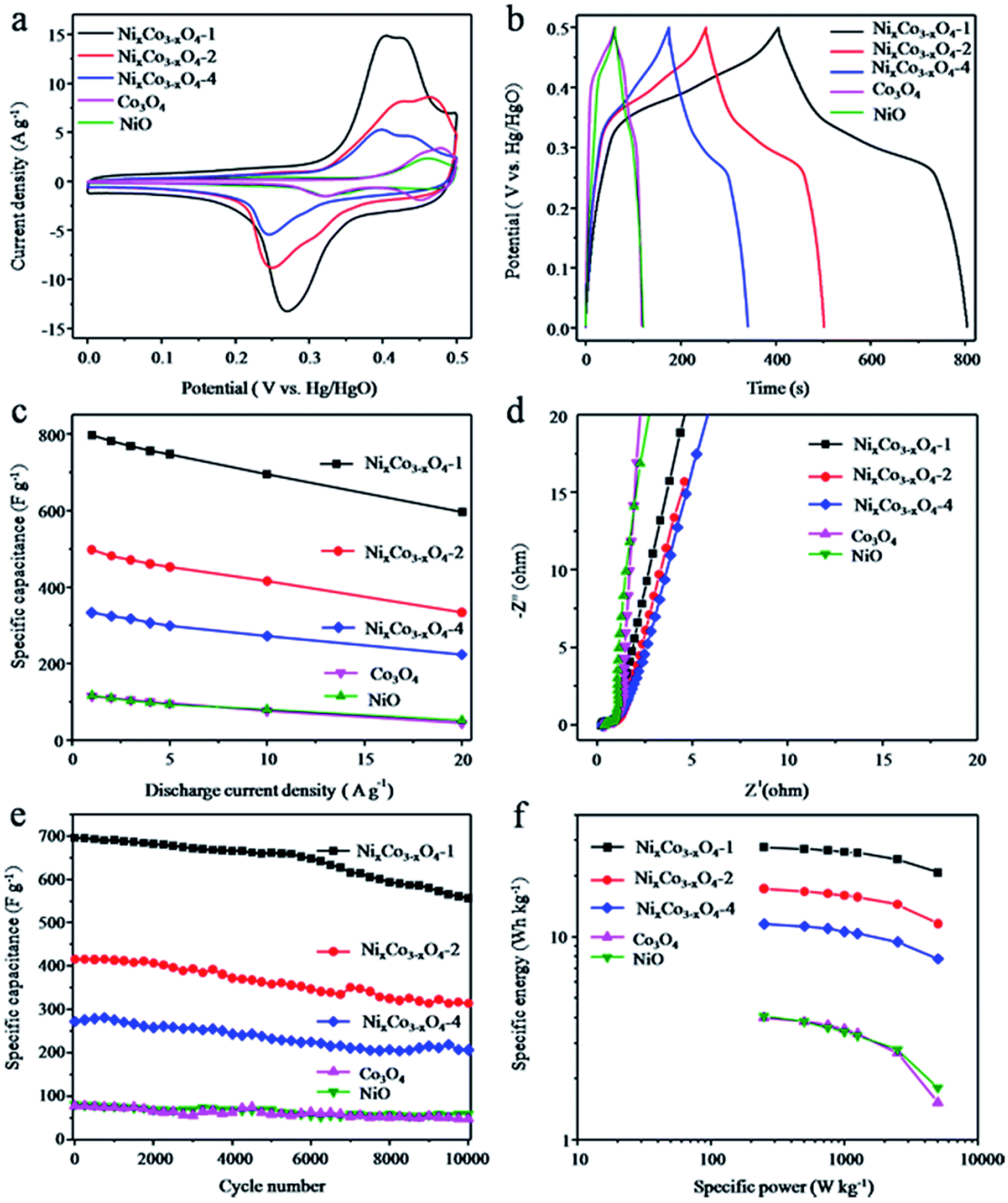

Figure 2.8 a) CV curves at 5 mVs^{-1} for the synthesized metal oxides and mixed metal oxides. (b) GCD at 1 Ag^{-1} for the metal oxides and mixed metal oxides. c) Specific capacitance for metal oxides and mixed metal oxides. d) EIS measurement in the range of 0.01 to 10^5 Hz for metal oxides and mixed metal oxides. e) Cycling stability at 10,000 cycles at 10 Ag^{-1} for metal oxides and mixed metal oxides. f) Ragos plots for metal oxides and mixed metal oxides.

Table 2.2: Storage capability of selected MOF-derived Ni and Zn-based electrodes in SCs.

MOF precursor	MOF-based electrode	Morphology	Specific surface area (m^2/g)	Electrolyte	Capacitance	Current density	Ref.
Ni-MOF	NiO	Nanospheres	66.8	3 M KOH	473 F g^{-1}	0.5 A g^{-1}	[80]
Ni-MOF	NiOx@NPC	Plate-like	1523	6 M KOH	581.3 Fg^{-1}	1 Ag^{-1}	[81]
Ni-ZnBTC	NiO/C	Fibrous	598	6 M KOH	14,926 F g^{-1}	0.25 A g^{-1}	[82]
Ni-MOF	NiO/C@CNF	Flower-like	446.98	3 M KOH	742 Fg^{-1}	1 Ag^{-1}	[71]
Ni-MOF	Ni(OH)2	Sphere-like	131.92	3 M KOH	982 Fg^{-1}	1 Ag^{-1}	[74]
Ni-MOF	$Ni(OH)_2$–MnO_2@CNi($OH)_2$–MnO_2@C	Nanosheet	204.1	1 M KOH	965.1 C g^{-1}	2 mA cm^{-2}	[83]
Ni-MOF	Ni(OH)x	Nanorod	186.8	6 M KOH	1698 F g^{-1}	1 A g^{-1}	[84]
Ni-MOF	$Ni(OH)_2$/MoS_2	NA	49.3	3M KOH	2192 $F.g^{-1}$	1 A g^{-1}	[85]
MOF-74(Ni)	$Ni_xCo_{3-x}O_{4-1}$	Ball-like (coarse)	92	6 M KOG	797 F g^{-1}	1 A g^{-1}	[79]
ZIF-67	$NiCo_2O_4$	Polyhedron	43.2	6M KOH	956 F g^{-1}	1 A g^{-1}	[78]

Co-ZIF/Ni	$Ni_xCo_{3-x}O_4$/rGO	Nanosheet	5.6	2 M KOH	102.13 F g^{-1}	1 A g^{-1}	[86]
ZIF-67	$NiCo_2O_4/Co_3O_4$	Nanoflakes	33.8	6 M KOH	1046 F g^{-}	1 A g^{-1}	[87]
ZIF-67	$Ni_xCo_{3-x}O_4$/CNTs	Nanocage	NA	2 M KOH	668 F/g	at 1 A g^{-1}	[88]
ZIF-8	ZnO@C@$NiCo_2O_4$	Nanosheet	NA	2 M KOH	2650 F g^{-1}	5 A g^{-1}	[89]
IF-Zn	ZnO@MOF@PANI	Nanoarrays	NA	3.0 M KCl	340.7 F g^{-1}	1.0 A g^{-1}	[90]
JUCC-155	$ZnCo_2O_4$	Quadrangular rod shape	55	6 M KOH	451 Fg-1	1 Ag-1	[24]
ZIF-8@ZIF-67	ZnO/Co_3O_4/NiO	Polyhedral	101.72	2 M KOH	1119.11 C g^{-1}	1 A g^{-1}	[91]
MOF-74(Zn)	ZnO-C	Rod-like	782.971		197.84 F /g	1 A g^{-1}	[63]
ZIF-8	PANI/ZnO@ZIF-8-CC	NA	1856	3 M KCl	3987 C/g	30 mA cm^2	[64]
Mixed Zn MOFs	$ZnMn_2O_4$/carbon	Nanorod	143.4	1 M Na_2SO_4	589 F g^{-1}	1 A g^{-1}	[92]

2.6 Conclusion

Transition metal-based MOFs and their composite materials have revolutionized the field of renewable and sustainable energy technologies. They have confirmed their potential as a good electrode candidate for energy storage applications, because they evidence several features seen in the parent MOFs, including a well-designed structural composition, large specific surface area, tunable porosity and bi-functionality.

This chapter provided a discussion of the potential of Ni and Zn-containing MOFs as useful templates and self-sacrificing precursors for the design of corresponding electrode materials (including oxides, hydroxides and mixed metal oxides). A summary of their application in SCs was also provided. Notably, MOF-based Zn and Ni-based electrodes can be fabricated via different routes, i.e. etching, annealing and hydrolyzing methods. While the annealing approach is a facile method used to ensure high-performance electrode materials for SC applications, the structural integrity of the resultant MOF may be threatened at a high temperature, which may compromise the electrode characteristics and so limit their storage performance. The etching process is good for preparing hollow-structured electrode materials, as it ensures an abundance of active sites on the fabricated materials, which are accessible to the electrolyte ions and enhance their SC performance. However, it may be limited by the high cost of MOF materials.

The MOF-hydrolyzing strategy is another important strategy that can be used to improve the supercapacitor performance of MOFs. It is unique in the sense that it allows the costly organic ligands to be recycled, and also supports large-scale synthesis of the electrode materials. However, the residual MOFs that emanate from incomplete hydrolysis of MOFs may be detrimental to the storage performance and cyclic stability of the resulting MOF-based electrodes.

The transformation of pristine Ni and Zn-based MOFs into derivative oxides, hydroxides and mixed-metal electrodes has been shown to deliver excellent specific capacitance and superior cycling stability. This can be ascribed to the high conductivity and the large specific surface area, which can facilitate fast migration of the electrolyte ions and increase the redox reaction. The performance of these materials can be improved further by grafting them onto electrically conductive materials, including carbon-based materials (CNTs, CNF, rGO and graphene) that have specific dimensions. However, it is crucial that the particle size of the composite electrode is kept small when modified with carbon materials, to ensure close proximity between the electrode materials containing Ni or Zn oxides and the conductive carbon substrate. Additionally, the morphology of the final composite also has a role to play in terms of the capacitive performance as electrode materials, since the unique morphology of these electrodes can help to shorten the pathways for the migration of electrolyte ions, enhance surface redox reactions and effectively improve the reaction kinetics.

Because of the low electrical conductivity and intense volume expansion associated with monometallic nickel and zinc oxides/hydroxides, researchers have also developed mixed-metal oxides containing nickel and zinc ions to improve their performance by exploring synergistic effects of the individual components. The superior electrical conductivity and richer redox sites confer on these materials a remarkably higher performance in terms of specific capacitance, energy/power density and cycling stability. It is equally important to note that incorporation of S^{2-} from MoS_2 or NiS_2 into the O^{2-} site can enhance the conductivity and capacitive performance.

Despite the considerable success recorded in terms of improving supercapacitor performance, some challenges with MOF-derived Zn and based electrodes still persist. One is the low cyclic stability experienced with some MOF-based metal oxides and a contrary trend in others. A clear grasp of the design mechanism, crystal growth and judicious selection of the MOF-precursors will help to improve electrochemical performance. Furthermore, the inadequate capacitance of MOF-based electrodes usually produces a low energy density in the supercapacitor. However, this can be remediated by modifying the surface characteristics, including particle size, to improve the wettability of the electrode to the electrolyte, which ensures superior energy density in the electrolyte. Last, but not least, the high cost of MOFs is another challenge that may limit their use in supercapacitor applications. Even though the MOF-hydrolyzing strategy offers great promise in this regard, research efforts have to be intensified to meet the requirements for industrial applications.

References

[1] A. M. Omer, "Energy, environment and sustainable development," *Renewable and Sustainable Energy Reviews*. 2008, doi: 10.1016/j.rser.2007.05.001.

[2] A. Du Pasquier, I. Plitz, S. Menocal, and G. Amatucci, "A comparative study of Li-ion battery, supercapacitor and nonaqueous asymmetric hybrid devices for automotive applications," *J. Power Sources*, 2003, doi: 10.1016/S0378-7753(02)00718-8.

[3] G. Yu *et al.*, "Enhancing the supercapacitor performance of graphene/MnO2 nanostructured electrodes by conductive wrapping," *Nano Lett.*, 2011, doi: 10.1021/nl2026635.

[4] M. Hadartz and M. Julander, "Battery-supercapacitor energy storage, Gothenburg,

Sweden: Chalmers University of Technology, (2008).

[5] T. Ma, H. Yang, and L. Lu, “Development of hybrid battery-supercapacitor energy storage for remote area renewable energy systems,” *Appl. Energy*, 2015, doi: 10.1016/j.apenergy.2014.12.008.

[6] M. Jayalakshmi and K. Balasubramanian, “Simple capacitors to supercapacitors - An overview,” *International Journal of Electrochemical Science*. 2008.

[7] J. Yan, Q. Wang, T. Wei, and Z. Fan, “Recent advances in design and fabrication of electrochemical supercapacitors with high energy densities,” *Adv. Energy Mater.*, 2014, doi: 10.1002/aenm.201300816.

[8] S. Zhang and N. Pan, “Supercapacitors performance evaluation,” *Advanced Energy Materials*. 2015, doi: 10.1002/aenm.201401401.

[9] R. Kötz and M. Carlen, “Principles and applications of electrochemical capacitors,” *Electrochim. Acta*, 2000, doi: 10.1016/S0013-4686(00)00354-6.

[10] Q. Zhang, E. Uchaker, S. L. Candelaria, and G. Cao, “Nanomaterials for energy conversion and storage,” *Chem. Soc. Rev.*, 2013, doi: 10.1039/c3cs00009e.

[11] Z. Lin *et al.*, “Materials for supercapacitors: When Li-ion battery power is not enough,” *Materials Today*. 2018, doi: 10.1016/j.mattod.2018.01.035.

[12] P. E. Lokhande, U. S. Chavan, and A. Pandey, “Materials and fabrication methods for electrochemical supercapacitors: Overview,” *Electrochem. Energy Rev.*, 2020, doi: 10.1007/s41918-019-00057-z.

[13] L. Chang and Y. Hang Hu, “Supercapacitors,” in *Comprehensive Energy Systems*, 2018.

[14] A. G. Pandolfo and A. F. Hollenkamp, “Carbon properties and their role in supercapacitors,” *Journal of Power Sources*. 2006, doi: 10.1016/j.jpowsour.2006.02.065.

[15] B. Chen, Y. Lü, K. Chen, Z. Sha, X. Liu, and Y. Liu, “Research progress of solid-state supercapacitors electrolytes and its classifications,” *Gaodianya Jishu/High Voltage Engineering*. 2019, doi: 10.13336/j.1003-6520.hve.20181205014.

[16] C. Lekakou, O. Moudam, F. Markoulidis, T. Andrews, J. F. Watts, and G. T. Reed,

"Carbon-based fibrous EDLC capacitors and supercapacitors," *J. Nanotechnol.*, 2011, doi: 10.1155/2011/409382.

[17] Z. Zhou and X. F. Wu, "High-performance porous electrodes for pseudosupercapacitors based on graphene-beaded carbon nanofibers surface-coated with nanostructured conducting polymers," *J. Power Sources*, 2014, doi: 10.1016/j.jpowsour.2014.03.096.

[18] H. Furukawa, K. E. Cordova, M. O'Keeffe, and O. M. Yaghi, "The chemistry and applications of metal-organic frameworks," *Science*. 2013, doi: 10.1126/science.1230444.

[19] L. Wang, Y. Han, X. Feng, J. Zhou, P. Qi, and B. Wang, "Metal-organic frameworks for energy storage: Batteries and supercapacitors," *Coordination Chemistry Reviews*, vol. 307. Elsevier B.V., pp.361–381, Jan. 15, 2016, doi: 10.1016/j.ccr.2015.09.002.

[20] A. Morozan and F. Jaouen, "Metal organic frameworks for electrochemical applications," *Energy and Environmental Science*. 2012, doi: 10.1039/c2ee22989g.

[21] F. S. Ke, Y. S. Wu, and H. Deng, "Metal-organic frameworks for lithium ion batteries and supercapacitors," *J. Solid State Chem.*, 2015, doi: 10.1016/j.jssc.2014.07.008.

[22] Y. Zhao, J. Liu, M. Horn, N. Motta, M. Hu, and Y. Li, "Recent advancements in metal organic framework based electrodes for supercapacitors," *Science China Materials*. 2018, doi: 10.1007/s40843-017-9153-x.

[23] Y. Liang, W. Yao, J. Duan, M. Chu, S. Sun, and X. Li, "Nickel cobalt bimetallic metal-organic frameworks with a layer-and-channel structure for high-performance supercapacitors," *J. Energy Storage*, 2021, doi: 10.1016/j.est.2020.102149.

[24] S. Chen *et al.*, "Porous ZnCo2O4 nanoparticles derived from a new mixed-metal organic framework for supercapacitors," *Inorg. Chem. Front.*, 2015, doi: 10.1039/c4qi00167b.

[25] W. Chu, Y. Hou, J. Liu, X. Bai, Y. Fang Gao, and Z. Cao, "Zn-Co phosphide porous nanosheets derived from metal-organic-frameworks as battery-type positive electrodes for high-performance alkaline supercapacitors," *Electrochim. Acta*, 2020, doi: 10.1016/j.electacta.2020.137063.

[26] Y. Zhang *et al.*, "Progress of electrochemical capacitor electrode materials: A review,"

International Journal of Hydrogen Energy. 2009, doi: 10.1016/j.ijhydene.2009.04.005.

[27] Y. Zhao *et al.*, "Metal organic frameworks for energy storage and conversion," *Energy Storage Materials*. 2016, doi: 10.1016/j.ensm.2015.11.005.

[28] R. Zhao, Z. Liang, R. Zou, and Q. Xu, "Metal-organic frameworks for batteries," *Joule*. 2018, doi: 10.1016/j.joule.2018.09.019.

[29] X. Li, X. Yang, H. Xue, H. Pang, and Q. Xu, "Metal–organic frameworks as a platform for clean energy applications," *EnergyChem*, 2020, doi: 10.1016/j.enchem.2020.100027.

[30] P. Simon and Y. Gogotsi, "Materials for electrochemical capacitors," *Nature Materials*. 2008, doi: 10.1038/nmat2297.

[31] H. X. Yang *et al.*, "Nickel nanoparticles incorporated into N-doped porous carbon derived from N-containing nickel-MOF for high-performance supercapacitors," *J. Alloys Compd.*, 2019, doi: 10.1016/j.jallcom.2018.12.259.

[32] C. Qu *et al.*, "Nickel-based pillared MOFs for high-performance supercapacitors: Design, synthesis and stability study," *Nano Energy*, 2016, doi: 10.1016/j.nanoen.2016.04.003.

[33] K. S. Park *et al.*, "Exceptional chemical and thermal stability of zeolitic imidazolate frameworks," *Proc. Natl. Acad. Sci. U. S. A.*, 2006, doi: 10.1073/pnas.0602439103.

[34] R. Díaz, M. G. Orcajo, J. A. Botas, G. Calleja, and J. Palma, "Co8-MOF-5 as electrode for supercapacitors," *Mater. Lett.*, 2012, doi: 10.1016/j.matlet.2011.10.046.

[35] Z. Liang, C. Qu, W. Guo, R. Zou, and Q. Xu, "Pristine metal–organic frameworks and their composites for energy storage and conversion," *Advanced Materials*. 2018, doi: 10.1002/adma.201702891.

[36] S. Sundriyal, H. Kaur, S. K. Bhardwaj, S. Mishra, K. H. Kim, and A. Deep, "Metal-organic frameworks and their composites as efficient electrodes for supercapacitor applications," *Coordination Chemistry Reviews*. 2018, doi: 10.1016/j.ccr.2018.04.018.

[37] M. Xue *et al.*, "Microfluidic etching for fabrication of flexible and all-solid-state micro supercapacitor based on MnO2 nanoparticles," *Nanoscale*, 2011, doi: 10.1039/c0nr00990c.

[38] F. X. Ma, L. Yu, C. Y. Xu, and X. W. Lou, “Self-supported formation of hierarchical NiCo2O4 tetragonal microtubes with enhanced electrochemical properties,” *Energy Environ. Sci.*, 2016, doi: 10.1039/c5ee03772g.

[39] K. Wang, H. Wu, Y. Meng, and Z. Wei, “Conducting polymer nanowire arrays for high performance supercapacitors,” *Small*. 2014, doi: 10.1002/smll.201301991.

[40] D. W. Wang, F. Li, Z. G. Chen, G. Q. Lu, and H. M. Cheng, “Synthesis and electrochemical property of boron-doped mesoporous carbon in supercapacitor,” *Chem. Mater.*, 2008, doi: 10.1021/cm801729y.

[41] P. Zhong *et al.*, “Annealing temperature–dependent electronic properties in hydrothermal TiO2 nanorod arrays,” *J. Solid State Electrochem.*, 2018, doi: 10.1007/s10008-017-3786-x.

[42] S. Wu, J. Liu, H. Wang, and H. Yan, “A review of performance optimization of MOF-derived metal oxide as electrode materials for supercapacitors,” *International Journal of Energy Research*. 2019, doi: 10.1002/er.4232.

[43] B. R. Wang, Y. Hu, Z. Pan, and J. Wang, “MOF-derived manganese oxide/carbon nanocomposites with raised capacitance for stable asymmetric supercapacitor,” *RSC Adv.*, 2020, doi: 10.1039/d0ra05494a.

[44] B. P. Reddy, K. Mallikarjuna, M. Kumar, M. C. Sekhar, Y. Suh, and S. H. Park, “Highly porous metal organic framework derived NiO hollow spheres and flowers for oxygen evolution reaction and supercapacitors,” *Ceram. Int.*, 2021, doi: 10.1016/j.ceramint.2020.09.172.

[45] X. Li, M. Zhang, L. Wu, Q. Fu, and H. Gao, “Annealing temperature dependent ZnCo2O4 nanosheet arrays supported on Ni foam for high-performance asymmetric supercapacitor,” *J. Alloys Compd.*, 2019, doi: 10.1016/j.jallcom.2018.09.197.

[46] M. H. Ervin, “Etching holes in graphene supercapacitor electrodes for faster performance,” *Nanotechnology*, 2015, doi: 10.1088/0957-4484/26/23/234003.

[47] Y. Wang *et al.*, “ZIF-8@MWCNT-derived carbon composite as electrode of high performance for supercapacitor,” *Electrochim. Acta*, 2016, doi:

10.1016/j.electacta.2016.07.019.

[48] S. Wang *et al.*, “Phototherapy: Metal-organic-framework-derived mesoporous carbon nanospheres containing porphyrin-like metal centers for conformal phototherapy (Adv. Mater. 38/2016),” *Adv. Mater.*, 2016, doi: 10.1002/adma.201670266.

[49] X. Deng, J. Li, S. Zhu, L. Ma, and N. Zhao, “Boosting the capacitive storage performance of MOF-derived carbon frameworks via structural modulation for supercapacitors,” *Energy Storage Mater.*, 2019, doi: 10.1016/j.ensm.2019.04.015.

[50] B. Xu, H. Zhang, H. Mei, and D. Sun, “Recent progress in metal-organic framework-based supercapacitor electrode materials,” *Coordination Chemistry Reviews*. 2020, doi: 10.1016/j.ccr.2020.213438.

[51] X. Xue *et al.*, “Hydrolysis of metal-organic framework towards three-dimensional nickel cobalt-layered double hydroxide for high performance supercapacitors,” *J. Energy Storage*, 2020, doi: 10.1016/j.est.2020.101649.

[52] Z. Xiao *et al.*, “Controlled hydrolysis of metal-organic frameworks: Hierarchical Ni/Co-layered double hydroxide microspheres for high-performance supercapacitors,” *ACS Nano*, 2019, doi: 10.1021/acsnano.9b02106.

[53] S. Zhang *et al.*, “Temperature controlled diffusion of hydroxide ions in 1D channels of Ni-MOF-74 for its complete conformal hydrolysis to hierarchical Ni(OH)2 supercapacitor electrodes,” *Nanoscale*, 2019, doi: 10.1039/c9nr02555c.

[54] H. Zhang *et al.*, “‘Hot’ alkaline hydrolysis of amorphous MOF microspheres to produce ultrastable bimetal hydroxide electrode with boosted cycling stability,” *Small*, 2019, doi: 10.1002/smll.201904663.

[55] A. Venkataraman, “Pseudocapacitors for energy storage,” *Pseudocapacitors for Energy Storage*, 2015, (Doctoral dissertation, Portland State University).

[56] F. Béguin and E. Frackowiak, *Supercapacitors: Materials, Systems, and Applications*. 2013, Poznan: Wiley-VCH Verlag GmbH & Co.

[57] Bakker, M.G., Frazier, R.M., Burkett, S., Bara, J.E., Chopra, N., Spear, S., Pan, S. and Xu,

C., 2012. Perspectives on supercapacitors, pseudocapacitors and batteries. *Nanomaterials and Energy*, *1*(3), pp.136-158.

[58] Q. Lu, J. G. Chen, and J. Q. Xiao, "Nanostructured electrodes for high-performance pseudocapacitors," *Angew. Chemie - Int. Ed.*, 2013, doi: 10.1002/anie.201203201.

[59] M. Selvakumar, D. Krishna Bhat, A. Manish Aggarwal, S. Prahladh Iyer, and G. Sravani, "Nano ZnO-activated carbon composite electrodes for supercapacitors," *Phys. B Condens. Matter*, 2010, doi: 10.1016/j.physb.2010.02.028.

[60] Y. Zhang *et al.*, "Carbon nanotube-ZnO nanocomposite electrodes for supercapacitors," *Solid State Ionics*, 2009, doi: 10.1016/j.ssi.2009.10.001.

[61] J. Xu, S. Liu, and Y. Liu, "Co3O4/ZnO nanoheterostructure derived from core-shell ZIF-8@ZIF-67 for supercapacitors," *RSC Adv.*, 2016, doi: 10.1039/c6ra07773k.

[62] Y. Zhang, H. Li, L. Pan, T. Lu, and Z. Sun, "Capacitive behavior of graphene-ZnO composite film for supercapacitors," *J. Electroanal. Chem.*, 2009, doi: 10.1016/j.jelechem.2009.07.010.

[63] L. Wang *et al.*, "Multifunctional ZnO-porous carbon composites derived from MOF-74(Zn) with ultrafast pollutant adsorption capacity and supercapacitance properties," *J. Colloid Interface Sci.*, 2019, doi: 10.1016/j.jcis.2019.07.015.

[64] X. M. Cao and Z. B. Han, "Hollow core-shell ZnO@ZIF-8 on carbon cloth for flexible supercapacitors with ultrahigh areal capacitance," *Chem. Commun.*, 2019, doi: 10.1039/c8cc09847f.

[65] H. Xiao, S. Yao, H. Liu, F. Qu, X. Zhang, and X. Wu, "NiO nanosheet assembles for supercapacitor electrode materials," *Prog. Nat. Sci. Mater. Int.*, 2016, doi: 10.1016/j.pnsc.2016.05.007.

[66] J. Y. Lee, K. Liang, K. H. An, and Y. H. Lee, "Nickel oxide/carbon nanotubes nanocomposite for electrochemical capacitance," *Synth. Met.*, 2005, doi: 10.1016/j.synthmet.2005.01.016.

[67] S. Wu, K. S. Hui, K. N. Hui, and K. H. Kim, "Correction: Ultrathin porous NiO nanoflake

arrays on nickel foam as an advanced electrode for high performance asymmetric supercapacitors," *J. Mater. Chem. A*, 2016, doi: 10.1039/c6ta90113a.

[68] B. Zhao *et al.*, "Monolayer graphene/NiO nanosheets with two-dimension structure for supercapacitors," *J. Mater. Chem.*, 2011, doi: 10.1039/c1jm13016a.

[69] J. Yan *et al.*, "Preparation of graphene nanosheet/carbon nanotube/polyaniline composite as electrode material for supercapacitors," *J. Power Sources*, 2010, doi: 10.1016/j.jpowsour.2009.11.028.

[70] S. Xiong *et al.*, "A high-performance hybrid supercapacitor with NiO derived NiO@Ni-MOF composite electrodes," *Electrochim. Acta*, 2020, doi: 10.1016/j.electacta.2020.135956.

[71] S. Shin and M. W. Shin, "Nickel metal–organic framework (Ni-MOF) derived NiO/C@CNF composite for the application of high performance self-standing supercapacitor electrode," *Appl. Surf. Sci.*, 2021, doi: 10.1016/j.apsusc.2020.148295.

[72] Z. Zhang *et al.*, "Ni-MOF derived NiO/C nanospheres grown in situ on reduced graphene oxide towards high performance hybrid supercapacitor," *J. Alloys Compd.*, 2019, doi: 10.1016/j.jallcom.2019.06.073.

[73] L. Yue *et al.*, "Ni-MOF coating MoS_2 structures by hydrothermal intercalation as high-performance electrodes for asymmetric supercapacitors," *Chem. Eng. J.*, 2019, doi: 10.1016/j.cej.2019.121959.

[74] Q. Tang, L. Ma, F. Cao, M. Gan, and F. Yan, "Different morphologies of Ni(OH) 2 derived from a MOF template for high performance supercapacitors," *J. Mater. Sci. Mater. Electron.*, 2019, doi: 10.1007/s10854-019-01240-0.

[75] W. H. Low, P. S. Khiew, S. S. Lim, C. W. Siong, and E. R. Ezeigwe, "Recent development of mixed transition metal oxide and graphene/mixed transition metal oxide based hybrid nanostructures for advanced supercapacitors," *Journal of Alloys and Compounds*. 2019, doi: 10.1016/j.jallcom.2018.10.102.

[76] F. Shi, L. Li, X. L. Wang, C. D. Gu, and J. P. Tu, "Metal oxide/hydroxide-based materials for supercapacitors," *RSC Advances*. 2014, doi: 10.1039/c4ra06136e.

[77] R. R. Salunkhe, Y. V. Kaneti, and Y. Yamauchi, “Metal-organic framework-derived nanoporous metal oxides toward supercapacitor applications: Progress and prospects,” *ACS Nano*. 2017, doi: 10.1021/acsnano.7b02796.

[78] Y. Liu, Z. Wang, Y. Zhong, M. Tade, W. Zhou, and Z. Shao, “Molecular design of mesoporous NiCo2O4 and NiCo2S4 with sub-micrometer-polyhedron architectures for efficient pseudocapacitive energy storage,” *Adv. Funct. Mater.*, 2017, doi: 10.1002/adfm.201701229.

[79] S. Chen, M. Xue, Y. Li, Y. Pan, L. Zhu, and S. Qiu, “Rational design and synthesis of NixCo3-xO4 nanoparticles derived from multivariate MOF-74 for supercapacitors,” *J. Mater. Chem. A*, 2015, doi: 10.1039/c5ta02557e.

[80] M. K. Wu, C. Chen, J. J. Zhou, F. Y. Yi, K. Tao, and L. Han, “MOF–derived hollow double–shelled NiO nanospheres for high–performance supercapacitors,” *J. Alloys Compd.*, 2018, doi: 10.1016/j.jallcom.2017.10.171.

[81] A. M. Al-Enizi *et al.*, “Synthesis of NiOx@NPC composite for high-performance supercapacitor via waste PET plastic-derived Ni-MOF,” *Compos. Part B Eng.*, 2020, doi: 10.1016/j.compositesb.2019.107655.

[82] Y. Yang *et al.*, “Dilute NiO/carbon nanofiber composites derived from metal organic framework fibers as electrode materials for supercapacitors,” *Chem. Eng. J.*, 2017, doi: 10.1016/j.cej.2016.08.132.

[83] J. Li *et al.*, “Hierarchically nanostructured Ni(OH)2–MnO2@C ternary composites derived from Ni-MOFs grown on nickel foam as high-performance integrated electrodes for hybrid supercapacitors,” *Electrochim. Acta*, 2020, doi: 10.1016/j.electacta.2020.136139.

[84] J. Xu, C. Yang, Y. Xue, C. Wang, J. Cao, and Z. Chen, “Facile synthesis of novel metal-organic nickel hydroxide nanorods for high performance supercapacitor,” *Electrochim. Acta*, 2016, doi: 10.1016/j.electacta.2016.06.090.

[85] W. Yang *et al.*, “MoS2/Ni(OH)2 composites derived from in situ grown Ni-MOF coating MoS2 as electrode materials for supercapacitor and electrochemical sensor,” *Colloids*

Surfaces A Physicochem. Eng. Asp., vol. 615, no. January, p.126178, 2021, doi: 10.1016/j.colsurfa.2021.126178.

[86] B. Xue, K. Li, Y. Guo, J. Lu, S. Gu, and L. Zhang, "Construction of zeolitic imidazolate frameworks-derived NixCo3−xO4/reduced graphene oxides/Ni foam for enhanced energy storage performance," *J. Colloid Interface Sci.*, 2019, doi: 10.1016/j.jcis.2019.09.005.

[87] D. Yu, B. Wu, L. Ge, L. Wu, H. Wang, and T. Xu, "Decorating nanoporous ZIF-67-derived NiCo2O4 shells on a Co3O4 nanowire array core for battery-type electrodes with enhanced energy storage performance," *J. Mater. Chem. A*, 2016, doi: 10.1039/c6ta04286d.

[88] B. Xue, K. Li, S. Gu, and J. Lu, "Zeolitic imidazolate frameworks (ZIFs)-derived NixCo3−xO4/CNTs nanocomposites with enhanced electrochemical performance for supercapacitor," *J. Colloid Interface Sci.*, 2018, doi: 10.1016/j.jcis.2018.06.077.

[89] W. Zeng *et al.*, "Metal-organic-framework-derived ZnO@C@NiCo2O4 core-shell structures as an advanced electrode for high-performance supercapacitors," *J. Mater. Chem. A*, 2016, doi: 10.1039/c6ta01510g.

[90] C. Zhu, Y. He, Y. Liu, N. Kazantseva, P. Saha, and Q. Cheng, "ZnO@MOF@PANI core-shell nanoarrays on carbon cloth for high-performance supercapacitor electrodes," *J. Energy Chem.*, 2019, doi: 10.1016/j.jechem.2018.11.006.

[91] L. Zhu, C. Hao, S. Zhou, X. Wang, T. Zhou, and Y. Guo, "Ternary ZnO/Co3O4/NiO inherited layered core-shell structure from a double template for high performance supercapacitor," *J. Mater.*, 2021, doi: 10.1016/j.jmat.2021.01.003.

[92] Z. Zhu, Z. Wang, Z. Yan, R. Zhou, Z. Wang, and C. Chen, "Facile synthesis of MOF-derived porous spinel zinc manganese oxide/carbon nanorods hybrid materials for supercapacitor application," *Ceram. Int.*, 2018, doi: 10.1016/j.ceramint.2018.07.310.

Chapter 3: Synthesis and application of flexible supercapacitors based on nanocomposites of MOFs

Abstract

Flexible supercapacitors are promising energy storage devices that could meet the growing demand for the next generation of flexible, wearable and portable electronic products. They offer several benefits, such as flexibility, a small size and high power density. However, the major drawback limiting large-scale use of supercapacitors is low energy density. Metal-organic frameworks (MOFs) have the potential to overcome this problem and have received considerable attention recently owing to their diverse structure and unique physicochemical property. The capacitance and rate performance of pristine MOFs can be limited by poor electrical conductivity, and low thermal and chemical stability. However, this can be resolved by fabricating MOF-based nanocomposites that contain electrically conductive components and have good stability.

This chapter provides an overview of recent advances in flexible supercapacitor electrode materials based on MOF nanocomposites and presents them in categories. First, the most popular pathways to synthesize MOF-based electrode materials and the quintessential design strategies for flexible supercapacitor devices are summarized and discussed. Second, the effects of the nanocomposite components on the performance of flexible supercapacitors is detailed, since there is a nexus between the structural composition of the electrode materials and the capacitive storage performance. The chapter concludes with a brief discussion of the possible research that could advance this emerging field. It is expected that this chapter will help researchers and industry make informed decisions concerning smart designs for flexible supercapacitor devices using MOF nanocomposites.

Keywords: Flexible supercapacitors, energy storage, MOFs, nanocomposites, energy density.

3.1 Introduction

The continuous depletion of the world's fossil fuel reserves and the associated environmental challenges have necessitated a search for clean and sustainable alternative energy sources [1]. The need to ensure that these resources satisfy both immediate and future needs has prompted a surge in demand for efficient energy storage systems.

Technological advancements have increased the demand for portable and wearable devices, which have become an integral part of life in the 21st century [2-3]. Supercapacitors (SCs) are emerging energy storage devices that are renowned for their high power density, long life span, excellent stability and quick charge-discharge rate [4]. Depending on the storage mechanism, supercapacitors can be categorized into electric double-layer capacitors (EDLCs), pseudocapacitors and hybrid supercapacitors (HSCs) [5]. While EDLC stores energy electrostatically, pseudocapacitors store energy by means of the Faradaic redox process. The third category (HSC) uses both these mechanisms [6].

The electrode material influences the preferred storage mechanism and, by extension, the performance of the SC. Although supercapacitors have gone through considerable transformation in the last few decades, their low energy density remains a significant drawback that limits their use in industrial-scale applications [7]. For example, carbon-based electrodes can barely meet the high energy density requirements; therefore, it is essential to fabricate flexible supercapacitor electrodes with an exceptional energy storage capacity.

Flexible SCs are characterized by being lightweight and eco-friendly, require a simple fabrication process, and offer outstanding mechanical flexibility and good tolerance to being folded or anchored on any surface. All of this means they are an excellent source of power for use in wearable electronics [8-9]. In order for flexible SCs to offer high storage performance, all their components must provide a high degree of flexibility. One of the ways to accomplish this is to employ flexible substrates as current collectors, e.g. carbon cloth (CC), carbon nanofibers, metal foils and wire [10]. Another approach to achieving flexibility in SCs is to develop binder-free electrode film to replace polymer-based binders, and so reduce their weight and thereby improve their performance [11]. The use of gel polymer-based electrolytes instead of aqueous-based electrolytes would also ensure that separators are eliminated, which would mean that ions are

transported more quickly [12]. These approaches geared towards attaining high flexibility in SCs must be optimized, in order to achieve high-energy, high-power density and long cycling stability. Examples of materials that exhibit remarkable physicochemical properties for use as flexible SCs include carbon-based nanomaterials such as graphene and carbon nanotubes (CNTs), as well as conductive polymers and metal oxides (ZnO, MnO_2, V_2O_5, TiO_2, etc.) [13-15].

Another material that is considered promising for use as a flexible supercapacitor is metal-organic frameworks (MOFs) built by coordinating metal nodes and organic linkers [16]. MOFs are unique because of their high specific surface area, good structure, exceptional porosity and high tunability, among other beneficial characteristics [17]. Because of these beneficial properties, MOFs have found practical application in various fields, such as sensing, catalysis, gas storage, drug delivery and energy storage [18-20].

Since the engineering work done by Yaghi et al. [21] about three decades ago, several other MOFs have been developed for flexible supercapacitor applications. They can be employed in three different ways, namely:

- Parent MOFs can be made to store energy using their internal surface via the EDLC mechanism or by redox reaction of their metal nodes.
- MOFs can also be pyrolyzed to produce porous carbon with high storage performance, because of the higher level of conductivity, which is attributed to carbon materials.
- Transforming MOFs into metal and metal oxides to store energy by way of the Faraidaic process (i.e. transfer of charges between the electrode and electrolyte) [21-22].

Unfortunately, these three approaches deliver limited specific capacitance and cycling stability, which prevents their use as a general template for the fabrication of MOF-derived flexible supercapacitors [23]. Several studies have been carried out to enhance the development of flexible supercapacitors using nanocomposites of MOFs [24-26], and the recent progress made with MOF-based nanocomposites that are used as flexible supercapacitor electrodes is discussed in this chapter. The focus is on the different methods used to prepare the MOF nanocomposites and their performance as flexible supercapacitors. The main challenges and prospects of MOF-based flexible supercapacitors are then outlined.

This chapter should provide insight that will help with fabricating flexible SCs in the future, based on MOF nanocomposites for scientific research and industrial applications.

3.2 Flexible supercapacitors

Flexible supercapacitors are the next generation power source, because of their flexibility, good durability, exceptional charge-discharge rate, good safety and high-power density [27]. For instance, flexible supercapacitors made of fibers can be woven or knitted into different shapes without compromising their original quality [28]. As shown in Figure 3.1, the major components of flexible supercapacitors are substrates, electrode materials and gel polymer-based electrolytes. These three parameters must be optimized carefully to obtain the flexibility required of a flexible supercapacitor [29]. Flexible SCs are often required to operate under different folding conditions or at bent angles, without breaking or significant loss in storage performance [30].

Electrode materials play a vital role in the performance of a flexible supercapacitor, and various electrodes have been employed, such as carbon-based material, conductive polymers and metal oxides [31]. Carbon-based materials have a storage mechanism that is guided by the EDLC storage mechanism and they are of great use because of their chemical inertness and excellent electrical conductivity [32]. The other types of electrode materials used for flexible SCs are pseudocapacitors, which comprise metal and metal oxides. Because pseudocapacitors rely on reversible redox reactions at the surface of the electrode, they have a better storage capacity than EDLCs; however, they also suffer from poor conductivity [33].

With the rapid growth in research on flexible SCs, elicited by the growing demand for flexible electronics, attention has shifted to MOFs and their nanocomposites, in terms of fabricating flexible SCs to enhance energy density and overall performance [34]. MOFs can achieve a high specific surface area, a tunable metal center for a redox reaction, and large accessible active sites with excellent porosity for rapid transportation of ions and electrons in the electrolytes [35].

With SCs, three kinds of MOFs are exploited - pristine MOFs and those pyrolyzed under an ambient atmosphere or an inert atmosphere. In this chapter, the use of pristine MOFs for flexible SCs is not applicable and only MOF nanocomposites that are designed to cater for the drawbacks of pristine MOFs are discussed. These drawbacks include low chemical/thermal stability and poor electrical conductivity that emanate from the insulating linkers in the structure. In one instance,

the conductivity of MOFs was improved via intercalation with the conjugated conductive substrates polyaniline (PANI), polypyrrole (PPy) and poly(3,4-ethylenedioxythiophene) (PEDOT) [36]. When conductive polymers are incorporated into pristine MOFs, it boosts the electrical conductivity of the derived MOF nanocomposites and enhances the Faradaic process at the electrode/electrolyte interface [36]. This strategy, as well as several others that have been reported in the literature in recent times, for transforming pristine MOFs into MOF nanocomposites for flexible supercapacitor applications, are the focus of the next section.

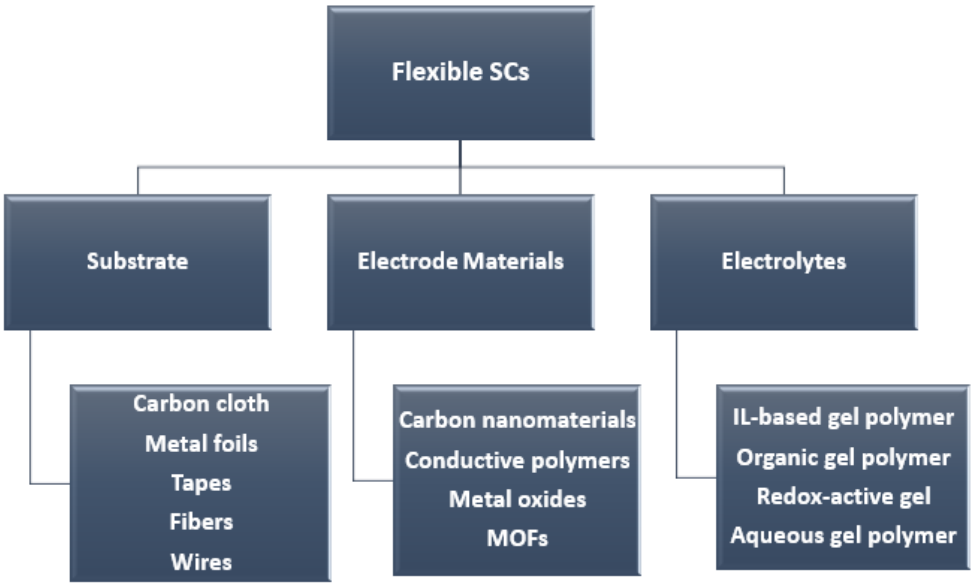

Figure 3.1 Classification of flexible supercapacitors into substrate, electrode materials and electrolytes.

3.3 Fabrication methods used to produce MOF nanocomposites

MOFs exhibit promising physicochemical properties for different applications, including supercapacitors, and their properties can be further enhanced in various ways. These include impregnating appropriate functional materials, post-synthetic functionalization, changing the organic linkers and making composites with appropriate materials [37]. Composite materials often exhibit good properties because of the synergistic effect of the constituents used to make the composite [38]. The potential use of MOFs increases every year, due to the ease of functionalization with other materials, such as metal nanoparticles and metal oxides, conductive polymers and carbon nanomaterials. It is possible to tune their functionality and surface characteristics, and (most importantly) improve their electrochemical energy storage performance

[39]; therefore, researchers have developed several strategies to incorporate functional materials into MOFs for enhanced flexible supercapacitor applications [40-42].

This chapter provides a brief introduction and explanation of the research work done in this field. Polymer-based materials are the most commonly-used compositing materials used to obtain the required properties in flexible SCs. They boost the physical and chemical properties of the nanocomposites, and offer intrinsic conductivity, which ultimately delivers high-performance flexible SCs [43]. Several reviews have reported on the fabrication strategies used to produce MOF nanocomposites, and the synthesis strategies can generally be categorized into four approaches that are discussed here: ship-in-a-bottle, bottle-around-a-ship, photodeposition and thermolysis.

3.3.1 Ship-in-a-bottle approach

This approach refers to the process of building a model ship inside a bottle. It involves immobilizing small nanoparticle precursors (the ship) on the MOF scaffolds (the bottle), which produces the target MOF nanocomposites upon additional in situ treatment [44]. As a result, the MOF composites encapsulate larger nanoparticles than the pores inside the frameworks, which are kept inside the lattice. The encapsulated species can vary from metal nanoparticles to metal oxides and from polymers to organometallics [45].

When this method is employed, numerous ‘guests’ can be incorporated, including metal nanoparticles and nanoclusters. Although the ship-in-a-bottle process is famously used with zeolite composites, its application has recently been extended to the MOF field [46]. In terms of fabricating MOF nanocomposites, there are many benefits associated with using the ship-in-a-bottle approach. These include: (i) ease of preparation; (ii) pure MOF nanocomposites can be formed; (iii) it eliminates the energy barrier challenge at the surface of two materials [47]. The major drawback when using this method is the difficulty in controlling (to a reasonable extent) the size, morphology and location of the guest molecules inside the framework structure [48].

The ship-in-a-bottle approach can further be classified into the following phases: grinding (solid phase); wet infiltration (liquid phase); chemical vapor deposition (gas); plasma arc deposition (plasma phase).

3.3.1.1 Solid grinding/Ball milling

This method involves grinding functional precursors with the parent MOFs (without using solvents), using the mortar or ball milling method [49]. The active precursors then diffuse into the pores of the MOF and are enclosed. This is followed by annealing at a high temperature in a reducing atmosphere and the nanoparticles are deposited onto MOFs to produce NP@MOF nanocomposite [50]. This method is a green, rapid synthesis method that can ensure synthesis of novel MOF nanocomposites. For instance, in 2020, Yu et al. reported synthesizing 3D Ag MOF-containing nanocomposites using a simple grinding method and used them as electrode materials for high-performance supercapacitor applications [51]. As shown in Figure 3.2, the obtained composite material - Ag-MOF and $[Ag_6Mo_7O_{24}]$@Ag-MOF - was acquired by grinding $Ag_6Mo_7O_{24}$ with trimesic acid (H_3BTC) in an ethanol solution. The synthesis was confirmed using different spectroscopic techniques - including TEM, XRD and EDX - which showed that Mo, Ag, C and O were uniformly distributed in the rod shape of $[Ag_6Mo_7O_{24}]$@Ag-MOF nanocomposites.

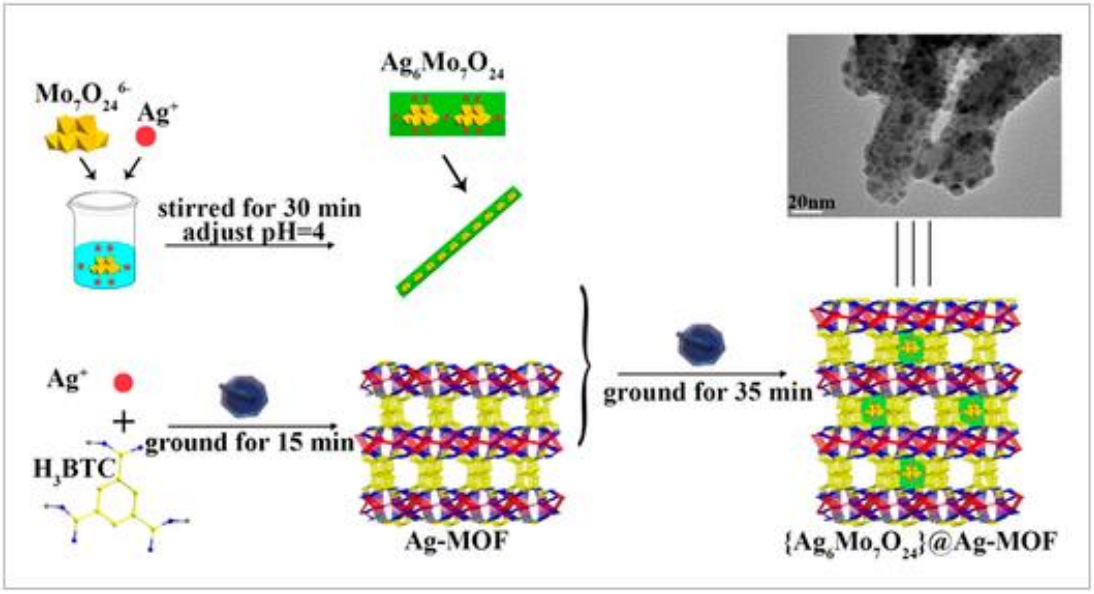

Figure 3.2 Synthesis pathway for MOF nanocomposites using the grinding method.
Source: Ref. [51]

3.3.1.2 Wet infiltration method

The wet infiltration method, otherwise known as the solution infiltration method, is a simple method that involves immersion of MOFs in a solution containing guest molecules as nanoparticle precursors [52]. The wet infiltration method can be extended to accommodate fluids (fluid infiltration), such as supercritical CO_2, which can penetrate the MOF structure to ensure uniform

distribution of the guest molecules [53]. The pore windows of MOFs need to be larger than the size of the guest molecules to allow diffusion of the guests into the MOF.

Farrusseng et al. employed a solution infiltration method to encapsulate various Fe and Ru complexes of phthalocyanines in MIL-101 with different sizes [54]. In another study, Houk and co-workers anchored silver nanoparticles on three different MOFs (MOF-508, HKUST-1 and MIL-68(In)) using the solution infiltration method [55], and solubility in water informed the choice of the selected MOFs. The process involved a water-ethanol (5:1 v/v) solution containing silver (I) nitrate being used to prepare the parent MOFs. The MOF powder was then transferred into the solution to form a slurry. Ag(I) was expected to reduce Ag(0) using ethanol as the reducing agent, with 100% yield during the infiltration process. Structural elucidation of the composite structure showed that the structural integrity of the MOFs was protected after the infiltration and that Ag_3 nanoclusters were found inside the MOF windows [55]. However, while small metal complexes satisfactorily diffused into the pores of the parent MIL-101, large complexes of approximately 2mm x 2mm only moved to the external surface of MIL-101 at the expense of the internal pores.

To overcome this drawback of the diffusion barrier, Tsung and his team pioneered a dissociative linker exchange strategy to incorporate large molecules with a diameter up to four times larger than the pores of the MOF [57]. Since then, a lot of research has been published (including that of Ma et al.) on using cobalt(II) phthalocyanine to encapsulate the MOF framework by facile *de novo* assembly of the constituting species of the guest molecule [58]. This overcomes the problem of encapsulating guest molecules bigger than the pores of the MOF [58].

3.3.1.3 Chemical vapor deposition

Chemical vapor deposition (CVD) is a technique used in nanofabrication that is known to be ideal for the fabrication of MOF nanocomposites [59]. Generally, this method involves three steps: (i) precursor vaporization; (ii) transporting the precursor via the gas phase; (iii) deposition of the target precursor onto the substrate [60]. To fabricate MOF nanocomposites via this method, the MOF substrate reacts via deposition with the vapor of the nanoparticle precursors. After deposition, heat treatment in a reducing atmosphere (e.g. H_2) transforms the nanoparticle precursors into nanoparticle-yielding NP@MOF nanocomposites. MOFs that are thermally stable with an appropriate pore size for the diffusion of the gaseous guest molecules are the best candidates for this strategy, including ZIF-based MOFs, MOF-5 and MOF-177. [61]. For instance,

Fischer et al. demonstrated that highly porous MOF-5 or IRMOF-1 could be reversibly loaded with metal-organic CVD metal precursors - such as Cu, Zn, Pt, Pd, Fe and Au [62] - as guest molecules, while preserving the MOF properties. It was further shown that the metal nanoparticle loading is size-selective and dependent on the vapor pressure of the precursors [62].

3.3.1.4 Arc plasma deposition

Another method used to synthesize MOF-based nanocomposites is arc plasma deposition (APD). It involves using arc plasma shots to deposit metal nanoparticles directly on the MOF substrates [63]. For instance, Sadakiyo et al. prepared Metal@MOFs nanocomposites using the APD method with the aid of an arc plasma gun containing a metallic cylinder as a metal precursor (Pt, Pd, or Au) [64]. (See Figure 3.3.) In that study, the MOF powder (up to 5 g) was placed inside the vacuum chamber and rotated continuously by stirring using a stirrer bar [64]. A water-cooling system was used to keep the temperature inside the pot at 18 ^{o}C. Different nanocomposites of ZIF-8 and MIL-101 were prepared by irradiating plasma shots inherent with varying precursors of metal onto the pristine MOFs in the frequency range of 1-2 Hz, and using an applied voltage of 140 V. Different loading percentages (wt%) of MOF nanocomposites were obtained by means of inductively coupled plasma atomic emission spectrometry (ICP-AES) analysis: Pt/ZIF-8 (0.82%), Pd/ZIF-8 (0.79%), Ru/ZIF-8 (0.93%) and Ru/MIL-101 (1.09%) [64].

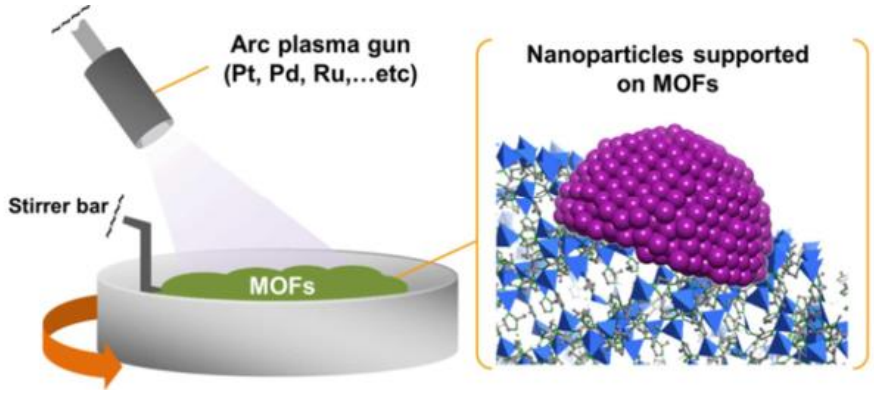

Figure 3.3 Scheme showing gram-scale synthesis of M@MOF composites using the APD method. Source: Ref. [64]

3.4 Bottle-around-a-ship approach

This approach, otherwise known as the template method, involves stabilizing the functional molecule or nanoparticles by capping agents or surfactants, which are then added to the MOF-

containing solution [65]. This method can help optimize the size and shape of the encapsulated particles, since they are formed before the framework is assembled. In addition, it can help minimize the formation of the nanoparticles on the external surface of the parent MOFs [66]. This method prefers MOFs with mild synthesis protocols to eliminate aggregation of molecules during the assembly of MOF nanocomposites.

The assembly of MOFs around active species has been well established with porphyrin moieties and polyoxometalates. Several studies have been done in this field by incorporating different moieties into MOFs to obtain MOF composites. For instance, Chang et al. successfully prepared keggin-type polyoxometallates (POM) in a defected Zr-based MOF, using the bottle-around-a-ship approach with $Mo^{5+/}Mo^{6+}$ ratios [67].

3.5 Photodeposition

This process involves semiconductor nanoparticles being uniformly deposited in situ onto the support surface in the presence of light [68]. For instance, a series of metal sulfides - including Ag_2S, CdS, MoS_2 and CuS) quantum dots - were deposited on MIL(Ti) [69]. The choice of MIL-101(Ti) was informed by its large surface area, ease of tunability and photo-responsiveness [69]. In another study, Wu and co-workers employed the photodeposition technique to deposit CdS nanorods on UiO-66(NH_2) at room temperature [70].

3.6 Thermolysis

This is the most widely used method to convert MOFs into different active materials. It ensures effective carbonization of the MOF template/precursor and uniform distribution of MOF nanocomposites without compromising the integrity of the MOF [71]. MOFs can be subjected to heat treatment under different atmospheres to produce metal oxide, carbon and their composites for use as a sacrificial template [72]. The carbonization atmosphere - including H_2, O_2, NH_3 and inert gases - needs to be optimized to eliminate air in the formation of MOF-based composites [73].

MOFs that are considered valuable precursors for use in producing nanocomposites have certain inherent properties, including tunable morphology, high stability and low cost. ZIF, MOF-74 and MIL-based MOFs are the leading precursor candidates for the fabrication of MOF nanocomposites for flexible supercapacitor applications [74]. This is due to the unsaturated metal center, and their

high flexibility and good stability. One study that used this method was reported by Wang et al. [75]. Mn-MIL-100 served as a template to fabricate different metal oxide and metal oxide/carbon nanocoposites under different heating conditions - see Figure 3.4. Filtration and reduction with graphene oxide (GO) yielded Mn_3O_4@C/rGO [75].

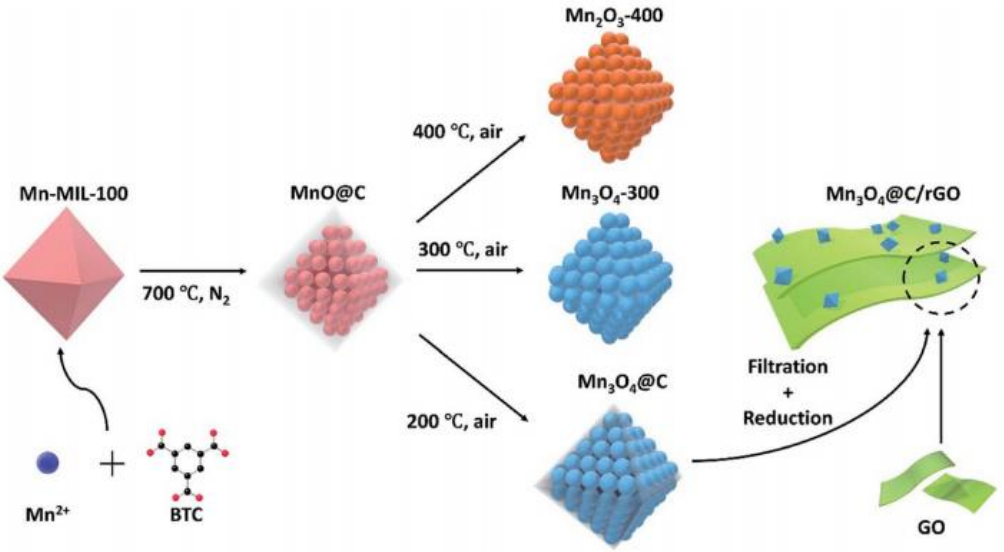

Figure 3.4 Thermolysis of Mn-MIL-100 into Mn_3O_4@C/rGO.
Source: Ref. [75]

3.7 Applications of MOF nanocomposites for flexible supercapacitors

MOFs, in addition to being employed as functional materials, may also be used as a template to create porous structures and nanocomposites, such as metal oxides, metal/metal oxides, nanocarbons, and metal oxide/carbon nanocomposites [76]. Only MOF-derived metal/metal oxide nanocomposites, MOF-derived carbon/redox polymer nanocomposites, MOF-derived metal oxide/carbon nanocomposites, and MOF/redox polymer nanocomposites for flexible supercapacitors are described in this chapter.

3.7.1 MOF-derived metal oxide/carbon nanocomposites

Transition metal oxides, including NiO, ZnO, Co_3O_4 and MnO_2, have outstanding redox properties and are regarded as promising candidates for energy storage devices such as flexible supercapacitors [77]. However, these materials are characterized by poor electrical conductivity, low chemical/thermal stability and a small specific surface area. Because of the beneficial characteristics of MOFs, MOF-derived metal oxides/CNTs can be designed to exhibit a high

surface area, which increases the quantity of accessible redox-active sites and improves the overall energy storage performance [78]. In addition, the incorporation of carbon content can help circumvent the low conductivity associated with metal oxides. Thus, MOF-derived metal oxide/carbon nanocomposites are promising electrode materials for use in flexible supercapacitor applications [79].

Zhang et al. employed a two-step thermal annealing process in Ar and air to produce Co_3O_4/C nanowire arrays from pristine Co-MOF [80]. Nickel foam (NF) was first used to improve the structural stability of the MOF-based electrodes and minimize electron/ion resistance by growing it in situ with the Co-MOF nanowire array [80]. Upon annealing in Ar, the Co-MOF was transformed to carbon, while the carbon reduced the cobalt ions. The final Co_3O_4/C nanocomposite was produced after annealing in air without compromising the structural integrity of the pristine MOF. When the composite material was used as the electrode material for flexible supercapacitors, it exhibited an areal capacitance of 1.32 F/cm^2 at a current density of 1 mA/cm^2, and showed good cyclic stability of 78.3% after 5000 cycles because of the synergistic effects of porous nanowire arrays and carbon [80].

Using one-step heat treatment of Co-BDC in nitrogen and oxygen gas flow, Dai and colleagues created a Co_3O_4@C nanocomposite alongside Co@C [81]. When employed in supercapacitor applications, Co3O4@C had a specific capacitance of 261 F/g at 1 A/g compared to 90 F/g for Co@C at the same current density. The energy and power density of asymmetric supercapacitors (ASCs) assembled using Co_3O_4@C and Co@C as the positive and negative electrodes, respectively, were 8.8 Wh kg^{-1} and 375 W kg^{-1}, respectively [81].

Wang et al. reported MOF-derived manganese oxide/carbon nanocomposites from two-step thermolysis in air and N_2 of Mn-MIL-100 [75]. MnO@C was first produced by annealing the parent MOF at 700 ^{o}C in an N_2 atmosphere. It was then converted to Mn_3O_4@C at 200 ^{o}C under airflow. Mn_3O_4@C-2 obtained after annealing MnO@C for 2h delivered the highest capacitance compared to other manganese oxide samples treated at 300 ^{o}C (Mn_3O_4) and 400 ^{o}C (Mn_2O_3). A flexible supercapacitor electrode fabricated from Mn_3O_4@C/reduced GO produced a volumetric capacitance of 328.4 F/cm^3 at 0.5 A/cm^3 [75].

3.7.2 MOF/carbon/redox polymer nanocomposites

The synergistic effects of combining MOFs, carbon and redox polymers will contribute significantly to enhancing the performance of flexible supercapacitors, because the incorporation of MOFs will result in a large surface area and high porosity. In addition, carbon will improve the conductivity and mechanical strength of MOFs. Similarly, redox polymers will also increase the conductivity and provide an avenue to connect all the active species in the space. They can also contribute to the overall storage performance through the Faradaic redox reaction [82].

Wang et al. developed flexible solid-state supercapacitors using MOFs interwoven by electrochemically-deposited PANI [83]. In the Wang et al. study, ZIF-67 was chosen as the storage material, while CC was selected for its mechanical flexibility and strength, and its contribution to the conductivity of the hybrid structure [83]. To make the composite with these components, a two-step process was employed, as shown in Figure 3.5. MOFs were coated onto the CC, followed by electrochemical deposition of PANI chains onto MOF to produce a flexible PANI-ZIF-67-CC, while preserving the structural architecture of MOF. The structural elucidation of the composite showed that the conductive PANI chains covered the interstitial open space and were well bridged with the crystal surface of MOF [83].

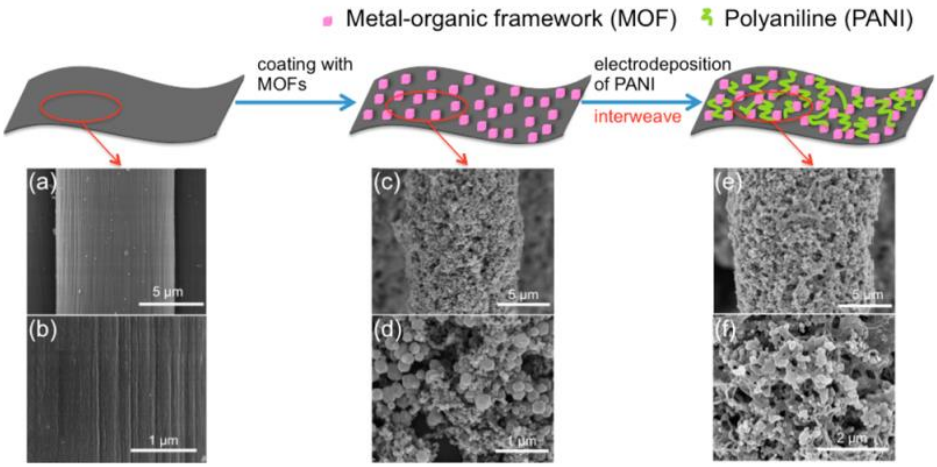

Figure 3.5 The two-step synthesis route of a flexible PANI-ZIF-67-CC electrode and SEM images of: (a and b) CC fibers; (c and d) after coating with the parent ZIF-67; (e,f) after electrodeposition of PANI
Source: Ref. [83]

When used as a supercapacitor electrode, the composite electrode delivered an outstanding areal capacitance of 2146 mF/cm^2 at a scan rate of 10 mV/s, due to the synergistic effects of the constituting components. A solid-state flexible supercapacitor device fabricated using PANI-ZIF-67-CC in a gel-like electrolyte (Figure 3.6) delivered a capacitance of 116 mF/cm^2 with a maximum energy density of 0.0161 mWh/cm^3 at 0.0044 mWh/cm^2 and excellent power density of 0.833 W/cm3 at 0.245 W/cm^2. In addition, the device retained 80% of its original capacitance after 2000 cycles at 0.1 mA/cm^2. Importantly, the energy performance of the device remained intact, even after twisting and bending, as shown in Fig 3.6 b-d. Furthermore, it successfully lit up the light-emitting diode (LED) bulb connected by two 14500 batteries for 30s [83].

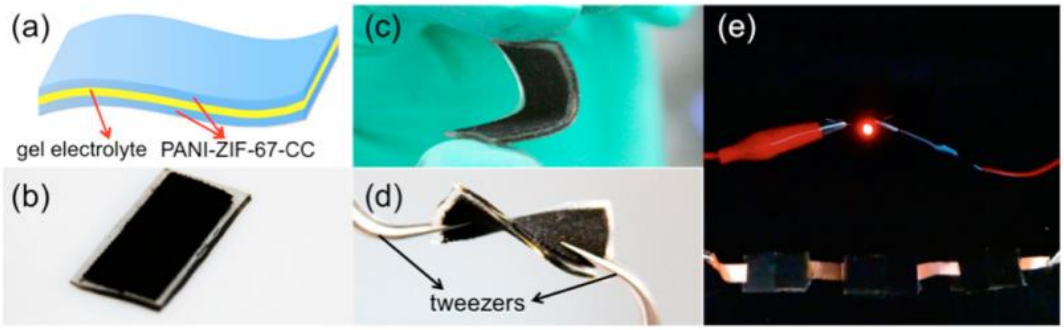

Figure 3.6(a): A flexible solid-state supercapacitor device made from PANI-ZIF-67-CC. Optical images of the fabricated device in: a (b) standard condition; (c) bent condition; (d) twisted condition. (e) Photograph of LED powered by three supercapacitors connected in series.
Source: Ref. [83]

Cheng et al. produced a flexible supercapacitor electrode consisting of ZnO@MOF/PANI coated on CC in a recent work, which will aid in the development of flexible electrode materials [84]. At 1 A/g, the flexible supercapacitor electrode had a capacitance of 340 F/g and preserved roughly 84 percent of its original value at 10 A/g, indicating strong rate capability. The electrode also demonstrated high cyclic stability, with 82% capacitance retention after 5000 cycles. The excellent storage performance found can be due to the synergistic effects of the different components that made up the ternary nanocomposites, which result in faster electron transport and more accessible redox-active sites [84].

3.7.3 MOF-derived metal/metal oxides nanocomposites

One promising way of obtaining high-performance flexible supercapacitor electrodes is by transforming pristine MOFs into metal oxide and incorporating an additional metal ion [85]. The

presence of redox metallic ion centers alone in the MOF structures will contribute to the pseudocapacitive energy storage of the composite. In contrast, extra metal ions will contribute additional properties, such as compositional and structural diversity, multi-functionality and stability. MOF-based metal/metal oxide nanocomposites exhibit excellent supercapacitor performance because of their good conductivity, high stability and suitable capacitance offered by the composite when compared to pristine metal-oxides [86].

Zheng et al. [87] reported on one study that deals with this problem. It entailed creating a Co3O4@Co-MOF and AC flexible supercapacitor device with a 1.5 V potential window that provided 192 mF/cm2 of areal capacitance at 0.5 mA/cm2 [87]. The composite electrode's outstanding stability resulted in great cycling stability, with around 100 percent capacitance retention after 400 bending cycles. This suggests that it might be a viable power source for flexible electronics [87].

Guan et al. recently described a flexible asymmetric supercapacitor device made of NiCo2O4 and carbon nanowalls with a specific capacitance of 89 F/g at 5 mA/cm^2 and excellent rate capabilities [88]. After 20,000 cycles, the device retained roughly 87 percent of its capacitance and had good bending capabilities at various bending angles.

3.7.4 MOF/redox polymer nanocomposites

The energy storage performance of MOFs can be reinforced by the incorporation of conductive polymers, especially PANI, which is known for its high electrical conductivity, high doping potential and ease of functionalization [89]. After incorporation, the composite electrode exhibited a light weight, high mechanical flexibility, low cost and (most importantly) the excellent storage capability characteristic of a flexible supercapacitor [90]. In 2018, Wang et al. coordinated PANI with unsaturated metal sites in MIL-101 via its electron-rich imine function to produce PANI/MIL-101 nanocomposites [91]. A flexible solid state supercapacitor device made from PANI/MIL-101 delivered a high specific capacitance of 80 F/g at a current density of 0.5 A/g, and an energy density and power density of 7 Wh/kg and 2000 W/kg, respectively, within a potential window of 0.8V. The CV and galvanostatic charge-discharge (GCD) experiments shown in Figure 3.7a and 3.7b were used to examine the flexibility of the supercapacitor electrode, and the device exhibited good mechanical flexibility after 1000 bending cycles at a contact angle of 180^o [91]. In addition, about 90% of the original capacitance was retained after 10,000 cycles, which suggests good cyclic

stability. (See Figure 3.7c.) For purposes of testing its use in practical applications, the fabricated flexible device was connected in a series of four cells and charged to 3.2 V at a current kept at 8 mA. The result showed that it could successfully light up an LED for 90s [91]. (See Figure 3.7d.)

Similarly, Iqbal and co-workers developed a battery-grade flexible device based on Co-MOF/PANI assembled with activated carbon (AC) and separated by a porous membrane [92]. The device delivered a specific capacitance of 104 C/g at 1 A/g, a maximum energy density of 23.2 Wh/kg and a power density of 4480 W/kg. It also showed good stability after 3000 cycles, i.e. 146% [92].

Lin et al. [93] used a simple non-calcined technique to build a solid-state asymmetric flexible supercapacitor device based on Co-BTC coated on a nanowire microsphere in 2021. While the nanowire architecture increased the MOFs' electronic conductivity, the microspherical shape improved the device's mechanical flexibility and stability. The manufactured gadget has an energy density of 34.4 Wh/kg and a maximum power density of 375 W/kg.

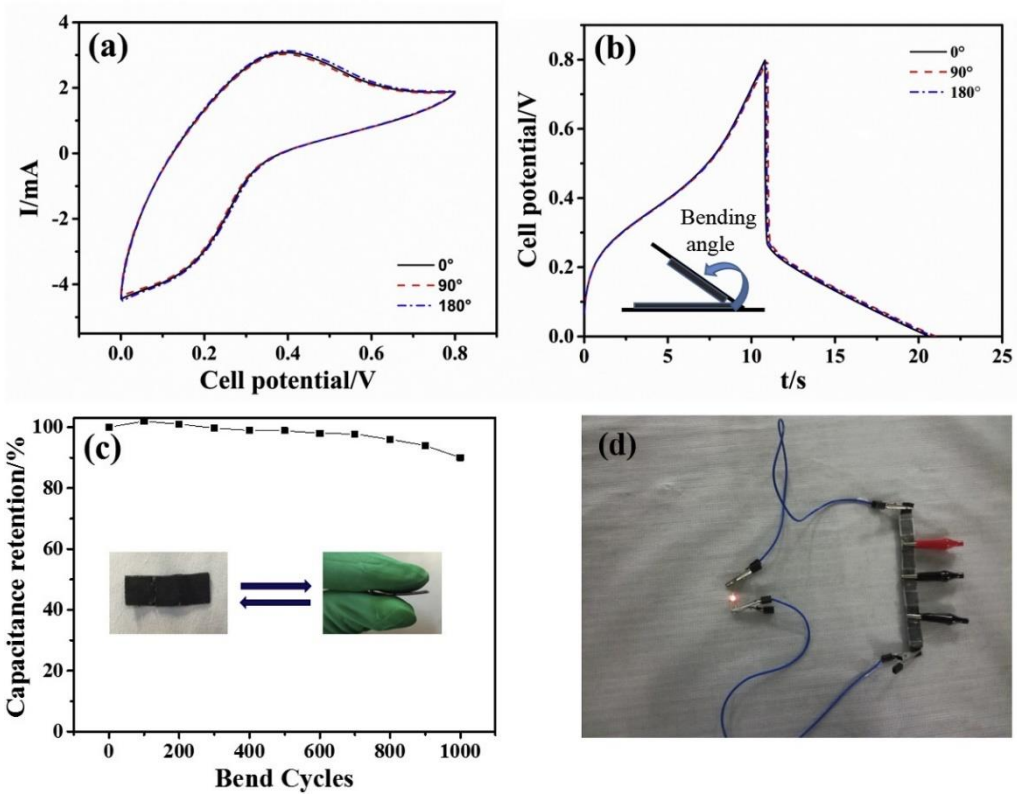

Figure 3.7 Electrochemical performance of device.
(a) CV curve of the MOF-based flexible supercapacitor at 20 mV/s scan rate for different bent angles. (b) GCD curve of the flexible supercapacitor at different angles. (c) Cyclic stability at different

bending cycles at 180º with the inset showing the mechanical folding test. (d) Photograph of LED connected by four cells.
Source: Ref. [91]

3.8 Conclusions

MOF nanocomposites have the requisite characteristics for fabricating high-performance supercapacitor electrodes, thereby overcoming the limitations of individual pristine MOFs. It has been established that MOF nanocomposites with optimized features - such as electrical conductivity, thermal and chemical stability and a flexible surface area - will deliver highly flexible energy storage devices.

This chapter provided a summarized discussion of different synthetic strategies used when constructing nanocomposites based on MOFs, including ship-in-a bottle, bottle-around-a-ship and thermolysis. Notably, thermolysis under different atmospheric conditions remains the most widely used method for the synthesis of MOF-based nanocomposites for flexible supercapacitor applications. The construction of MOF-based nanocomposites can expand the family of flexible supercapacitors. The most important MOF nanocomposites for use in flexible supercapacitor applications are summarized in Table 3.1. The key points relating to these nanocomposites are as follows:

- Various MOFs can be used as a sacrificial template or a precursor to obtain distinct MOF nanocomposites, such as MOF/conductive polymer, metal oxide/metal and MOF/redox polymer.
- Different MOF precursors and functional species produce different nanocomposites with a distinct structure, shape and composition. Therefore, choosing the parent MOF and compositing material must be done carefully for high-performance flexible supercapacitor applications.
- Composite MOF-derived nanoparticles - such as conductive polymers, carbon and metal oxides - have various functions that can successfully improve the performance of flexible devices in terms of energy/power density, flexibility and cycle life. This could be attributed to the synergistic effects of the individual components that make up the composite.

Despite the considerable success recorded with using MOF-based nanocomposites in flexible supercapacitor applications, some challenges remain, such as:

- The vast majority of MOFs were not initially designed for flexible supercapacitor applications, which limits their storage performance, even after incorporating compositing materials.

- The most widely used negative electrode used in the assembly of flexible devices is AC. However, it has a limited capacitance of 200 F/g. To balance the charge between positive and negative electrodes, the loading of the negative electrode is always higher than the loading of the positive electrode, and this limits the energy density value.
- The high cost of MOFs is another concern in terms of the commercialization of MOF-based nanocomposites.

To overcome these problems, the following research directions are proposed:

- Researchers need to intensify research efforts into the design of new composite materials for MOF-derived nanoparticles to be used as the electrode material in supercapacitor applications. They should also ensure that the synergy between the original MOFs and compositing materials is properly understood for proper optimization of the storage performance.
- Attention should be paid to other negative electrodes, apart from activated carbon, in order to deliver high energy density devices.
- The high cost of MOFs can be reduced by using metal waste, and inexpensive and low-grade materials as starting materials.

To conclude, applications for

flexible supercapacitors involving MOF nanocomposites are still largely at the lab scale, and the number of synthesis protocols available in the literature is limited. Nonetheless, future research should exploit various advanced materials to construct MOF-based nanocomposites with improved properties for use in flexible supercapacitor devices for industrial-scale applications.

Table 3.1: Summary of the flexible supercapacitor performance of MOF-based nanocomposites.

Pristine MOF	MOF nanocomposite	Electrolyte	Capacitance	Energy density	Cyclic stability	Flexibility (bending cycles)	Ref.
ZIF-67	PANI-ZIF-67-CC	H_2SO_4/PVA gel	35 mF cm^{-2} at 0.05 mA cm^{-2}	0.0044 mWh cm^{-2}	80% (2000)	Optical images showed capacitance remained intact after bending and twisting.	[83]
Co-MOF	Co3O4@Co-MOF	Gel-based electrolyte	192 mF cm^{-2} at 0.5 mA cm^{-2}	21.6 mW h cm^{-3}	96% (5000)	99.7% (400 cycles)	[87]
MIL-101	PANI/MIL-101	PVA/H_2SO_4	371 F/g at 0.5	7 Wh kg^{-1}	81% (10000)	90% (1000 cycles)	[91]
Co-BTC	Co-BTC/NWM	1 M NaOH	657 F/g at 0.5 A/g		81% (3000)	-	[93]
UiO-66	PANI/UiO-66	PVA/H_2SO_4	1015 F/g at 1 A/g	78.8 Wh/kg	84% (3500)	90% (800 cycles)	[94]
Cu-MOF	Cu-MOF@CC		1812 mF/cm^2 @ 1 mA/cm^2	3.14 mWh/cm^3	90% (2000)	-	[95]
HKUST-1	PEDOT/HKUST-15G-CNTF	PVA/H_3PO_4 gel	37.8 mF/cm^2 at 5 mV/s	2.1 mW/cm at 0.4 mA/cm^2	89% (700)	Optical images taken at different angles show high flexibility.	[96]

ZIF-67	ZIF-67/rGO	0.2 M $K_3[Fe(CN)_6]^{+1}$ M Na_2SO_4	326 F/g at 3 A/g	25.5 Wh /kg	88.8% (1000)	-	[97]
ZIF-67	ZIF-67-Ppy	Na_2SO_4/PVA gel	225.8 mF cm^{-2} at 0.04 mA cm^{-2}	0.0113 mWh cm^{-2}	-	Optical images show good flexibility up to 180 ^{o}	[98]

3.6 References

1. Hoel, M. and Kverndokk, S., 1996. Depletion of fossil fuels and the impacts of global warming. *Resource and Energy Economics*, *18*(2), pp.115-136.
2. Tomico, O., Hallnäs, L., Liang, R.H. and Wensveen, S.A., 2017. Towards a next wave of wearable and fashionable interactions. *International Journal of Design*, *11*(3).
3. Melumad, S., Hadi, R., Hildebrand, C. and Ward, A.F., 2020. Technology-augmented choice: How digital innovations are transforming consumer decision processes. *Customer Needs and Solutions*, *7*, pp.90-101.
4. Chen, S., Yang, G., Jia, Y. and Zheng, H., 2016. Facile synthesis of CoWO4 nanosheet arrays grown on nickel foam substrates for asymmetric supercapacitors. *ChemElectroChem*, *3*(9), pp.1490-1496.
5. Markoulidis, F., Dawe, A. and Lekakou, C., 2021. Electrochemical double-layer capacitors with lithium-ion electrolyte and electrode coatings with PEDOT: PSS binder. *Journal of Applied Electrochemistry*, *51*(3), pp.373-385.
6. Salanne, M., Rotenberg, B., Naoi, K., Kaneko, K., Taberna, P.L., Grey, C.P., Dunn, B. and Simon, P., 2016. Efficient storage mechanisms for building better supercapacitors. *Nature Energy*, *1*(6), pp.1-10.
7. Kumar, Y., Rawal, S., Joshi, B. and Hashmi, S.A., 2019. Background, fundamental understanding and progress in electrochemical capacitors. *Journal of Solid State Electrochemistry*, *23*(3), pp.667-692.
8. Dubal, D.P., Kim, J.G., Kim, Y., Holze, R., Lokhande, C.D. and Kim, W.B., 2014. Supercapacitors based on flexible substrates: An overview. *Energy Technology*, *2*(4), pp.325-341.
9. Sugumaran, C.P., 2020. A flexible, cost-effective, and eco-friendly solid state supercapacitor based on PVA/KCl/carbon black nanocomposite. *Ionics*, *26*(3), pp.1465-1473.
10. Gopi, C.V.M., Vinodh, R., Sambasivam, S., Obaidat, I.M. and Kim, H.J., 2020. Recent progress of advanced energy storage materials for flexible and wearable supercapacitor: From design and development to applications. *Journal of Energy Storage*, *27*, p.101035.
11. Wang, Y., Qu, Q., Gao, S., Tang, G., Liu, K., He, S. and Huang, C., 2019. Biomass derived carbon as binder-free electrode materials for supercapacitors. *Carbon*, *155*, pp.706-726.

12. Wang, Z., Li, H., Tang, Z., Liu, Z., Ruan, Z., Ma, L., Yang, Q., Wang, D. and Zhi, C., 2018. Hydrogel electrolytes for flexible aqueous energy storage devices. *Advanced Functional Materials*, *28*(48), p.1804560.
13. Shown, I., Ganguly, A., Chen, L.C. and Chen, K.H., 2015. Conducting polymer-based flexible supercapacitor. *Energy Science & Engineering*, *3*(1), pp.2-26.
14. Hillier, N., Yong, S. and Beeby, S., 2020. The good, the bad and the porous: A review of carbonaceous materials for flexible supercapacitor applications. *Energy Reports*, *6*, pp.148-156.
15. Yu, A., Roes, I., Davies, A. and Chen, Z., 2010. Ultrathin, transparent, and flexible graphene films for supercapacitor application. *Applied Physics Letters*, *96*(25), p.253105.
16. Cherusseri, J., Pandey, D., Kumar, K.S., Thomas, J. and Zhai, L., 2020. Flexible supercapacitor electrodes using metal–organic frameworks. *Nanoscale*, *12*(34), pp.17649-17662.
17. González, C.M.O., Kharisov, B.I., Kharissova, O.V. and Quezada, T.E.S., 2021. Synthesis and applications of MOF-derived nanohybrids: A review. *Materials Today: Proceedings*.
18. Goetjen, T.A., Liu, J., Wu, Y., Sui, J., Zhang, X., Hupp, J.T. and Farha, O.K., 2020. Metal–organic framework (MOF) materials as polymerization catalysts: A review and recent advances. *Chemical Communications*, *56*(72), pp.10409-10418.
19. Szczęśniak, B., Choma, J. and Jaroniec, M., 2018. Gas adsorption properties of hybrid graphene-MOF materials. *Journal of Colloid and Interface Science*, *514*, pp.801-813.
20. Otun, K.O., Liu, X. and Hildebrandt, D., 2020. Metal-organic framework (MOF)-derived catalysts for Fischer-Tropsch synthesis: Recent progress and future perspectives. *Journal of Energy Chemistry*, *51*, pp.230-245.
21. Yang, J., Ma, Z., Gao, W. and Wei, M., 2017. Layered structural Co-based MOF with conductive network frames as a new supercapacitor electrode. *Chemistry–A European Journal*, *23*(3), pp.631-636.
22. Wu, S., Liu, J., Wang, H. and Yan, H., 2019. A review of performance optimization of MOF-derived metal oxide as electrode materials for supercapacitors. *International Journal of Energy Research*, *43*(2), pp.697-716.

23. Xie, W., Wang, Y., Zhou, J., Zhang, M., Yu, J., Zhu, C. and Xu, J., 2020. MOF-derived CoFe2O4 nanorods anchored in MXene nanosheets for all pseudocapacitive flexible supercapacitors with superior energy storage. *Applied Surface Science*, *534*, p.147584.
24. Xu, X., Shi, W., Liu, W., Ye, S., Yin, R., Zhang, L., Xu, L., Chen, M., Zhong, M. and Cao, X., 2018. Preparation of two-dimensional assembled Ni–Mn–C ternary composites for high-performance all-solid-state flexible supercapacitors. *Journal of Materials Chemistry A*, *6*(47), pp.24086-24091.
25. Liu, X., Guan, C., Hu, Y., Zhang, L., Elshahawy, A.M. and Wang, J., 2018. 2D metal–organic frameworks derived nanocarbon arrays for substrate enhancement in flexible supercapacitors. *Small*, *14*(43), p.1702641.
26. Zhou, S., Kong, X., Zheng, B., Huo, F., Strømme, M. and Xu, C., 2019. Cellulose nanofiber@ conductive metal–organic frameworks for high-performance flexible supercapacitors. *ACS Nano*, *13*(8), pp.9578-9586.
27. Kim, S.K., Kim, H.J., Lee, J.C., Braun, P.V. and Park, H.S., 2015. Extremely durable, flexible supercapacitors with greatly improved performance at high temperatures. *ACS nano*, *9*(8), pp.8569-8577.
28. Shao, G., Yu, R., Zhang, X., Chen, X., He, F., Zhao, X., Chen, N., Ye, M. and Liu, X.Y., 2020. Making stretchable hybrid supercapacitors by knitting non-stretchable metal fibers. *Advanced Functional Materials*, *30*(35), p.2003153.
29. Palchoudhury, S., Ramasamy, K., Gupta, R.K. and Gupta, A., 2019. Flexible supercapacitors: A materials perspective. *Frontiers in Materials*, *5*, p.83.
30. Liang, J., Tian, B., Li, S., Jiang, C. and Wu, W., 2020. All-printed MnHCF-MnOX-based high-performance flexible supercapacitors. *Advanced Energy Materials*, *10*(12), p.2000022.
31. Xie, P., Yuan, W., Liu, X., Peng, Y., Yin, Y., Li, Y. and Wu, Z., 2020. Advanced carbon nanomaterials for state-of-the-art flexible supercapacitors. *Energy Storage Materials*.
32. Choi, C., Lee, J.A., Choi, A.Y., Kim, Y.T., Lepró, X., Lima, M.D., Baughman, R.H. and Kim, S.J., 2014. Flexible supercapacitor made of carbon nanotube yarn with internal pores. *Advanced Materials*, *26*(13), pp.2059-2065.
33. Yi, C.Q., Zou, J.P., Yang, H.Z. and Xian, L.E.N.G., 2018. Recent advances in pseudocapacitor electrode materials: Transition metal oxides and nitrides. *Transactions of Nonferrous Metals Society of China*, *28*(10), pp.1980-2001.

34. Ajdari, F.B., Kowsari, E., Shahrak, M.N., Ehsani, A., Kiaei, Z., Torkzaban, H., Ershadi, M., Eshkalak, S.K., Haddadi-Asl, V., Chinnappan, A. and Ramakrishna, S., 2020. A review on the field patents and recent developments over the application of metal organic frameworks (MOFs) in supercapacitors. *Coordination Chemistry Reviews*, *422*, p.213441.
35. Sundriyal, S., Kaur, H., Bhardwaj, S.K., Mishra, S., Kim, K.H. and Deep, A., 2018. Metal-organic frameworks and their composites as efficient electrodes for supercapacitor applications. *Coordination Chemistry Reviews*, *369*, pp.15-38.
36. Wang, Y., Ding, Y., Guo, X. and Yu, G., 2019. Conductive polymers for stretchable supercapacitors. *Nano Research*, pp.1-10.
37. Yue, T., Xia, C., Liu, X., Wang, Z., Qi, K. and Xia, B.Y., 2021. Design and synthesis of conductive metal-organic frameworks and their composites for supercapacitors. *ChemElectroChem*, *8*(6), pp.1021-1034.
38. Shin, S. and Shin, M.W., 2021. Nickel metal–organic framework (Ni-MOF) derived NiO/C@ CNF composite for the application of high performance self-standing supercapacitor electrode. *Applied Surface Science*, *540*, p.148295.
39. Choudhary, R.B., Ansari, S. and Purty, B., 2020. Robust electrochemical performance of polypyrrole (PPy) and polyindole (PIn) based hybrid electrode materials for supercapacitor application: A review. *Journal of Energy Storage*, *29*, p.101302.
40. Liu, X., Zhang, L. and Wang, J., 2020. Design strategies for MOF-derived porous functional materials: Preserving surfaces and nurturing pores. *Journal of Materiomics*.
41. Lu, X.F., Fang, Y., Luan, D. and Lou, X.W.D., 2021. Metal–organic frameworks derived functional materials for electrochemical energy storage and conversion: A mini review. *Nano Letters*, *21*(4), pp.1555-1565.
42. Tian, D., Wang, C. and Lu, X., 2021. Metal–organic frameworks and their derived functional materials for supercapacitor electrode application. *Advanced Energy and Sustainability Research*, p.2100024.
43. Zhao, D., Zhang, Q., Chen, W., Yi, X., Liu, S., Wang, Q., Liu, Y., Li, J., Li, X. and Yu, H., 2017. Highly flexible and conductive cellulose-mediated PEDOT: PSS/MWCNT composite films for supercapacitor electrodes. *ACS Applied Materials & Interfaces*, *9*(15), pp.13213-13222.

44. Xiao, M., Zhao, C., Chen, H., Yang, B. and Wang, J., 2012. “Ship-in-a-bottle” growth of noble metal nanostructures. *Advanced Functional Materials*, *22*(21), pp.4526-4532.
45. Corma, A. and Garcia, H., 2004. Supramolecular host-guest systems in zeolites prepared by ship-in-a-bottle synthesis. *European Journal of Inorganic Chemistry*, *2004*(6), pp.1143-1164.
46. De Decker, J., Folens, K., De Clercq, J., Meledina, M., Van Tendeloo, G., Du Laing, G. and Van der Voort, P., 2017. Ship-in-a-bottle CMPO in MIL-101 (Cr) for selective uranium recovery from aqueous streams through adsorption. *Journal of hazardous materials*, *335*, pp.1-9.
47. Wang, G., Li, Y. and Jin, Z., 2020. “Ship in a bottle” design of ZIF-9@ CoAl LDH hybrid compound as a high performance asymmetric supercapacitor. *New Journal of Chemistry*, *44*(18), pp.7528-7540.
48. Evans, J.D., Sumby, C.J. and Doonan, C.J., 2014. Post-synthetic metalation of metal–organic frameworks. *Chemical Society Reviews*, *43*(16), pp.5933-5951.
49. Szczęśniak, B., Borysiuk, S., Choma, J. and Jaroniec, M., 2020. Mechanochemical synthesis of highly porous materials. *Materials Horizons*, *7*(6), pp.1457-1473.
50. Wei, T.H., Wu, S.H., Huang, Y.D., Lo, W.S., Williams, B.P., Chen, S.Y., Yang, H.C., Hsu, Y.S., Lin, Z.Y., Chen, X.H. and Kuo, P.E., 2019. Rapid mechanochemical encapsulation of biocatalysts into robust metal–organic frameworks. *Nature Communications*, *10*(1), pp.1-8.
51. Zhao, X., Gong, L., Wang, C., Wang, C., Yu, K. and Zhou, B., 2020. A facile grinding method for the synthesis of 3D Ag metal–organic frameworks (MOFs) containing Ag6Mo7O24 for high-performance supercapacitors. *Chemistry–A European Journal*, *26*(20), pp.4613-4619.
52. Guo, Z., Zheng, W., Yan, X., Dai, Y., Ruan, X., Yang, X., Li, X., Zhang, N. and He, G., 2020. Ionic liquid tuning nanocage size of MOFs through a two-step adsorption/infiltration strategy for enhanced gas screening of mixed-matrix membranes. *Journal of Membrane Science*, *605*, p.118101.
53. Miao, Y., Zhang, K., Liu, B., Lin, W., Zhang, H., Lu, Y. and Yao, J., 2012. Ferrofluid-infiltrated microstructured optical fiber long-period grating. *IEEE Photonics Technology Letters*, *25*(3), pp.306-309.

54. Kockrick, E., Lescouet, T., Kudrik, E.V., Sorokin, A.B. and Farrusseng, D., 2011. Synergistic effects of encapsulated phthalocyanine complexes in MIL-101 for the selective aerobic oxidation of tetralin. *Chemical Communications*, *47*(5), pp.1562-1564.
55. Houk, R.J., Jacobs, B.W., Gabaly, F.E., Chang, N.N., Talin, A.A., Graham, D.D., House, S.D., Robertson, I.M. and Allendorf, M.D., 2009. Silver cluster formation, dynamics, and chemistry in metal−organic frameworks. *Nano Letters*, *9*(10), pp.3413-3418.
56. Morabito, J.V., Chou, L.Y., Li, Z., Manna, C.M., Petroff, C.A., Kyada, R.J., Palomba, J.M., Byers, J.A. and Tsung, C.K., 2014. Molecular encapsulation beyond the aperture size limit through dissociative linker exchange in metal–organic framework crystals. *Journal of the American Chemical Society*, *136*(36), pp.12540-12543.
57. Morabito, J.V., Chou, L.Y., Li, Z., Manna, C.M., Petroff, C.A., Kyada, R.J., Palomba, J.M., Byers, J.A. and Tsung, C.K., 2014. Molecular encapsulation beyond the aperture size limit through dissociative linker exchange in metal–organic framework crystals. *Journal of the American Chemical Society*, *136*(36), pp.12540-12543.
58. Li, B., Zhang, Y., Ma, D., Ma, T., Shi, Z. and Ma, S., 2014. Metal-cation-directed de novo assembly of a functionalized guest molecule in the nanospace of a metal–organic framework. *Journal of the American Chemical Society*, *136*(4), pp.1202-1205.
59. Yu, J., Mu, C., Yan, B., Qin, X., Shen, C., Xue, H. and Pang, H., 2017. Nanoparticle/MOF composites: Preparations and applications. *Materials Horizons*, *4*(4), pp.557-569.
60. Stassin, T., Stassen, I., Marreiros, J., Cruz, A.J., Verbeke, R., Tu, M., Reinsch, H., Dickmann, M., Egger, W., Vankelecom, I.F. and De Vos, D.E., 2020. Solvent-free powder synthesis and MOF-CVD thin films of the large-pore metal–organic framework MAF-6. *Chemistry of Materials*, *32*(5), pp.1784-1793.
61. Huang, J.K., Saito, N., Cai, Y., Wan, Y., Cheng, C.C., Li, M., Shi, J., Tamada, K., Tung, V.C., Li, S. and Li, L.J., 2020. Steam-assisted chemical vapor deposition of zeolitic imidazolate framework. *ACS Materials Letters*, *2*(5), pp.485-491.
62. Hermes, S., Schröder, F., Amirjalayer, S., Schmid, R. and Fischer, R.A., 2006. Loading of porous metal–organic open frameworks with organometallic CVD precursors: Inclusion compounds of the type [L n M] a@ MOF-5. *Journal of Materials Chemistry*, *16*(25), pp.2464-2472.

63. Yoshimaru, S., Sadakiyo, M., Staykov, A., Kato, K. and Yamauchi, M., 2017. Modulation of the catalytic activity of Pt nanoparticles through charge-transfer interactions with metal–organic frameworks. *Chemical Communications*, *53*(50), pp.6720-6723.
64. Sadakiyo, M., Yoshimaru, S., Kasai, H., Kato, K., Takata, M. and Yamauchi, M., 2016. A new approach for the facile preparation of metal–organic framework composites directly contacting with metal nanoparticles through arc plasma deposition. *Chemical Communications*, *52*(54), pp.8385-8388.
65. Bogaerts, T., Van Yperen-De Deyne, A., Liu, Y.Y., Lynen, F., Van Speybroeck, V. and Van der Voort, P., 2013. Mn-salen@ MIL101 (Al): A heterogeneous, enantioselective catalyst synthesized using a 'bottle around the ship' approach. *Chemical Communications*, *49*(73), pp.8021-8023.
66. Chen, D.M., Zhang, N.N., Liu, C.S. and Du, M., 2017. Dual-emitting Dye@ MOF composite as a self-calibrating sensor for 2, 4, 6-trinitrophenol. *ACS Applied Materials & Interfaces*, *9*(29), pp.24671-24677.
67. Chang, X., Yang, X.F., Qiao, Y., Wang, S., Zhang, M.H., Xu, J., Wang, D.H. and Bu, X.H., 2020. Confined heteropoly blues in defected Zr-MOF (bottle around ship) for high-efficiency oxidative desulfurization. *Small*, *16*(14), p.1906432.
68. Lin, R., Shen, L., Ren, Z., Wu, W., Tan, Y., Fu, H., Zhang, J. and Wu, L., 2014. Enhanced photocatalytic hydrogen production activity via dual modification of MOF and reduced graphene oxide on CdS. *Chemical Communications*, *50*(62), pp.8533-8535.
69. Liang, R., Jing, F., Shen, L., Qin, N. and Wu, L., 2015. M@ MIL-100 (Fe)(M= Au, Pd, Pt) nanocomposites fabricated by a facile photodeposition process: Efficient visible-light photocatalysts for redox reactions in water. *Nano Research*, *8*(10), pp.3237-3249.
70. Shen, L., Liang, S., Wu, W., Liang, R. and Wu, L., 2013. CdS-decorated UiO–66 (NH 2) nanocomposites fabricated by a facile photodeposition process: An efficient and stable visible-light-driven photocatalyst for selective oxidation of alcohols. *Journal of Materials Chemistry A*, *1*(37), pp.11473-11482.
71. Feng, L., Yuan, S., Zhang, L.L., Tan, K., Li, J.L., Kirchon, A., Liu, L.M., Zhang, P., Han, Y., Chabal, Y.J. and Zhou, H.C., 2018. Creating hierarchical pores by controlled linker thermolysis in multivariate metal–organic frameworks. *Journal of the American Chemical Society*, *140*(6), pp.2363-2372.

72. Huang, K.X., Hua, J., Chang, G.G., Li, Z., Tian, G., Chen, M.J., Li, J.X., Ke, S.C., Yang, X.Y. and Chen, B., 2021. Confined thermolysis for oriented N-doped carbon supported Pd toward stable catalytic and energy storage applications. *Small*, *17*(22), p.2002811.
73. Yan, X., Li, X., Yan, Z. and Komarneni, S., 2014. Porous carbons prepared by direct carbonization of MOFs for supercapacitors. *Applied Surface Science*, *308*, pp.306-310.
74. Wang, D.G., Liang, Z., Gao, S., Qu, C. and Zou, R., 2020. Metal-organic framework-based materials for hybrid supercapacitor application. *Coordination Chemistry Reviews*, *404*, p.213093.
75. Wang, R., Hu, Y., Pan, Z. and Wang, J., 2020. MOF-derived manganese oxide/carbon nanocomposites with raised capacitance for stable asymmetric supercapacitor. *RSC Advances*, *10*(57), pp.34403-34412.
76. Emam, H.E., Abdelhameed, R.M. and Ahmed, H.B., 2020. Adsorptive performance of MOFs and MOF containing composites for clean energy and safe environment. *Journal of Environmental Chemical Engineering*, p.104386.
77. Wu, Z., Zhu, Y., Ji, X. and Banks, C.E., 2016. Transition metal oxides as supercapacitor materials. In *Nanomaterials in Advanced Batteries and Supercapacitors* (pp.317-344). Springer, Cham.
78. Adarsh, N.N., 2017. Metal–organic framework (MOF)–derived metal oxides for supercapacitors. In *Metal Oxides in Supercapacitors* (pp.165-192). Elsevier.
79. Javed, M.S., Shaheen, N., Hussain, S., Li, J., Shah, S.S.A., Abbas, Y., Ahmad, M.A., Raza, R. and Mai, W., 2019. An ultra-high energy density flexible asymmetric supercapacitor based on hierarchical fabric decorated with 2D bimetallic oxide nanosheets and MOF-derived porous carbon polyhedra. *Journal of Materials Chemistry A*, *7*(3), pp.946-957.
80. Zhang, C., Xiao, J., Lv, X., Qian, L., Yuan, S., Wang, S. and Lei, P., 2016. Hierarchically porous Co 3 O 4/C nanowire arrays derived from a metal–organic framework for high performance supercapacitors and the oxygen evolution reaction. *Journal of Materials Chemistry A*, *4*(42), pp.16516-16523.
81. Dai, E., Xu, J., Qiu, J., Liu, S., Chen, P. and Liu, Y., 2017. Co@ Carbon and Co 3 O 4@ Carbon nanocomposites derived from a single MOF for supercapacitors. *Scientific Reports*, *7*(1), pp.1-11.

82. Neisi, Z., Ansari-Asl, Z. and Dezfuli, A.S., 2019. Polyaniline/Cu (II) metal-organic frameworks composite for high performance supercapacitor electrode. *Journal of Inorganic and Organometallic Polymers and Materials*, *29*(6), pp.1838-1847.
83. Wang, L., Feng, X., Ren, L., Piao, Q., Zhong, J., Wang, Y., Li, H., Chen, Y. and Wang, B., 2015. Flexible solid-state supercapacitor based on a metal–organic framework interwoven by electrochemically-deposited PANI. *Journal of the American Chemical Society*, *137*(15), pp.4920-4923.
84. Zhu, C., He, Y., Liu, Y., Kazantseva, N., Saha, P. and Cheng, Q., 2019. ZnO@ MOF@ PANI core-shell nanoarrays on carbon cloth for high-performance supercapacitor electrodes. *Journal of Energy Chemistry*, *35*, pp.124-131.
85. Yan, J., Wang, H., Jin, B., Zeng, M. and Peng, R., 2021. Cu-MOF derived Cu/Cu2O/C nanocomposites for the efficient thermal decomposition of ammonium perchlorate. *Journal of Solid State Chemistry*, *297*, p.122060.
86. Kaneti, Y.V., Tang, J., Salunkhe, R.R., Jiang, X., Yu, A., Wu, K.C.W. and Yamauchi, Y., 2017. Nanoarchitectured design of porous materials and nanocomposites from metal-organic frameworks. *Advanced Materials*, *29*(12), p.1604898.
87. Zheng, S., Li, Q., Xue, H., Pang, H. and Xu, Q., 2020. A highly alkaline-stable metal oxide@ metal–organic framework composite for high-performance electrochemical energy storage. *National Science Review*, *7*(2), pp.305-314.
88. Guan, C., Liu, X., Ren, W., Li, X., Cheng, C. and Wang, J., 2017. Rational design of metal-organic framework derived hollow NiCo2O4 arrays for flexible supercapacitor and electrocatalysis. *Advanced Energy Materials*, *7*(12), p.1602391.
89. Eftekhari, A., Li, L. and Yang, Y., 2017. Polyaniline supercapacitors. *Journal of Power Sources*, *347*, pp.86-107.
90. Guo, S., Zhu, Y., Yan, Y., Min, Y., Fan, J., Xu, Q. and Yun, H., 2016. (Metal-organic framework)-Polyaniline sandwich structure composites as novel hybrid electrode materials for high-performance supercapacitor. *Journal of Power Sources*, *316*, pp.176-182.
91. Wang, Q., Shao, L., Ma, Z., Xu, J., Li, Y. and Wang, C., 2018. Hierarchical porous PANI/MIL-101 nanocomposites based solid-state flexible supercapacitor. *Electrochimica Acta*, *281*, pp.582-593.

92. Iqbal, M.Z., Faisal, M.M., Ali, S.R., Farid, S. and Afzal, A.M., 2020. Co-MOF/polyaniline-based electrode material for high performance supercapattery devices. *Electrochimica Acta*, *346*, p.136039.
93. Zhang, H., Wang, J., Sun, Y., Zhang, X., Yang, H. and Lin, B., 2021. Wire spherical-shaped Co-MOF electrode materials for high-performance all-solid-state flexible asymmetric supercapacitor device. *Journal of Alloys and Compounds*, *879*, p.160423.
94. Shao, L., Wang, Q., Ma, Z., Ji, Z., Wang, X., Song, D., Liu, Y. and Wang, N., 2018. A high-capacitance flexible solid-state supercapacitor based on polyaniline and metal-organic framework (UiO-66) composites. *Journal of Power Sources*, *379*, pp.350-361.
95. Li, D.J., Lei, S., Wang, Y.Y., Chen, S., Kang, Y., Gu, Z.G. and Zhang, J., 2018. Helical carbon tubes derived from epitaxial Cu-MOF coating on textile for enhanced supercapacitor performance. *Dalton Transactions*, *47*(16), pp.5558-5563.
96. Fu, D., Li, H., Zhang, X.M., Han, G., Zhou, H. and Chang, Y., 2016. Flexible solid-state supercapacitor fabricated by metal-organic framework/graphene oxide hybrid interconnected with PEDOT. *Materials Chemistry and Physics*, *179*, pp.166-173.
97. Sundriyal, S., Shrivastav, V., Kaur, H., Mishra, S. and Deep, A., 2018. High-performance symmetrical supercapacitor with a combination of a ZIF-67/rGO composite electrode and a redox additive electrolyte. *ACS Omega*, *3*(12), pp.17348-17358.
98. Xu, X., Tang, J., Qian, H., Hou, S., Bando, Y., Hossain, M.S.A., Pan, L. and Yamauchi, Y., 2017. Three-dimensional networked metal–organic frameworks with conductive polypyrrole tubes for flexible supercapacitors. *ACS Applied Materials & Interfaces*, *9*(44), pp.38737-38744.

Chapter 4: Dual-ligand Metal-Organic framework-derived supercapacitor electrodes for improved energy storage

Abstract

Because of its high capacitance value, low cost, and stability, nickel oxide (NiO) has emerged as a viable active material for the production of supercapacitor electrodes. The weak conductivity of NiO, on the other hand, has an impact on its electrochemical energy storage ability. A double-linker MOF approach was used in this study, with a pristine nickel-based metal-organic framework (Ni-MOF) being synthesized by solvothermal synthesis and subsequently changed into nickel oxide and nickel oxide/nickel composite electrodes by heating in air at various temperatures. With NiO/Ni calcined at 400 degrees Celsius, the best supercapacitor performance was attained (753 Fg^{-1} at 1 Ag^{-1}). The electrode material was cyclically stable as well, with 90% of the capacitance staying constant after 1000 cycles. With respect to the scan rates of the investigated electrodes, electrochemical kinetics investigation revealed the pseudocapacitive behavior of the MOF-derived electrode materials. The method described in this paper might be applied to develop alternative materials for use in high-performance supercapacitor applications.

Keywords: Nickel oxide, cycle, energy storage, capacitance, kinetics

4.1 Introduction

Fossil fuels have unquestionably grown significance in the energy industry during the last several decades, as their use continues to rise as a result of the world's growing population and technological improvements [1]. Biomass and other natural resources can be used to produce electricity [2]. All these problems can be overcome by shifting our attention to other sources of energy such as renewables. Electrochemical devices such as supercapacitors can be used to store this energy to make them valuable for future use [3].

Supercapacitors, also known as ultracapacitors, are high-efficiency energy storage devices with low internal resistance that may yield high energy density due to their unique storing mechanism [4,5]. Supercapacitors outlast regular batteries and offer a higher power density. They are also easier to maintain. Materials that form the brainbox of supercapacitors are numerous and include but not limited to carbon materials, metal oxides among others [6-10].

Although starting materials are critical to supercapacitor performance, they all have disadvantages. For instance, metal oxides have better capacitance value but low electrical conductance, whereas carbon-based compounds conduct better and show better performance [11,12]. The polymers that can conduct electricity show good performance, but their stability is low [13]. Other materials with intriguing properties have made hot research headlines around the globe in seeking to fabricate supercapacitors with superior performance [14,15].

Because of their interesting features such as ease of functionalization, flexibility among others, metal-organic frameworks (MOFs) have recently emerged as promising candidates for the fabrication of electrode materials for supercapacitor applications [16]. Despite these advantages, MOFs' weakness to conduct electricity and limited response to thermal behavior may restrict their storage performance [17]. MOFs are, therefore, either converted into derivative compounds such as oxides of metals to alleviate this problem, or form a composite with others while their structures remain intact [18].

Metal oxide study has been stepped up in order to eliminate the organics found in MOF structures while also converting metal nodes to oxides of metals without much effect on pore properties [19]. He et al., for example, used calcination at various temperatures to produce nickel oxide with hexagonal shape from parent metal-organic frameworks while maintaining the structure of the

pristine MOF [20]. At a current density of 1 A/g, the MOF-derived NiO had capacitance value of 485 F/g and retained around 87 percent after 5000 cycles. Han et al., for example, used the same nickel-MOF as a platform to create a three-dimensional nickel oxide with outstanding supercapacitor performance [21]. However, when compared to NiO's of 2,584 F/g, the capacitance of the synthesized electrode was small. As a result, their potential usage as supercapacitors may be limited [22]. Incorporating a functional substituent into metal-organic framework-based materials, on the other hand, will give better storage capacity, because metals generally when added increase conductivity and reduce the length between the electrode and the metal and hence store energy more strongly [23]. As a result, as has been widely documented in the literature [24-27], a method has to be established to successfully incorporate the needed features without presenting new sources of carbon. As a result, nickel oxide electrode will be positioned to provide exceptional storage performance.

This chapter describes the facile preparation of a nickel oxide/nickel electrode materials using a dual-ligand metal-organic framework method. MOFs that possess larger surface areas tend to interact more closely with the electrolyte ions, leading to poor electrochemical energy storage performance, since organic linkers frequently utilized in MOFs serve to manage the porosity and the manner with which the ions conduct electricity. As a consequence, the original nickel-MOF with two linkers was used in conjunction with precise fabrication circumstances to produce electrodes interesting characteristics. Surprisingly, the Ni-MOF founded on double-linkers has never been reported to be instrumental in the design of supercapacitors.

The pristine nickel-metal organic framework, which is made up of H_3BTC (benzenetricarboxylic acid) and 2-methylimidazole (2-MeIM) as ligands, was annealed at several temperatures to find the optimal range for the derivative electrodes to store the maximum energy. In comparison, the as-prepared nickel oxide/nickel electrode material performed well due to the synergistic effects of the generated NiO with Ni. The derivative nickel oxide/nickel composite electrode shown excellent performance of 753 F/g at 1 current density (A/g) during electrochemical testing, and the highest energy density of 26 Wh/kg and a power density of 2393 W/kg. The electrode showed good rate capability after 1000 charge-discharge cycles, with ninety percent preservation of the original material. Furthermore, knowledge of the created materials' storage device showed their

pseudocapacitive activity. Oxides of other metals and their composites can also be made using this method.

4.2 Experimental

4.2.1 Preparation of Ni-MOF

The solvothermal approach was used to make the double-linker Ni-MOF, with minor alterations to the method published in the literature [28]. 1.5 mmol nickel nitrate salt, 1.5 mmol 2-methylimidazole, and 1.5 mmol H_3BTC were dissolved in 105 mL DMF and agitated continuously at room temperature for 40 minutes. After being moved to a Teflon-lined autoclave, the solution was heated at 150 ^oC for 2 days. The mixture was centrifuged and carefully rinsed with DMF and then ethanol after the reaction. To make a double-linker Ni-MOF, the powder was dried overnight in a vacuum oven at 70 ^oC.

4.2.2 Preparation of a Nickel oxide/nickel composite electrode

The NiO/Ni composite materials were made by heating the Ni-MOF dual ligand at 400, 500, and 600 ^oC in air for 3 h at 5 $^oCmin^{-1}$. The resultant products were named after each temperature respectively.

4.2.3 Preparation of the working electrode

Three pieces of nickel foam (NF) (1cm x 1cm) were soaked in 20 mL 3 M hydrochloric acid under sonication for 1 hour to remove surface oxides before being coated with active ingredients. The foam was then thoroughly washed in water and then ethanol before being dried in a vacuum oven overnight. The working electrodes were subsequently made by combining an 8:1:1 (w/w) ratio of the MOF-based nickel oxide/nickel composite material, carbon black, and a PTFE binder in a homogenous slurry. This was applied on a clean nickel foam current collector and dried for 12 hours in a vacuum oven at 70 degrees Celsius. After crushing the Ni foam at 10 bar for 10s, the functioning electrode was achieved. The active substance weighed 3.5 to 4.5 mg, based on the change in mass between the nickel foam before and after loading. This preparation procedure is illustrated in Figure 4.1.

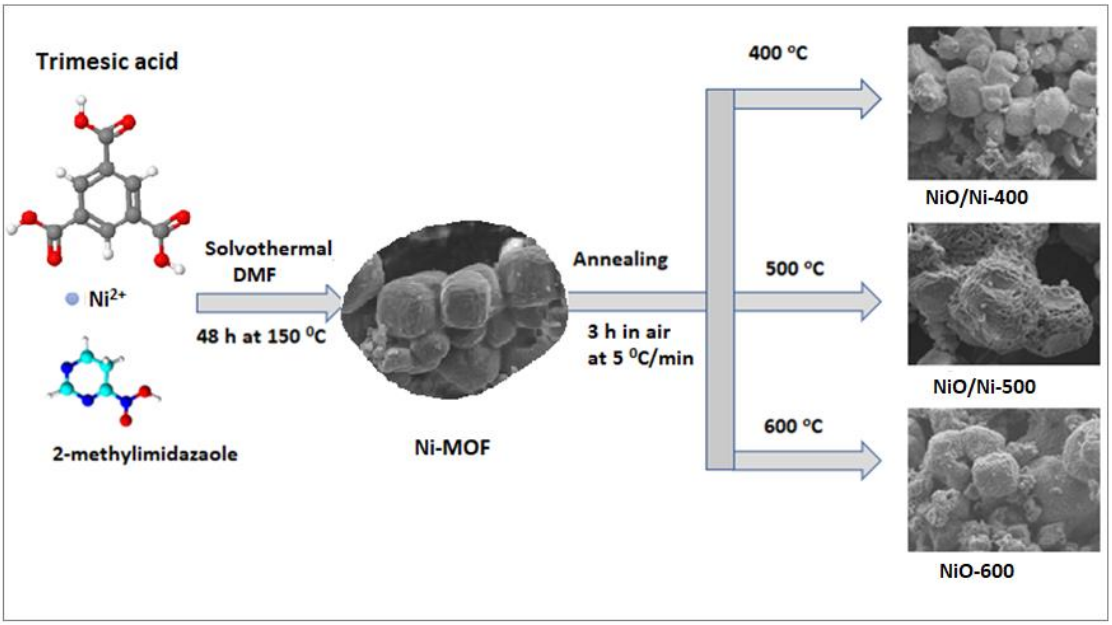

Figure 4.1. The production of nickel oxide/nickel composite electrodes from dual ligand nickel-MOF is depicted.

4.2.4 Electrochemical characterizations

Electrochemical testing of the electrode materials was carried out using a three-electrode configuration in a 3 M KOH electrolyte solution, with NiO/Ni as the working electrode, platinum as the counter electrode, and Ag/AgCl as the reference electrode. Using cyclic voltammetry (CV), galvanostatic charge-discharge (GCD), and electrochemical impedance spectroscopy, the electrochemical properties of the synthesized electrodes were determined (EIS). In the potential range of -0.1 to 0.5 V, the CV was conducted at various scan speeds. GCD studies were carried out using a voltage range of 0-0.5 V and between 1 and 10 A/g. A frequency range of 0.01 to 100 kHz was used for the EIS study.

4.3 Results and discussion

4.3.1 Thermal performance

Thermal gravimetric analysis was employed to test the stability under heat of the dual ligand nickel-MOF in a nitrogen environment. Figure 4.2 depicts the results. The moisture attached to the Ni-MOF surface caused the Ni-MOF to lose 15.9% of its weight at around 110 ^{o}C. Similarly, the weight reduction of 50.6 percent (from 280 to 350 ^{o}C) might be attributable to the Ni-MOF double-

framework linker's disintegration. Consequently, the final heating temperature of the pristine MOF for the preparation of nickel oxide and nickel oxide/nickel materials was set to 400 ºC..

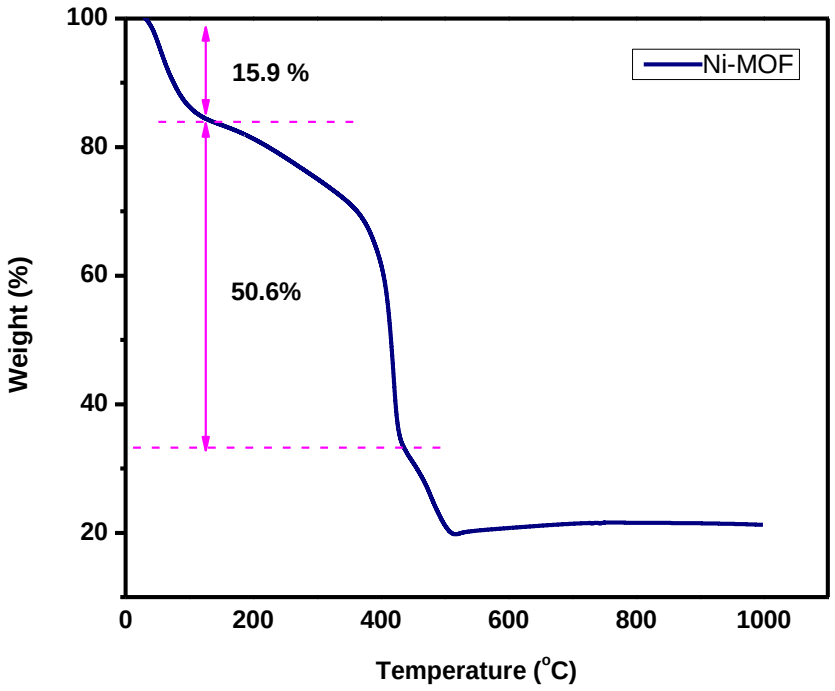

Figure 4.2 TGA plot of mixed-linker Ni-MOF

4.3.2 Phase crystallinity and chemical composition

The crystalline phase and composition of the original dual ligand MOF and the derived nickel oxide electrodes were shown by XRD analysis. The as-prepared dual ligand nickel MOF displays unique peaks ranging from 5 to 30º, which follows the conventional nickel-MOF structure, as shown in Figures 4.3a and 4.3b. This demonstrates that the double-linker technique worked [29]. It also ensured that the resultant nickel oxide and nickel oxide/nickel electrodes were accurately regulated.

The (111), (200), (220), (311), and (222) planes of nickel oxide (JCPDS No: 01-075-0197) were assigned to the standard peaks as indicated in the literature [30]. Similarly, the peaks at 44.5º, 51.8º, and 76.3º (2 theta), the metallic nickel (Ni) ascribed to the (111), (200), and (220) planes (JCPDS 00-004-0850) was detected [31]. At annealing temperatures of 400 ºC and 500 ºC, both verified the effective synthesis of NiO/Ni. The Ni peaks, on the other hand, vanished totally at 600

^{o}C due to the oxidation of Ni to nickel oxide at elevated temperatures, allowing only nickel oxide to develop. Figure 4.3 shows that the conversion of dual ligand MOF into phase pure nickel oxide and nickel oxide/nickel was complete since there were no contamination peaks in the XRD.

Figure 4.3c shows the Fourier Transform Infrared spectra of the nickel-MOF as synthesized, as well as the nickel oxide and nickel oxide/nickel produced by annealing under air at various temperatures. The O-H stretching depicts the coordinated water attached to the parent MOF, with a large peak at 3208 cm^{-1}. The aromatic HCs on the MOF ligand, which are clearly absent in the treated materials, can also be attributed to the strong peaks at 1545, 1428, 1345, and 1098 cm^{-1}. This shows that the framework has been successfully decomposed. The C=O stretching in Ni-MOF is responsible for the band at 1614 cm^{-1}. The Ni-O stretching mode is conserved for metal-organic framework-based nickel oxide and nickel oxide/nickel [32], as seen by the band at 465 cm^{-1}. Other absorption peaks in the calcined materials at 3669 cm^{-1} and 1401 cm^{-1}, respectively, at 400 ^{o}C and 500 ^{o}C, might be ascribed to the moisture vanishing after thermal treatment (600 ^{o}C). The obtained electrode materials' steep peak at 1063 cm^{-1} might be attributed to the -CO bending vibration, which matches to CO_2 absorption from the environment [33].

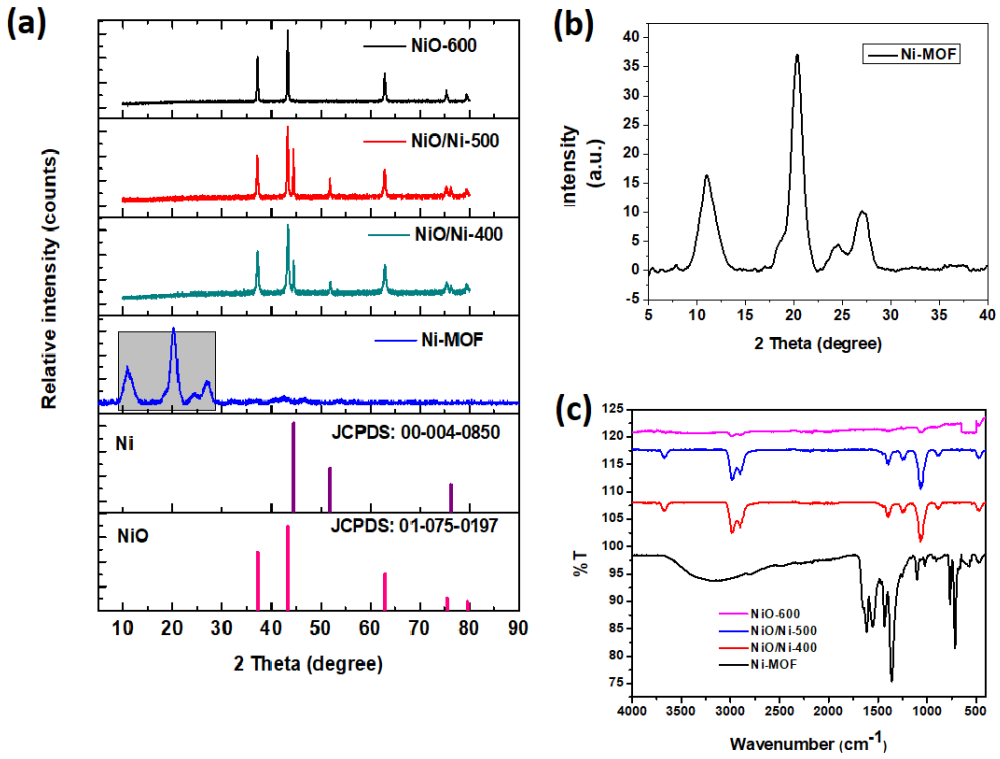

Figure 4.3: Characterization using (a) XRD patterns of the prepared materials. (b) Inset of the XRD pattern of Ni-MOF. (c) FTIR of nickel-MOF and the nickel oxide-derived materials

4.3.2 Surface morphology and elemental composition

SEM and transmission electron microscopy were used to examine the shape and composition of dual ligand MOF and its derivatives electrodes (TEM). The shape of the original nickel-MOF was retained at different heating conditions, according to the SEM data shown in Fig 4.4 (a-d), but the derivative electrodes had a more porous structure. The framework breakdown in Ni-MOF was validated by this. Furthermore, partial oxidation of Ni occurred at lower temperatures (400 ^{o}C and 500 ^{o}C), resulting in the production of NiO supported on Ni. At 600 ^{o}C, however, the metallic Ni fully oxidized to NiO, leaving just NiO behind. The elemental composition of the parent MOF can be seen in the EDS spectra, with Ni, O, and C as the primary ingredients, whereas Ni and O are the main constituents of the nickel oxide/nickel and nickel oxide electrodes. (For further information, see Figure 4.4 e-i.) The existence of a low-intensity C component in MOF-derived electrodes, on the other hand, is due to carbon covering used in analysis

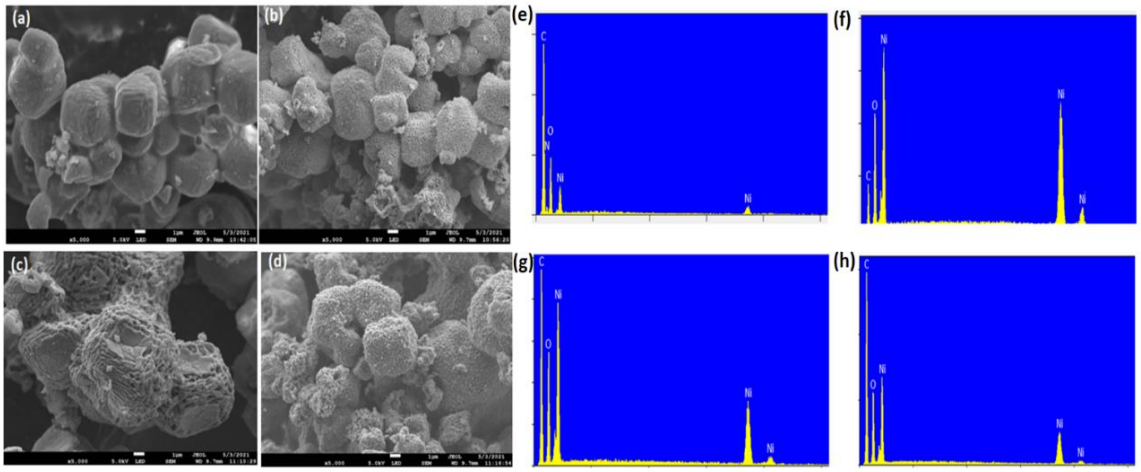

Figure 4.4 SEM and EDX images respectively of the (a,e) Ni-MOF and nickel oxide/nickel and nickel at 400 ºC (b,f) 500 ºC, (d,h) 600 ºC

Figure 4.5(a-d) displays TEM images of the generated NiO/Ni-400, NiO/Ni-500, and NiO electrodes, as well as the associated histogram (Figure 4.5(e-h)), which offer further information about the shape, size, and status of the agglomeration. The calcination of Ni-MOF double-linkers produced nanometer-sized spherical nickel-oxide-nickel composites (Figure 4.5 (b-c)) and NiO-600 electrodes with a rod-like form (Figure 4.5d). When linked to the original Ni-MOF of 59.2 nm, the 400, 500, and 600 ºC showed a well-dispersed morphology, a smooth surface, and a lesser size of 18.50 nm, 17.1 nm, and 49.51 nm, respectively. This demonstrates that the calcination temperature had an effect on the particle size of MOF-derived electrodes, and that the decline in particle size was due to the framework's disintegration into derived metal oxides.

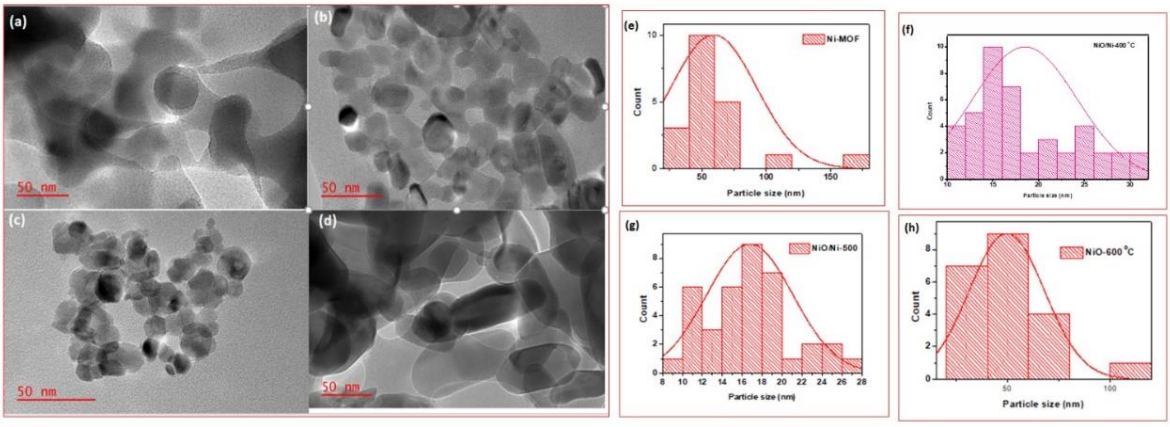

Figure 4.5 TEM images of: (a) Ni-MOF; (b) NiO/Ni-400; (c) NiO/Ni-500; (d) NiO-600. Particle size distribution histograms

4.3.3 Physisorption characteristics

Figure 4.5(a-d) shows TEM images of the calcined materials at 400, 500, and 600 ^{o}C electrodes, as well as the related histogram (Figure 4.5(e-h)), which offer further data about the agglomeration's structure, size, and state. Calcination of Ni-MOF double-linkers led to spherical composites (Figure 4.5 (b-c)) and rod-like nickel oxide-600 electrodes (Figure 4.5d). All the three electrodes displayed particle sizes of 18.50.7 nm, 17.1 nm, and 49.51.3 nm respectively, respectively, when compared to the original MOF of 59.2 nm. This shows that the calcination temperature had an influence on the particle size of the derivatives, and that the particle size reduction was due to the framework disintegrating into generated metal oxides. Likewise, when the ultimate calcination temperature increased, the surface areas and pore diameters decreased. The pore size distribution estimated using the BJH adsorption technique is shown in Figure 4.6b. It has pore sizes ranging from 5-50 nm, which is typical of mesoporous materials. The synthesized electrodes' mesoporous shape is critical for boosting electron and ion transport at the electrode-electrolyte interface, as well as providing an excess of active sites for fast electrochemical reactions.

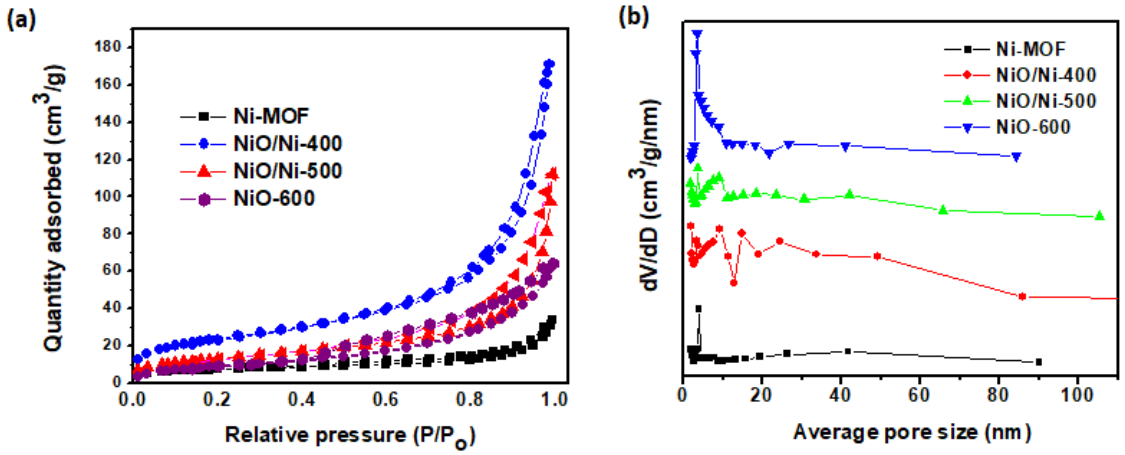

Figure 4.6 Nitrogen adsorption-desorption results. (a) of the parent Ni-MOF and MOF-derived = materials (b) pore size distribution of nickel-MOF and derivative electrodes

Electrochemical performance

The electrochemical activities of the three electrodes in a basic electrolyte using 3 electrodes were assessed based on EIS, cyclic voltammetry and GCD results. Figure 4.7 (a-c) displays the typical cyclic voltammetry curves of the three materials at different scan rates up to 100 mV/s. The curves show pseudocapacitive behavior in the examined potential window and was retained at increased

scan speeds, indicating a high rate competence for supercapacitors. The three curves all displayed oxidation-reduction peaks that may be attributed to the Faradaic chemistry, which is stated as:

$$NiO + OH^- \leftrightarrow NiOOH + e^- \quad (4.4)$$

Besides, when the scan rate increases, both the cathodic and anodic peaks change to higher and lower potential, implying that the Faradaic reaction is regulated by the ion diffusion mechanism [34]. Equally, because the slope of the relationship between the peak current and the square root of the scan rates ($v^{1/2}$) is proportional to the diffusion coefficient, the bigger the slope, the greater the coefficient of diffusion, and the stronger the ion-diffusion procedure of the materials [35]. As a result, the slope of the compared materials shows that nickel oxide/nickel-400 had the most effective ion-diffusion process.

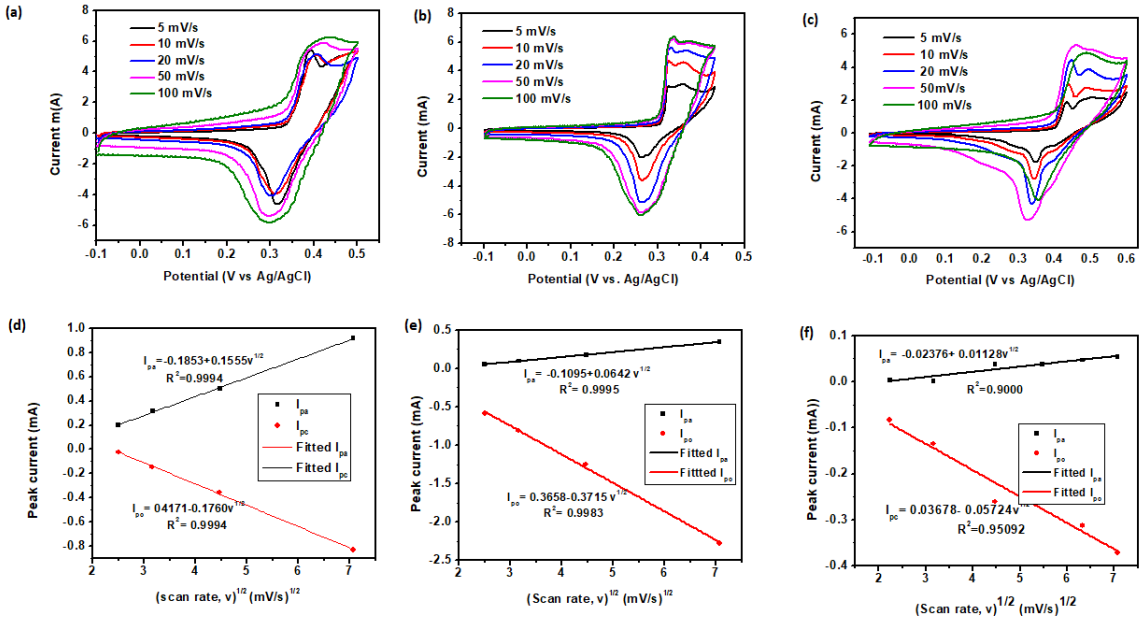

Figure 4.7 Supercapacitor activity of the electrodes. (a-c) CV curves in 3 M basic (KOH) electrolyte and (d-f) the link between the peak current against scan rates for the three electrodes

Figure 4.8 depicts GCD testing performed in the 0 to 0.5 voltage potential window at various current densities (a-d). For all three-electrode materials, the non-linearity of the charge-discharge curves against tested scan rates is typical of pseudocapacitive behavior, as evident in the CV curves [36]. At a current density of 1, the GCD curves were compared and it was observed that the nickel oxide/nickel-400 material has the most extended discharge time, suggesting the best storage

activity (See Figure 4.8a for further information.) Figure 4.8b-d further shows that when the current density increases, the specific capacitance of all three electrodes drops, which may be related to the inadequate reduction-oxidation activity at increased current density. When the capacitance was enhanced to 10 A/g using the electrode calcined at 400 ^{o}C, nearly 85% of the original capacitance valuewas preserved. The active components leaking from the materiak during reaction might be to due to the decrease in capacitance value of nickel oxide/nickel-400 offers the best rate capacity when compared to other electrode materials, such as nickel oxide/nickel-500 (50 percent retention) and nickel oxide-600 (78 percent holding). (For further information, see Figure 4.9a.). Nickel oxide/nickel-400 offers the best rate capacity when compared to other electrode materials, such as nickel oxide/nickel-500 (50 percent retention) and NiO-600 (78 percent holding). (For further information, see Figure 4.9a.) Nickel oxide/nickel rate capacity might be due to its large surface area, as well as the increased conductivity provided by the added Ni. This value, as shown in Table S4.2, is better than certain similar to nickel oxide supercapacitors and equivalent to others. For example, Moholkar and co-workers noted that nickel oxide produced by the solvothermal technique capacitance to a high value of 132 F/g at current density of 1 A/g in basic electrolyte solution [37], whereas Cai and his team established up to 381 F/g at 1 A/g for the composite of nickel oxide and nickel supercapacitor electrode [38]. In addition, the energy density and power density were calculated using equations 4.2 and 4.3, as shown in Table 4.1.

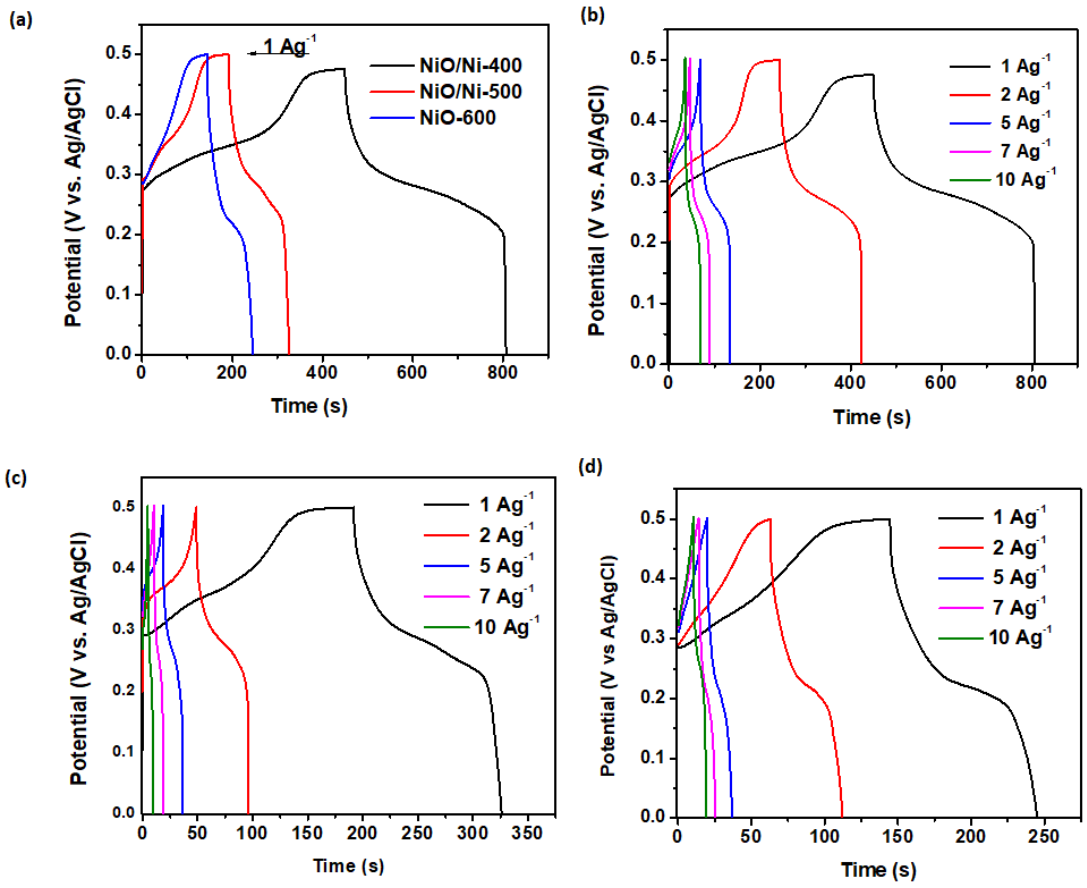

Figure 4.8 Galvanostatic charge-discharge curves of: (a) the comparison of the three electrodes at 1 Ag^{-1}; (b) NiO/Ni-400; (c) NiO/Ni-500; (d) NiO-600.

Moreover, cyclic stability is critical to a supercapacitor's performance in real-world applications [39]. As a result, unceasing cycling experiments at 5 A/g for 1000 cycles were used to appraise the behavior of the three electrodes. As shown in Figure 4.9b, for nickel oxide/nickel-400, Nickel oxide/nickel-500, and nickel oxide-600, respectively, 90 percent, 80 percent, and 85 percent of the original capacitance was kept. Electrochemical impedance spectroscopy was used in a frequency range of 0.01 to 100 kHz to further examine the exact conductance of the electrode materials. Figure 4.9c shows the Nyquist plots that resulted. In the low-frequency range, all of the materials showed a straight line, showing exceptional capacitive performance. The obtained Rs of the solutions for the three materials calcined at 400, 500, and 600 ^{o}C was respectively found to be 0.83, 0.14, and 0.94, based on the intercept of the real axis of the curve obtained from the electrochemical circuit fitting in Figure 4.9c. Meanwhile, the Rct for the charge transferred within the electrolyte ions was respectively 0.5, 0.9, and 1.0. The low charge-transfer resistance for the

nickel oxide/nickel at 400 ^{o}C indicates good electrical conductance, which has a significant impact on the high specific capacitance. The Ragone diagram (energy density versus power density) of the produced electrode materials is shown in Figure 4.9d. The power density of 265 W/kg, the nickel oxide/Ni-400 electrode produced the highest energy density of 26 Wh/kg. The energy density had decreased to 22.6 Whkg^{-1} at a maximum power density of 2390 Wkg^{-1}, which is greater than the synthesized NiO/Ni-500 and NiO-600, as well as some of the reported NiO-based electrodes, such as porous NiO, CNT@NiO, NiCo2O4/N-rGO, and Ni/NiO [40-43]. The preservation of the capacitance values to a great extent among other for the electrode material at 400 ^{o}C make it a befitting material for outstanding supercapacitor performance, according to this research.

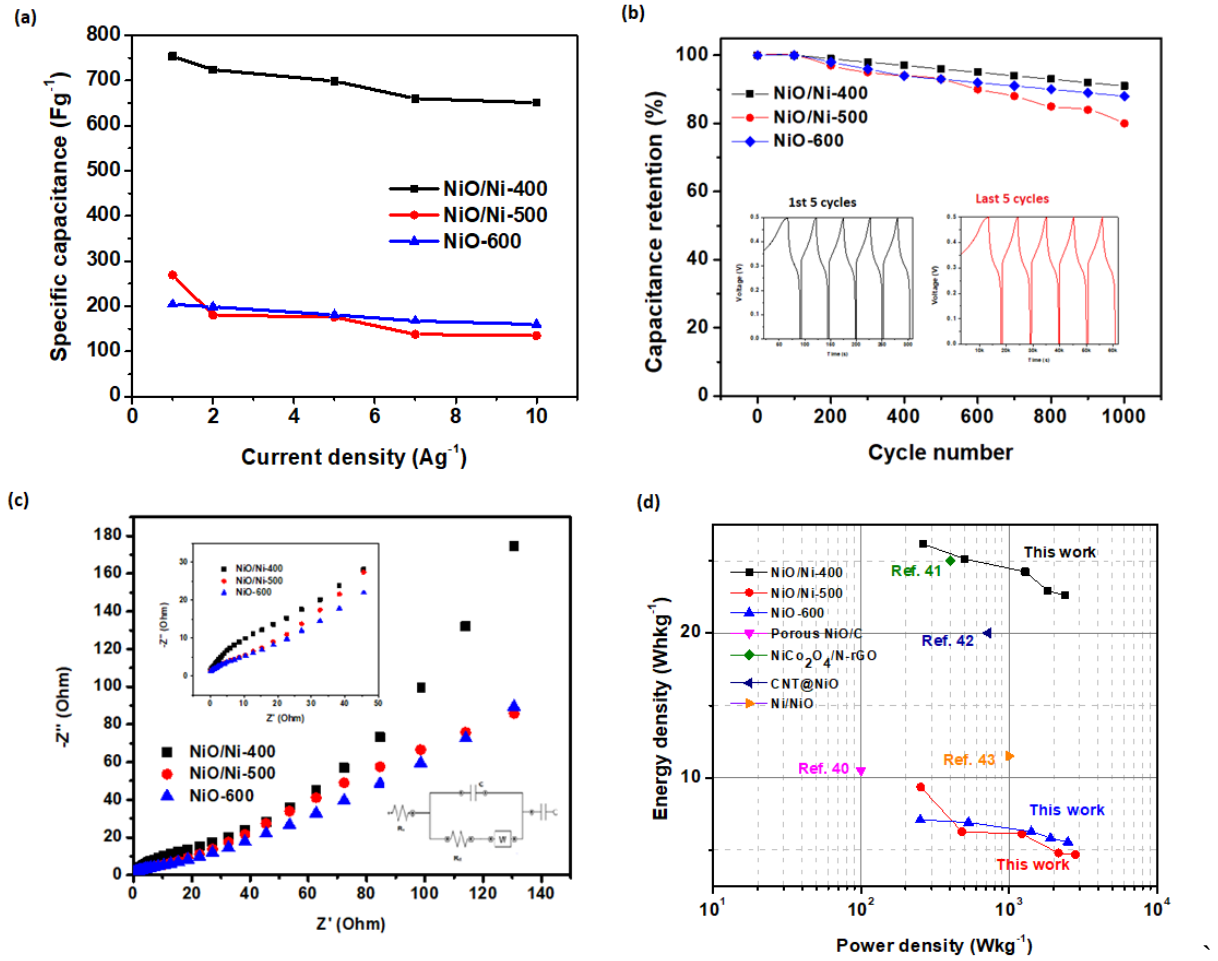

Figure 4.9: (a) Capacitance values of MOF-derived nickel oxides and nickel oxide/nickel electrodes. (b) Cycling stability tests. (c) EIS plots (d) Ragon plots

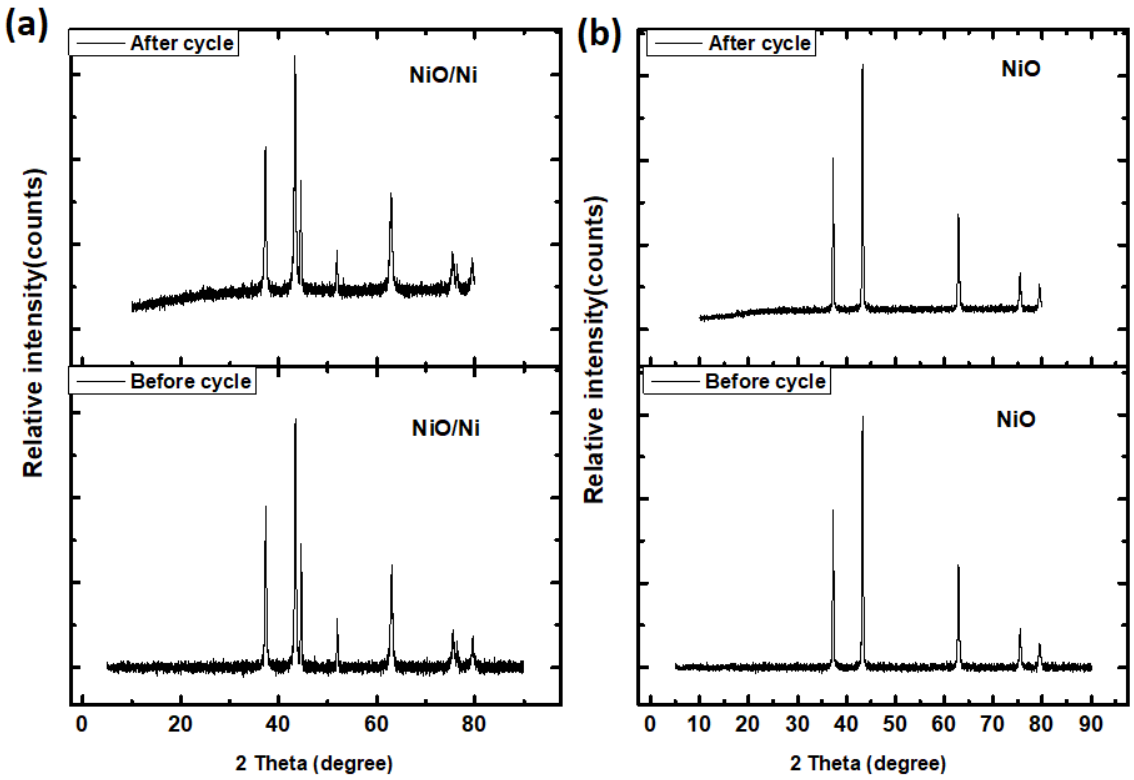

Figure 4.10: XRD patterns of (a) NiO/Ni and (b) NiO after 1000 charge-discharge cycles.

Table 4.1 Electrochemical performance of the NiO/Ni and NiO electrodes

Sample/ Current density	Specific capacitance (F/g)			Energy density (Wh/kg)			Power density (W/kg)		
	NiO/Ni-400	NiO/Ni-500	NIO-600	NiO/Ni-400	NiO/Ni-400	NIO 600	NiO/Ni-400	NiO/Ni-500	NIO-600
1 A/g	753.41	269.44	204.75	26.160	9.35	7.11	264.54	253.23	250.86
2 A/g	724.14	180.63	198.93	25.14	6.27	6.9	500.10	480.42	532.21
5 A/g	698.46	176.19	180.82	24.25	6.11	6.28	1283.68	1223.47	1412.5
7 A/g	660.12	138.16	168.22	22.92	4.79	5.83	1833.68	2158.84	1909.09
10 A/g	650.92	135.06	160.39	22.60	4.68	5.55	2393.09	2813.91	2500.02

After the electrochemical reaction, SEM and TEM were used to examine the surface appearance and structure of the spent electrode materials (NiO and NiO/Ni), as well as the materials' durability after cycling stability tests. (For further information, see Figure 4.11.) Interestingly, the materials'

form and size remained almost intact, which explains the high rate performance found at greater current densities.

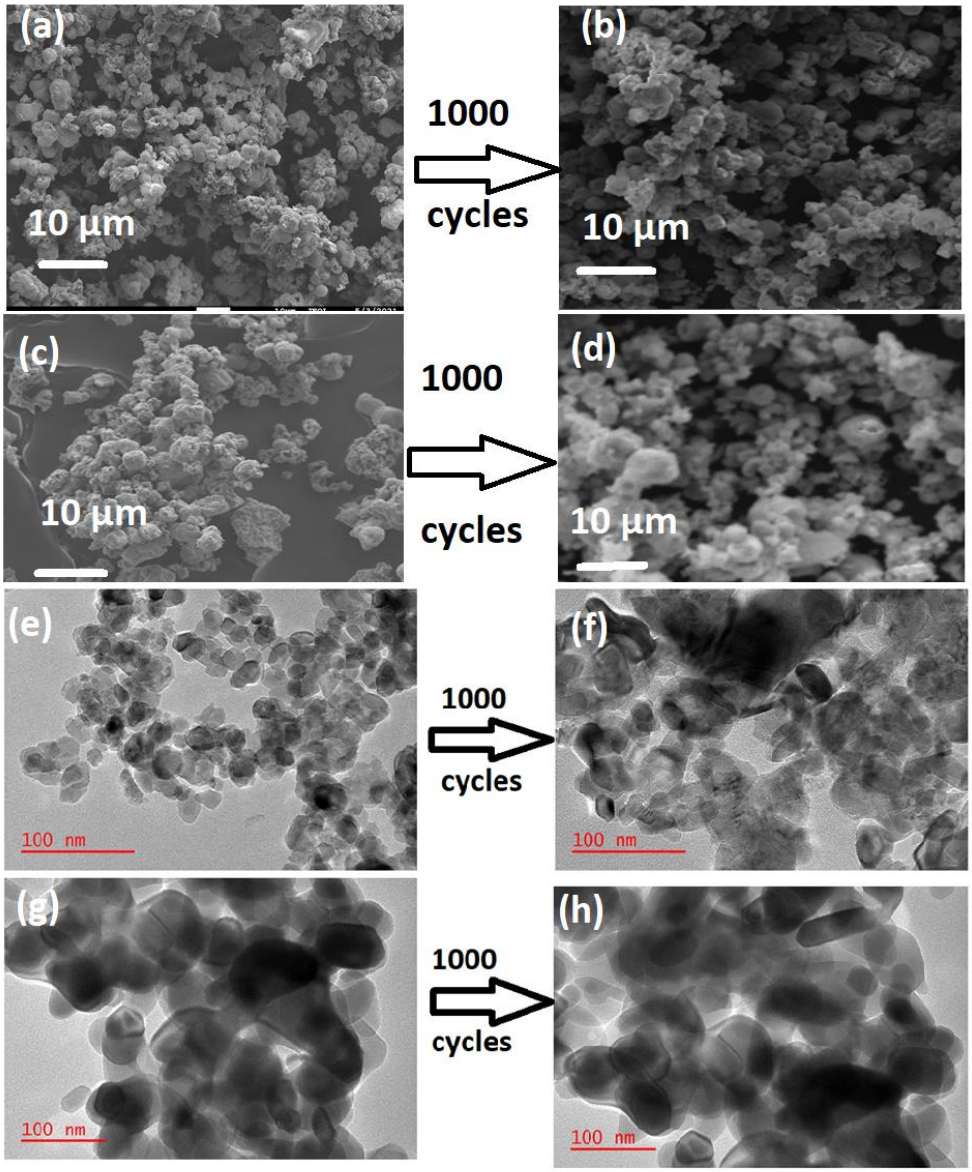

Figure 4.11: SEM images of NiO/Ni-400 (a, b) and NiO-600 (c, d) after 1000 cycles; TEM images

The current (I) and the scan rate (v) relationship can be investigated using Figure 4.10a and equations 4.5 and 4.6 to better understand the mechanism of the top ranking electrode, nickel oxide/nickel-400.

$$i = i_{capacitive} + i_{diffusion} = av^b \quad (4.5)$$

$$\log i = \log a + b \log v \quad (4.6)$$

The parameters a and b are the changeable and may be calculated using the logi and logv curves. When b = 1, the mechanism is surface-controlled; when b equals 0.5, the mechanism is diffusion-controlled [44].

$$i\,(V) = k_1 v + k_2 v^{1/2} \quad (4.7)$$

$$i\,(V)/ v^{1/2} = k_1 v^{1/2} + k_2 \quad (4.8)$$

I (V), $k_1 v$, and $k_2\ v^{1/2}$ denote the total current at any given potential window V, as well as percentages of capacitive and diffusion process, respectively. The values of k_1 (slope) and k_2 (intercept) from the straight line, which correspond to the contribution percentages from the capacitive and diffusion-controlled processes, respectively, were computed from the plot of $I\,(V)/v^{1/2}$ against $v^{1/2}$. (For further information, see Figure 4.12c.) Diffusion-controlled behavior is often observed in battery-like electrodes, but surface-controlled processes have been observed in capacitive and pseudocapacitive electrode materials [45]. The quick reduction-oxidation performance, which permitted outstanding rate capability and reversibility at high scan rates, the capacitive-controlled input to total charge storage increased with a rise in the material scan rate.

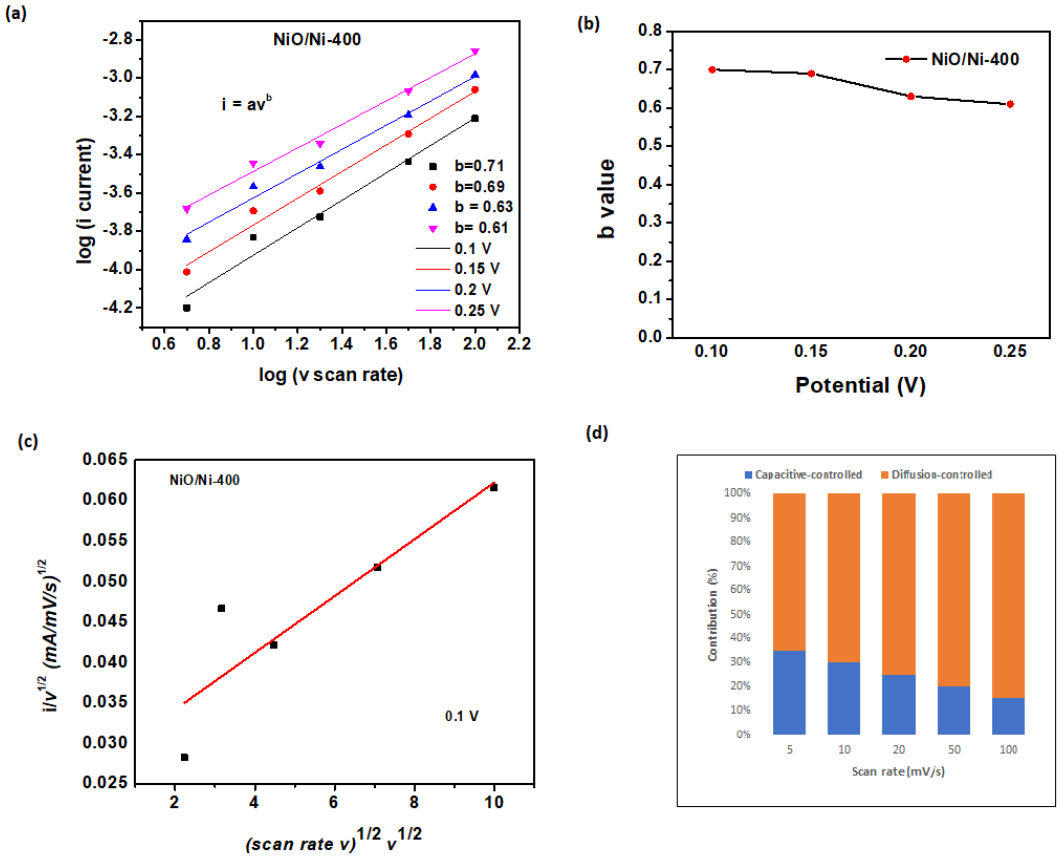

Figure 4.12: Kinetic results of the diffusion and capacitive-controlled processes of the synthesized nickel oxide/nickel electrode materials.

4.4 Conclusion

In conclusion, heating the pristine MOF at varied temperatures, a simple dual ligand method was established to produce nickel oxide and nickel oxide/nickel composite electrodes. Also, to the large surface properties, the best performing electrodes has the combined advantages of redox activity and conductivity. The structural composition, and physicochemical features of the resultant electrode materials were all influenced by the heating conditions. The materials synthesized at 400 degrees Celsius had a capacitance value of 753 F/g, as well as a notable rate capability (up to 85% retention at 10A/g) and strong cycling performance. Furthermore, the material had a high energy density of 26 Wh/kg as well as a good power density. The kinetic result established that all the materials exhibited diffusion-controlled process at different scan rates. This study is critical to fabricating other valuable supercapacitor electrode materials based on metal-organic frameworks

with excellent performance and also holds a great promise towards development of flexible storage devices.

4.6 References

1. J.W. Halloran Extraction of hydrogen from fossil fuels with production of solid carbon materials, Int. J. Hydrog. Energy, 33 (2008), pp.2218-2224.
2. R.A. Barreto Fossil fuels, alternative energy and economic growth Econ. Model., 75 (2018), pp.196-220.
3. X. Li, B. Wei Supercapacitors based on nanostructured carbon Nano Energy, 2 (2013), pp.159-173.
4. M.F. El-Kady, Y. Shao, R.B. Kaner Graphene for batteries, supercapacitors and beyond Nat. Rev. Mater., 1(2016), pp.1-14.
5. L. Li, L., E.B. Secor, K.S. Chen, J. Zhu, X. Liu, T.Z. Gao, J.W.T. Seo, Y. Zhao, and M.C. Hersam High-Performance Solid-State Supercapacitors and Microsupercapacitors Derived from Printable Graphene Inks. Advanced Energy Materials, 6(20) (2016), p.1600909.
6. L.L. Zhang, T. Wei, W. Wang, X.S. Zhao Manganese oxide–carbon composite as supercapacitor electrode materials Microporous Mesoporous Mater., 123 (2009), pp.260-267.
7. R. Dubey, V. Guruviah Review of carbon-based electrode materials for supercapacitor energy storage Ionics 25 (2019), pp.1419-1445.
8. K.R. Thines, E.C. Abdullah, M. Ruthiraan, N.M. Mubarak, M. Tripathi A new route of magnetic biochar-based polyaniline composites for supercapacitor electrode materials J. Anal. Appl. Pyrol., 121 (2016), pp.240-257.
9. Z.S. Iro, C. Subramani, S.S. Dash A brief review on electrode materials for supercapacitor Int. J. Electrochem. Science, 11 (2016), pp.10628-10643.
10. W. Fan, C. Zhang, W.W. Tjiu, K.P. Pramoda, C. He, T. Liu Graphene-wrapped polyaniline hollow spheres as novel hybrid electrode materials for supercapacitor applications ACS Appl. Mater. Interfaces, 5 (2013), pp.3382-3391.
11. E. Frackowiak Carbon materials for supercapacitor application Phys. Chem. Chem. Phys. 9 (2007), pp.1774-1785.

12. Y. Wang, J. Guo, T. Wang, J. Shao, D. Wang, Y.W. Yang Mesoporous transition metal oxides for supercapacitors Nanomaterials, 5 (2015), pp.1667-1689.
13. Y. Wang, Y. Ding, X. Guo, G. Yu Conductive polymers for stretchable supercapacitors Nano Res., 12 (2019), pp.1-10.
14. S. Chen, W. Xing, J. Duan, X. Hu, Z. Qiao Nanostructured morphology control for efficient supercapacitor electrodes J. Mater. Chem. A, 1 (2013) pp. 2941-2954.
15. L. Borchardt, M. Oschatz, S. Kaskel Tailoring porosity in carbon materials for supercapacitor applications Mater. Horiz, 1 (2014), pp.157-168.
16. A. Mohanty, D. Jaihindh, Y.P. Fu, S.P. Senanayak, L.S. Mende, A Ramadoss An extensive review on three dimension architectural metal-organic frameworks towards supercapacitor application J. Power Sources, 488 (2021), p.229444.
17. K.B. Wang, Q. Xun, Q. Zhang Recent progress in metal-organic frameworks as active materials for supercapacitors Energy Chem, 2 (2020), p.100025.
18. X. Gao, Y. Dong, S. Li, J. Zhou, L. Wang, B. Wang MOFs and COFs for batteries and supercapacitors Electrochem. Energy R., 3 (2020), pp.81-126.
19. Z. Zhu, Z. Wang, Z. Yan, R. Zhou, Z. Wang, C. Chen Facile synthesis of MOF-derived porous spinel zinc manganese oxide/carbon nanorods hybrid materials for supercapacitor application Ceram. Int., 44 (2018), pp.20163-20169.
20. S. Gao, Y. Sui, F. Wei, J. Qi, Q. Meng, Y. He Facile synthesis of nickel metal–organic framework derived hexagonal flaky NiO for supercapacitors J. Mate Sci: Mater. Electron, 29 (2018), pp. 2477-2483.
21. Y. Han, S. Zhang, N. Shen, D. Li, X. Li MOF-derived porous NiO nanoparticle architecture for high performance supercapacitors Mater. Lett., 188 (2017), pp.1-4.
22. G. Cheng, W. Yang, C. Dong, T. Kou, Q. Bai, H. Wang, Z. Zhang Ultrathin mesoporous NiO nanosheet-anchored 3D nickel foam as an advanced electrode for supercapacitors J. Mater. Chem. A, 3 (2015), pp.17469-17478.
23. Y. Li, Y. Xu, W. Yang, W. Shen, H. Xue, H. Pang MOF-derived metal oxide composites for advanced electrochemical energy storage Small, 14 (2018), pp.1704435.
24. S. Vijayakumar, S. Nagamuthu, G. Muralidharan Porous NiO/C nanocomposites as electrode material for electrochemical supercapacitors ACS Sustain. Chem. Eng., 1 (2013), pp.1110-1118.

25. L. Yu, G. Wan, X. Peng, Z. Dou, X. Li, Wang K, S. Lin, G. Wang Fabrication of carbon-coated NiO supported on graphene for high performance supercapacitors RSC Adv., 6 (2016), pp.14199-14204.
26. T. Liu, L. Zhang, B Cheng, W. You, J. Yu Fabrication of a hierarchical NiO/C hollow sphere composite and its enhanced supercapacitor performance Chem. Commun., 54 (2018), pp.3731-3734.
27. Z. Zhang, H. Huo, J. Gao, Z. Yu, F. Ran, L. Guo, S. Lou, T. Mu, X. Yin, Q. Wang, G. Yin Ni-MOF derived NiO/C nanospheres grown in situ on reduced graphene oxide towards high performance hybrid supercapacitor J. Alloys Compd., 801 (2019), pp.158-165.
28. Q. Zeng, L. Wang, X. Li, W. You, J. Zhang, X. Liu, M. Wang, R. Che Double ligand MOF-derived pomegranate-like Ni@ C microspheres as high-performance microwave absorber Appl. Surf. Sci., 538 (2021), p.148051.
29. T. Wang, Q. Zhou, X. Wang, J. Zheng, X. Li MOF-derived surface modified Ni nanoparticles as an efficient catalyst for the hydrogen evolution reaction J. Mater. Chem. A, 3 (2015), pp.16435-16439.
30. V. Sudha, S.M.S. Kumar, R. Thangamuthu Synthesis and characterization of NiO nanoplatelet and its application in electrochemical sensing of sulphite J. Alloys Compd., 744 (2018), pp.621-628.
31. X. Li, A. Dhanabalan, C. Wang Enhanced electrochemical performance of porous NiO–Ni nanocomposite anode for lithium-ion batteries J. Power Sources, 196 (2011), pp. 9625-9630.
32. S.H. Ahn, A. Manthiram Hierarchical tri-functional electrocatalysts derived from bimetallic–imidazolate framework for overall water splitting and rechargeable zinc–air batteries J. Mater. Chem. A, 7 (2019), pp.8641-8652.
33. S.T. Navale, V.V. Mali, S.A. Pawar, R.S. Mane, M. Naushad, F.J. Stadler, V.B. Patil Electrochemical supercapacitor development based on electrodeposited nickel oxide film RSC Adv., 5 (2015), pp.51961-51965.
34. Chao, D., Zhu, C., Yang, P., Xia, X., Liu, J., Wang, J., Fan, X., Savilov, S.V., Lin, J., Fan, H.J. and Shen, Z.X., 2016. Array of nanosheets render ultrafast and high-capacity Na-ion storage by tunable pseudocapacitance. *Nature Communications*, *7*(1), pp.1-8.

35. C. Zhang, L. Qian, K. Zhang, S. Yuan, J. Xiao, S. Wang Hierarchical porous Ni/NiO core–shells with superior conductivity for electrochemical pseudo-capacitors and glucose sensors J. Mater. Chem. A, 3 (2015), pp.10519-10525.
36. S. Cheng, L. Yang, Y. Liu, W. Lin, L. Huang, D. Chen, C.P. Wong, M. Liu Carbon fiber paper supported hybrid nanonet/nanoflower nickel oxide electrodes for high-performance pseudo-capacitors J. Mater. Chem. A, 1 (2013), pp.7709-7716.
37. S.D. Dhas, P.S. Maldar, M.D. Patil, A.B. Nagare, M.R. Waikar, R.G Sonkawade, A.V. Moholkar Synthesis of NiO nanoparticles for supercapacitor application as an efficient electrode material Vacuum, 181 (2020), p.109646.
38. X. Tong, D. Zhou, M. Qiu, Y. Zhou, Y. Ai, X. Guo, J. Zhang, Y. Cai, Q. Kong Biomorphic NiO/Ni with a regular pore-array structure as a supercapacitor electrode material Eur. J. Inorg. Chem., 6(2021), pp.562-566.
39. Y. Song, T.Y. Liu, X.X. Xu, D.Y. Feng, Y. Li, X.X. Liu Pushing the cycling stability limit of polypyrrole for supercapacitors Adv. Funct. Mater., 25 (2015), pp. 4626-4632.
40. D.W. Wang, F. Li, H.M. Cheng Hierarchical porous nickel oxide and carbon as electrode materials for asymmetric supercapacitor J. Power Sources, 185 (2008), pp. 1563-1568.
41. C. Huang, Y. Ding, C. Hao, S. Zhou, X. Wang, H. Gao, L. Zhu, J. Wu PVP-assisted growth of Ni-Co oxide on N-doped reduced graphene oxide with enhanced pseudocapacitive behavior Chem. Eng. J., 378 (2019), p.122202.
42. H. Yi, H. Wang, Y. Jing, T. Peng, X. Wang Asymmetric supercapacitors based on carbon nanotubes@ NiO ultrathin nanosheets core-shell composites and MOF-derived porous carbon polyhedrons with super-long cycle life J. Power Sources, 285 (2015), pp.281-290.
43. A-K Singh, D. Sarkar, G-G Khan, K. Mandal Unique hydrogenated Ni/NiO core/shell 1D nano-heterostructures with superior electrochemical performance as supercapacitors J. Mater Chem A., 1 (2013), pp.12759–12767
44. Y. Jiang, J. Liu Definitions of pseudocapacitive materials: A brief review Energy Environ. Mater. 2 (2019), pp.30-37.
45. J.B. Cook, H.S. Kim, T.C. Lin, C.H. Lai, B. Dunn, S.H. Tolbert Pseudocapacitive charge storage in thick composite MoS_2 nanocrystal-based electrodes Adv. Energy Mater., 7 (2017), p.1601283.

Chapter 5: Self-assembled Zn-functionalized Ni-MOFs as binder-free electrodes for electrochemical energy storage application

Abstract

Zinc-functionalized nickel metal-organic framework (Zn/Ni-MOF) composite electrodes were grown directly on nickel foam (NF), fabricated using solvothermal synthesis and used as binder-free electrodes for electrochemical energy storage applications. The structural characteristics of the composite materials were analyzed by X-ray diffraction (XRD), scanning electron microscopy (SEM), energy dispersive X-ray (EDX), nitrogen adsorption-desorption surface area analysis, Fourier Transform Infrared Spectroscopy (FTIR), thermal gravimetric analysis (TGA) and Raman spectroscopy. The structural elucidation revealed that flower-decorated ball-shape microstructures were obtained from Zn functionalization of the pristine Ni-MOF microsheets. They also showed a high surface area and different pore characteristics. The electrochemical performance measured when using a 3M KOH electrolyte solution indicated that Zn-doped Ni-MOF containing Zn/Ni in the ratio 1:2 (ZNN1) exhibited the best performance. The maximum specific capacitance was 391 Fg^{-1} at a current density of 1 Ag^{-1}, which indicated that it retained about 70% of its initial value at 10 Ag^{-1}. This indicates good rate capability. The electrode also possessed a maximum energy and power density of 12 Wh kg^{-1} and 2000 Wkg^{-1}, respectively, with a high cycling stability of 93% after 1000 cycles. The enhanced electrochemical performance of ZNN1 was attributed to an increase in the surface area and electrical conductivity of Ni-MOF, following the incorporation of an optimum concentration of Zn dopant. The charge storage mechanism was predominantly controlled by the diffusion process, which suggests that the method employed in this study is promising for the fabrication of pseudocapacitive materials.

Keywords: Ni-MOF, Zn dopant, binder-free electrodes, pseudocapacitive, microsheets.

Graphical Abstract

Zn-doped Ni-MOFs were fabricated and used, for the first time, as free-standing electrodes for supercapacitor applications. The optimum Zn/Ni concentration delivered the best performance with respect to specific capacitance and energy/power density, and was linked to the textural properties and low charge transfer resistance of the electrode materials. The storage mechanism was further probed using electrochemical kinetics.

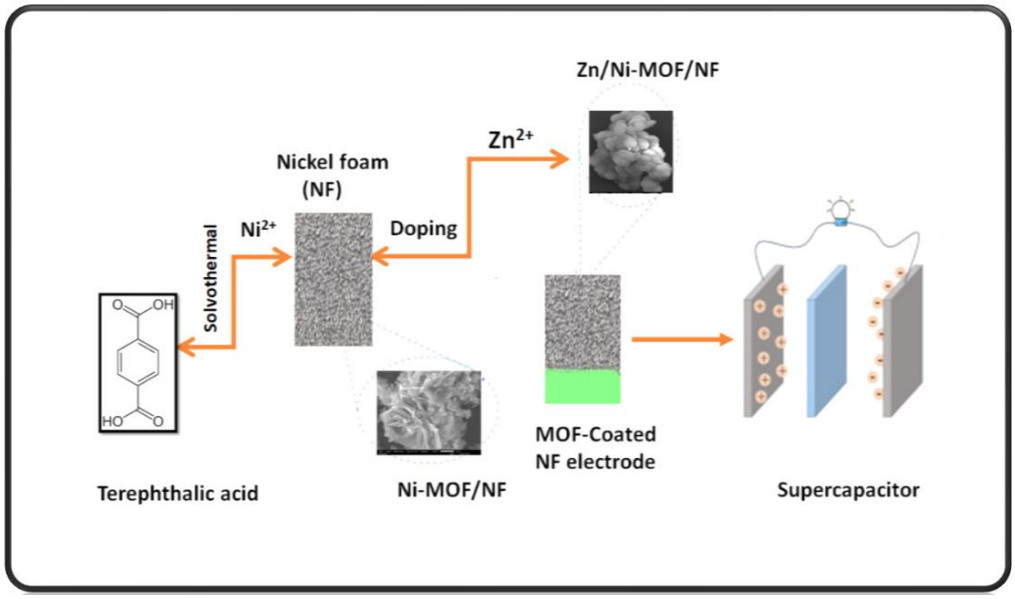

5.1 Introduction

High energy demands have stimulated research interest in clean and sustainable energy storage systems, in response to the problem of ongoing depletion of fossil resources and the accompanying environmental challenges [1]. To prepare these clean energy alternatives for future use, they need to be stored properly using smart devices [2]. Supercapacitors are considered one of the promising energy storage devices designed for the next generation of wearable and electronic devices, due to their high-power density, fast charge-discharge rate and exceptional cycling stability [3-4]. Supercapacitors can therefore be considered a suitable replacement for lithium-ion batteries (LIBs) in some applications where high power density and good cyclic stability are a high priority [5].

The performance of a supercapacitor is strongly influenced by the physicochemical properties of the electrode materials [6-7]. Great strides have been recorded in the past few decades with the development of high-performance electrode materials for supercapacitor applications – such as transition metal oxides, carbon-based materials, sulfides, hydroxides and conducting polymers - but constraints are still inherent in these materials, especially at a low energy density [8-10]. Thus, it is still a challenge to design a supercapacitor device that will deliver both high energy density and good energy density with respect to the novel materials and new structural architecture being used.

Metal-organic frameworks (MOFs) were first reported on about two decades ago. They are porous materials assembled from the coordination of metal ions and organic ligands [11]. They have attracted attention in the field of supercapacitor applications because of their high specific surface area, well-defined structure, high porosity and ease of functionalization of MOFs, and can also be used as flexible supercapacitors [12-13]. Unfortunately, the performance of MOFs in supercapacitor applications - which is measured in terms of energy/power density, capacitance values and cycling stability - can be severely hampered by low electrical conductivity and weak chemical/thermal stability [14]. Many approaches have been proposed to overcome this constraint and to improve the conductivity and stability, and ultimately enhance the energy storage performance of MOFs [15-17].

Functionalization of pristine MOFs with transition metals such as Zn^{2+}, Co^{2+}, Mo^{2+}, Ni^{2+}, Cd^{2+} and Co^{2+}/Zn^{2+} is one effective strategy that can enhance their conductivity and chemical stability while increasing the surface characteristics [18-20]. For instance, Yang et al. reported self-assembled Mo-doped Ni-MOF nanosheets and used them as electrode materials for an enhanced battery-type supercapacitor application [21]. The Mo-doping enhanced both the electrical conductivity and stability of the pristine MOF, and this translated into an increase in the electrochemical performance of the Mo-doped Ni-MOF. The electrode material with a Mo/Ni molar ratio of 1:1 delivered the best performance, with a specific capacitance of 802 Cg^{-1} at 1 Ag^{-1} compared to 435 Cg^{-1} for Ni-MOF at the same current density. In addition, the material exhibited good cyclic stability of 96% after 20,000 cycles, while the fabricated battery-type supercapacitor device showed an outstanding energy density of 59 $Whkg^{-1}$ at a power density of 802 Wkg^{-1} [21].

Chen et al. used HCl as a modulator to prepare hierarchical spherical Zn-doped Ni-MOF for supercapacitor applications using a microwave method [22]. The rational adjustment of the amount of Zn dopant (Zn/Ni: 0.07) delivered an optimum Zn-doped Ni MOF with a high specific capacitance of 237.4 mA h g^{-1} at a current density of 1 Ag^{-1}. It also retained 88% of its original value at 4000 cycles, which indicates good cycling stability. The superior performance of the electrode material was attributed to its structural properties, as well as the optimum concentration of Zn^{2+} used for doping [22].

Most studies involving transition metal-doped MOFs to improve the performance of supercapacitors have employed high molecular weight polymeric binders, such as polyvinyl pyrrolidine (PVP) and polytetrafluoroethylene (PTFE) [21-23], to prepare the working electrodes. However, the use of binders can decrease the accessible areas of the electrode material and limit transportation of charges and ions between the electrode and the electrolytes, thereby impeding the overall electrochemical energy storage performance [24]. To address this issue, binder-free electrodes can be used to fabricate electrode materials for high-performance supercapacitor applications [25-27]. This is done by growing active materials directly on different substrates, including Ni foam, Al foil, graphite sheets and carbon cloth [28].

This section reports on self-assembled synthesis and optimization of Zn-functionalized Ni-MOF, which was grown directly on an NF support using a solvothermal approach without the use of binders. This synthetic approach was used to fix MOFs on the Ni substrate with different concentrations of transition metal dopants. The fabricated electrodes were subsequently used as binder-free electrodes for supercapacitor applications, and showed beneficial characteristics such as good textural properties. Furthermore, the Dunn method was used to probe the kinetics and electrochemical energy storage mechanisms of the fabricated binder-free electrodes [29].

5.2 Experiment

5.2.1 Materials

All the reagents used in this study were analytical grade, except for the HCl, and all the reagents were used as received and without further purification. The major reagents used were zinc nitrate hexahydrate ($Zn(NO_3)_2.6H_2O$)), nickel chloride hexahydrate ($NiCl_2 \cdot 6H_2O$), terephthalic acid (benzene-1,4-dicarboxylic acid, BDC), dimethylformamide (DMF) and hydrochloric acid (HCl).

5.2.2 Synthesis of binder-free Ni-MOF

Before the reaction, Ni foam was cut into 2 cm x 2 cm pieces and cleaned thoroughly with 3 M HCl. The pristine Ni-MOF microsheets were obtained by means of facile solvothermal synthesis. Typically, 3 mmol of $Ni(NO_3)_2.6H_2O$ and 3 mmol of BDC were dissolved in a 60 mL DMF solution. After stirring for 30 minutes, 2 mL of 0.4 M NaOH was added to the mixture before it was transferred into a 50 mL Teflon-lined steel autoclave. A piece of cleaned NF was then immersed in the reaction mixture. The autoclave was capped tightly, heated at 120 ^oC for 12 h and then allowed to cool to room temperature. Finally, the free-standing greenish Ni-MOF grown on the NF was carefully removed, rinsed thoroughly with DMF and ethanol three times, and dried in a vacuum oven at 60 ^oC overnight. The sample was labelled as Ni-MOF/NF.

5.2.3 Synthesis of binder-free Zn-doped Ni-MOF

The synthesis of Zn-doped Ni-MOFs grown directly on NF followed the preparation method used for Ni-MOF, as described above, except for the dissolution of different concentrations of $Zn(Ac)_2.2H_2O$. The resultant Zn-doped Ni-MOF/NF with different concentrations of $Zn(Ac)_2.2H_2O$ and molar ratios of 0.5, 1.0 and 1.5 for Zn/Ni) were denoted as ZNN1, ZNN2 and ZNN3, respectively.

5.2.4 Material characterization

X-ray diffraction (XRD) patterns were recorded on a Rigaku SmartLab diffractometer to identify the surface crystallinity and purity of doped and undoped samples. The chemical structures of the samples were analyzed using Fourier transform infrared (FTIR) spectroscopy (Vertex 70 model). Scanning electron microscopy (SEM, JSM-7100L, JEOL), coupled with energy dispersive spectroscopy (EDS), was used to characterize the morphology and chemical composition of the samples. The Brunauer-Emmett-Teller (BET) method was used to analyze the specific surface area under liquid nitrogen at 77K, using a Micromeritics Tristar II instrument. The pore size and pore volume were measured using the Barrett-Joyner-Halenda (BJH) method. Prior to BET measurement, the samples were de-gassed under vacuum at 150 ^oC for 12 h.

5.2.5 Electrochemical measurements

A PGSTAT 302N AUTOLAB was used to evaluate the electrochemical performance of the fabricated electrodes. The cyclic voltammetry (CV), galvanostatic charge-discharge (GCD) and electrochemical impedance spectroscopy (EIS) measurements were carried out in a three-electrode configuration using Ag/AgCl as the reference electrode, platinum as the counter electrode, and the binder-free electrodes as the working electrode. The electrolyte used was a 3M KOH alkaline solution. The specific capacitance (C (F/g)), energy density (E (Wh/kg)) and power density (P (W/kg)) were calculated based on equations (5.1 - 5.3).

$$C = \frac{I \times \Delta t}{m \times \Delta V} \quad (5.1)$$

$$E = \frac{C \times (\Delta V)^2}{7.2} \quad (5.2)$$

$$P = \frac{3600E}{\Delta t} \quad (5.3)$$

In these equations: I(A) is the discharge current; Δt (s) represents the discharge time; m(g) is the mass of active material; ΔV (V) denotes the discharge potential window.

5.3 Results and discussion

5.3.1 Characterization of undoped and Zn-doped Ni-MOF

Figure 5.1 illustrates the design strategy of the binder-free Zn-doped Ni-MOF electrodes. The doping ratios of metal ion in ZNN were controlled by incorporating the Zn source. The free-standing Ni-MOF was first grown directly on the NF through solvothermal synthesis, using $Ni(NO_3)_2.6H_2O$ as the metal source and terephthalic acid as the organic linker. A green surface was produced, which was different from the untreated NF. Afterwards, the addition of Zn metal to the pristine MOF, using a similar solvothermal approach, resulted in ZNN with a greenish surface. Both the doped and undoped Ni-MOF were subsequently characterized and tested for electrochemical performance

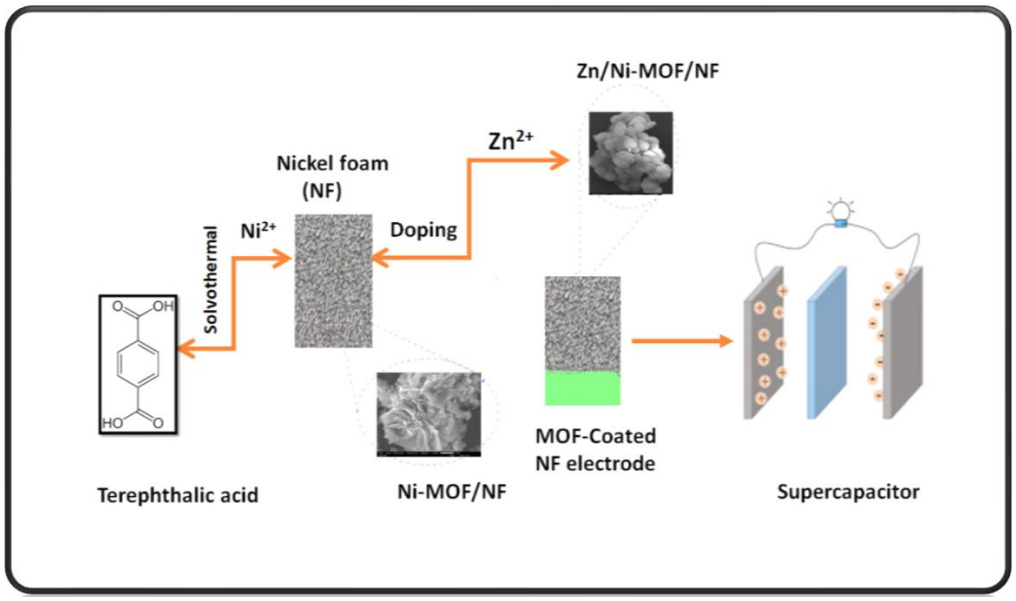

Figure 5.1 Illustration of the synthesis of undoped and Zn-doped Ni-MOF on nickel foam used as the binder-free electrodes.

The surface morphology of the binder-free electrodes was first characterized by SEM, as shown in Figure 5.2 (a-d). The pristine Ni-MOF (without Zn doping) exhibited a microsheet structure that transformed to a flower-like microsphere upon the addition of the Zn dopant. However, the nature of the microspheres and the flowers on them vary with the concentration of the dopant. Notably, both the Zn and Ni ions compete to form microspheres during doping, hence the slight difference in the morphologies of the doped samples. The addition of large concentrations of Zn resulted in large agglomerations of the flower shaped crystals growing on the microspheres. Thus, it is safe to conclude that the morphology of the Zn-doped Ni-MOF is influenced by the amount of Zn dopant used. Of all the samples, ZNN1 exhibited the best morphology in terms of smoothness, uniformity and interconnection between its particles. (See Figure 5.2b.) A well interconnected and uniform morphology is critical to enhancing the electrochemical energy storage performance, because of the advantage of rapid diffusion of electrolyte ions.

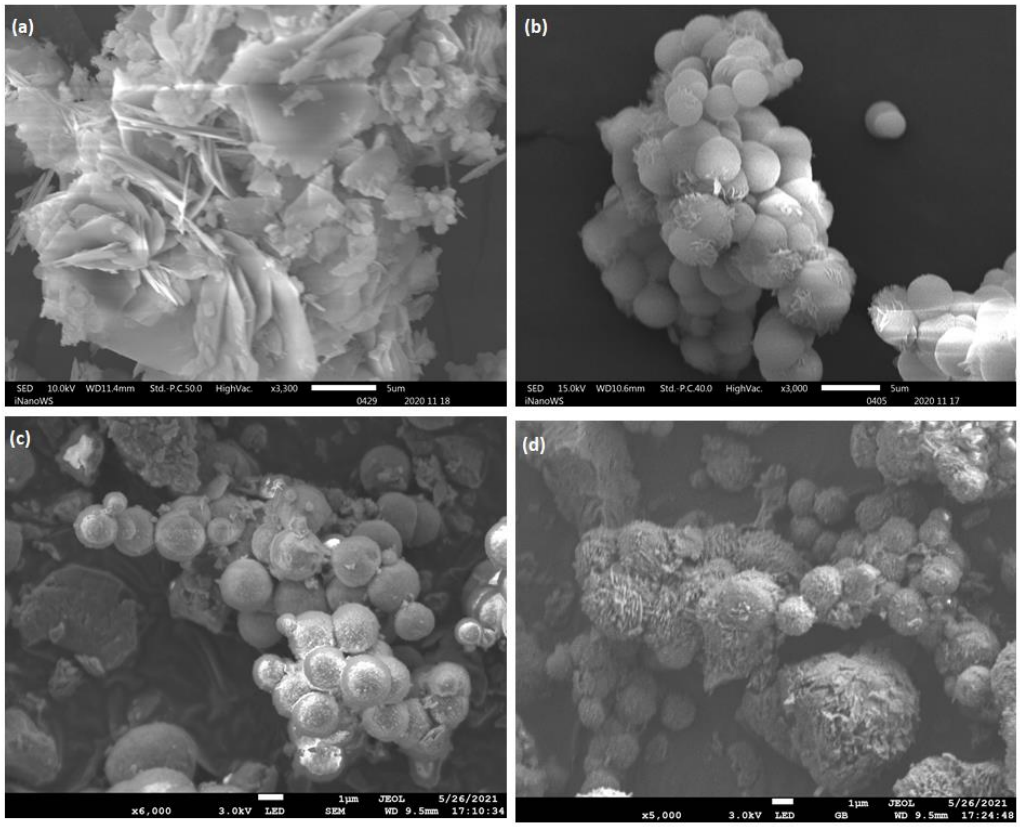

Figure 5.2 SEM images of: (a) pristine MOF and Zn-doped Ni-MOFs; (b) Zn/Ni=0.5 (ZNN1); (c) Zn/Ni=1 (ZNN2); (d) Zn/Ni=1.5 (ZNN3).

The elemental composition of undoped and doped samples was also examined using EDS, as depicted in Figure 5.3. The spectrum analysis revealed the presence of: C, O and Ni for the pristine MOFs; C, O, Ni and Zn with ratios of Zn/Ni of 0.5, 1 and 1.5, respectively, for the ZNN1, ZNN2 and ZNN3 samples. Hence, the EDS result confirmed successful Zn doping and a similar trend to that seen with Zn/Ni, except for a slight difference with ZNN3, which may be due to the strong competition posed by Ni against Zn at a high concentration.

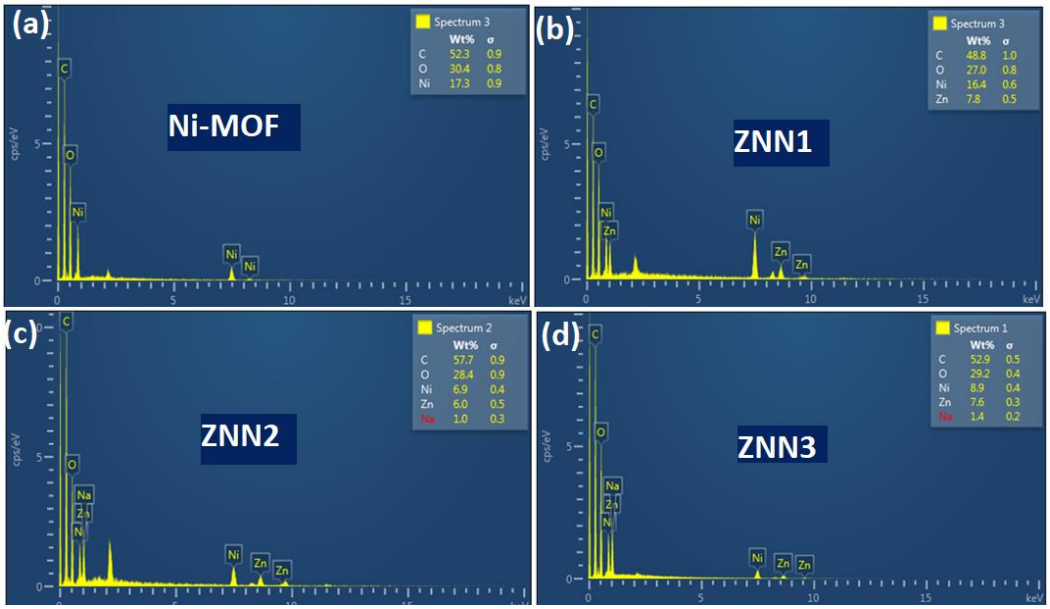

Figure 5.3 EDX spectra of the doped and un-doped Ni-MOFs.

The XRD and FTIR spectra of the samples are shown in Figure 5.4. It shows peaks at $2\theta = 2\text{-}20^{o}$ that are characteristic of Ni-MOF [30]. All the doped samples exhibited very similar diffraction patterns; however, some variation was observed during the doping, notably with an increase in the intensity of the peaks with a corresponding increase in the doping concentration. This trend implies that the larger Zn dopant ions are partially substituted by the Ni ions, which shows the influence of doping on the structure [31].

The FTIR spectra of the free-standing samples are shown in Figure 5.4b. The results agree with the literature on doping MOF structures with metal ions, i.e. it revealed almost identical peaks. However, a slight difference was seen between the symmetric and asymmetric modes in the fingerprint region (below 1500 cm^{-1}), which increased with Zn doping. This signals the effect of Zn doping on the MOF structure. The peak at 3690 cm^{-1} represents the O-H stretching vibration. The absorption bands at 1140 cm^{-1} and 1090 cm^{-1} indicate the aromatic -CH stretching vibration [32].

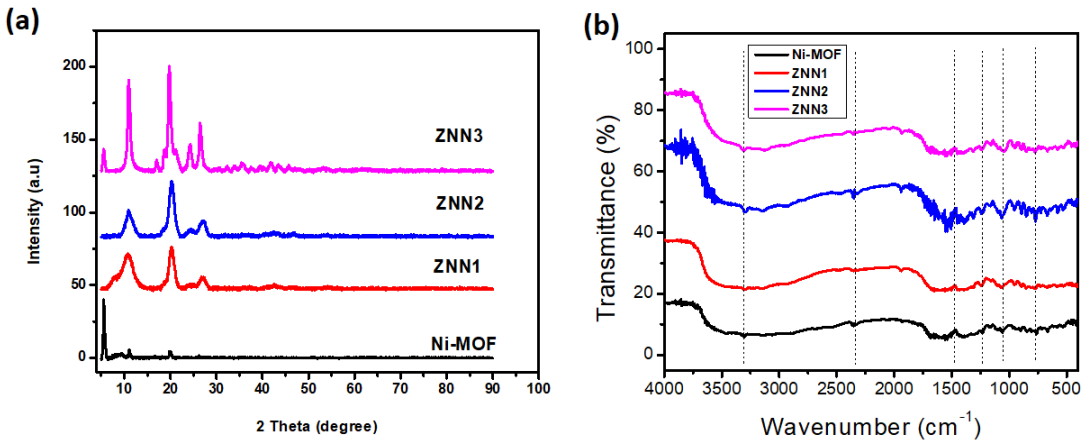

Figure 5.4 Characterization results showing the (a) XRD patterns and (b) FTIR spectra of the undoped and Zn-doped Ni-MOF materials.

Surface area and pore size distribution are two key parameters that influence the performance of a supercapacitor electrode [33]. Therefore, nitrogen adsorption-desorption analysis was conducted to determine the surface areas of the prepared samples. As shown in Figure 5.5, all samples exhibited a type IV isotherm with obvious hysteresis loops between adsorption and desorption, which indicates that the samples are mesoporous in nature [34]. The BET surface area and pore characteristics are indicated in Table S5.1. It shows a trend of an increase in surface area with the incorporation of the Zn dopant. An increase in surface area translates into enhanced electrochemical performance, as it increases the active interface between the electrode and the electrolyte. Overall, ZNN1 had the highest surface area (117.8 m^2/g) and an average pore size of 12.4 nm. Thus, it is expected that ZNN1 will possess the best electrochemical activity, based on its high surface area and optimum pore size.

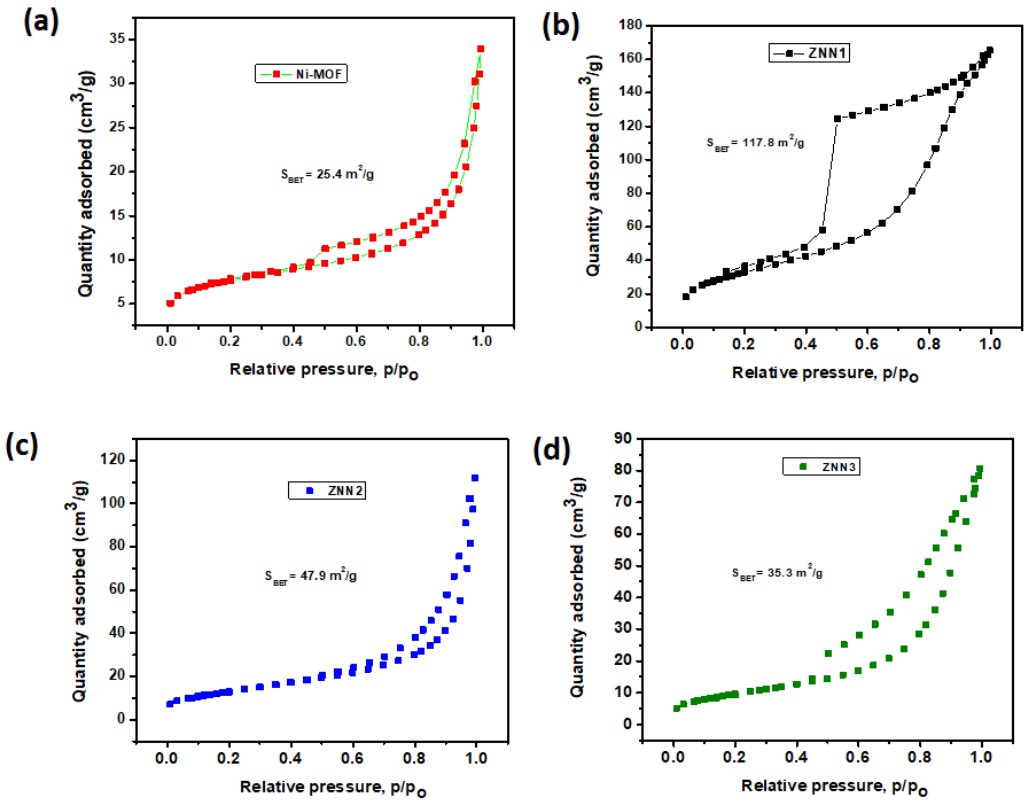

Figure 5.5 Nitrogen adsorption-desorption BET isotherms of: (a) Ni-MOF; (b) ZNN1; (c) ZNN2; (d) ZNN3.

5.3.2 Electrochemical performance

The electrochemical properties of the as-synthesized samples were characterized by CV, GCD and EIS in a three-electrode configuration using 3M KOH aqueous electrolyte, in order to evaluate the potential of the free-standing Zn-doped Ni-MOF for supercapacitor applications. Figure 5.6a depicts the CV curves of Ni-MOF without and with Zn dopant, at different concentrations, measured at a fixed scan rate of 5 mV/s and a potential window of -0.2 V and 0.5 V. Noticeably, the doped materials showed a higher peak current and area than the undoped materials, which indicates an improvement in electrochemical performance after Zn doping. Also, ZNN1 exhibited the largest integrated CV area, which indicates that it has the best performance. The results obtained agreed with the characterization results, including BET.

In addition, the CV curves showed two pairs of redox peaks, which is typical of pseudocapacitive behavior [35]. An increase in the scan rate did not affect the overall shape of the CV curves, which confirms an outstanding rate capability for storing energy. However, there was an increase in the

area under the curves with an increase in the scan rate, while the potential for oxidation and reduction peaks shifted slightly towards a higher and a lower potential, respectively. This could be attributed to either polarization of the electrode materials or an increase in ohmic resistance.

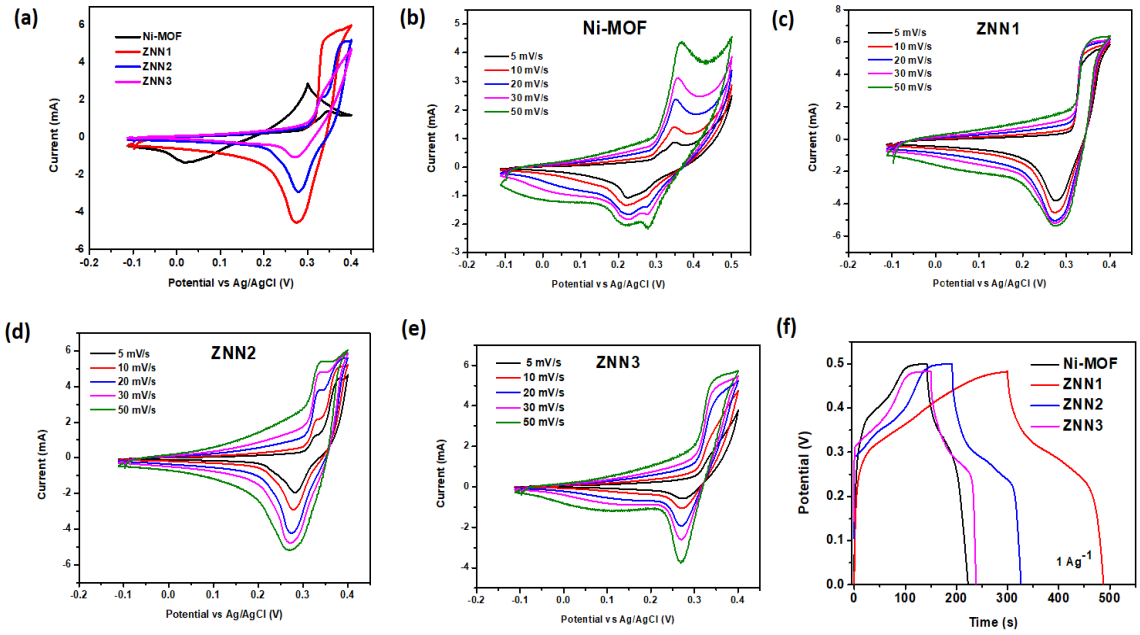

Figure 5.6 CV curves of: (a) comparison of undoped and Zn-doped electrode Ni-MOF; (b) Ni-MOF; (c) ZNN1; (d) ZNN2 (e) ZNN3; (f) comparison of the GCD curves of undoped and Zn-doped Ni-MOF.

The GCD curves at various current densities are compared in Figure 5.7. The non-linearity of the GCD curves is further proof of the pseudocapacitive behavior of the electrode materials, which agrees with the CV results [36]. Interestingly, it is obvious that the process of discharging Zn-doped materials requires more time than is required with the pristine material, which also indicates better performance. ZNN1 showed the highest specific capacitance at different current densities, which is similar to what was seen with the CV results. In addition, there was a gradual decrease in the specific capacitance values with an increase in current density. This could be ascribed to a reduction in the utility of the active material because of the rapid redox reaction, and probably because of slow kinetics with ion transfer in the material at a high current density.

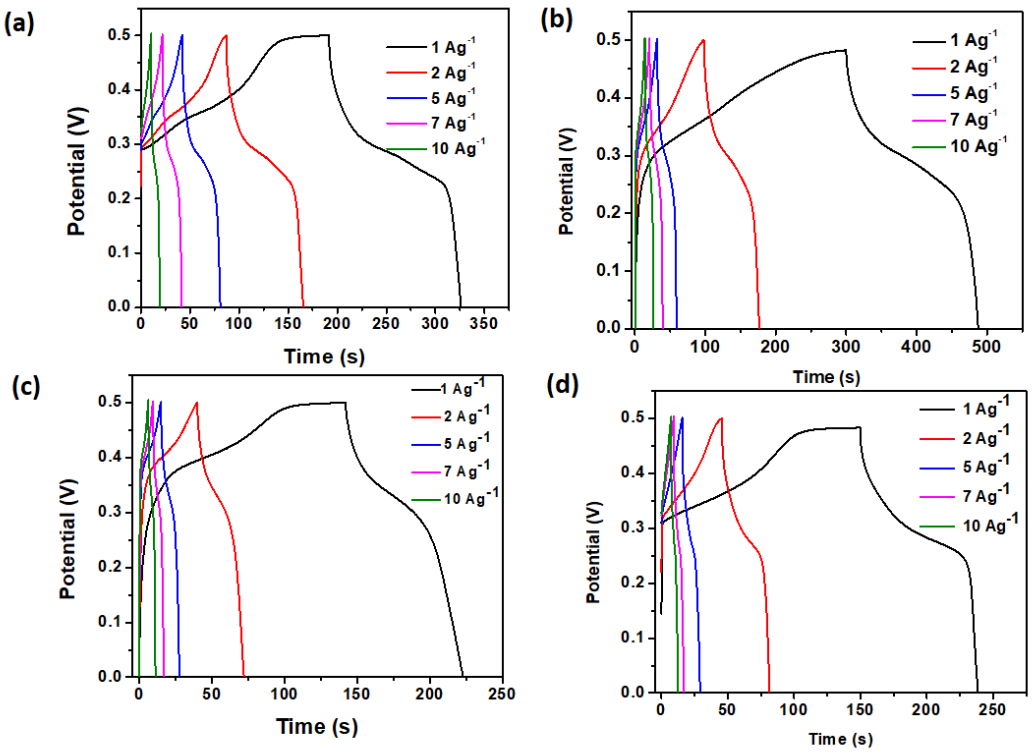

Figure 5.7 GCD curves of (a) Ni-MOF (b) ZNN1 (c) ZNN2 (d) ZNN3 at different current densities.

Equations (5.1), (5.2) and (5.3) were used to calculate the specific capacitance, energy density and power density of the electrode materials, respectively, and these were then compared to the GCD curves. (See Figure 5.8a.) The doped samples (ZNN1, ZNN2 and ZNN3) exhibited higher specific capacitance values than the undoped (pure free-standing Ni-MOF) electrode. As the Zn concentration increased, the capacitance values decreased accordingly. ZNN1 attained a maximum specific capacitance of 391 F/g at a current density of 1 A/g and retained up to 75% at 10 A/g, which is an indication of good rate capability. ZNN also delivered a maximum energy density and power density of 1700 Wh/kg and 12 W/kg, respectively.

The corresponding values obtained for the energy and power density of the other materials are shown in Table S5.2. Similarly, Table 5.1 provides a comparison of the electrochemical performance of the ZNN1 electrode with that of related materials that have already been established in the literature. ZNN1 compared favorably and had better specific capacitance than some materials, which may be attributed to the synergy between its uniform microsphere and optimum Zn doping.

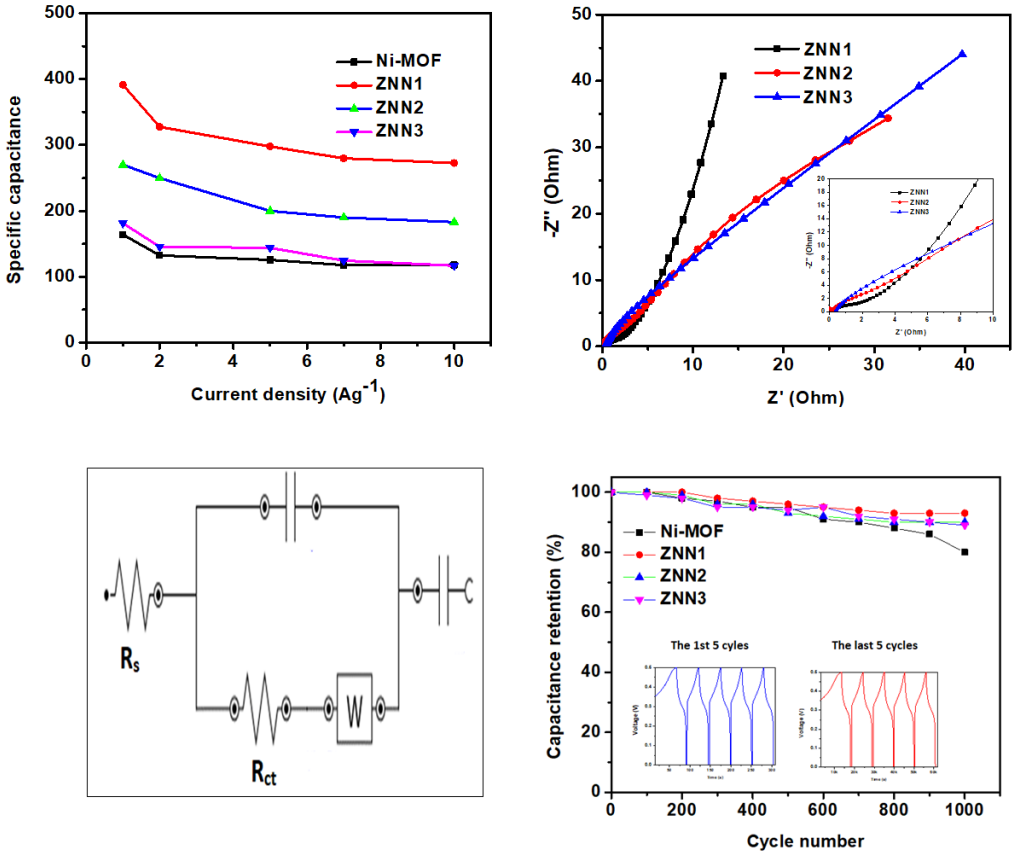

Figure 5.8 (a) Specific capacitance of the electrode materials at different current density levels. (b) Nyquist plots of the electrode materials measured at a frequency range of 100 kHz to 0.01 kHz. (c) Equivalent electrochemical circuit used to fit the Nyquist plot. (d) Cycling performance of the electrode materials measured at 5 A/g.

EIS was also used to probe the high performance of ZNN1 in comparison to other Zn-doped electrodes (ZNN2 and ZNN3) using the Nyquist plot. (See Figure 5.8b.) The inset shows the enlarged spectra for the mid- and high-frequency regions. The electrochemical circuit used to fit the Nyquist plots is shown in Figure 5.8c. At low frequency regions, all three EIS spectra displayed a liner curve and a quasi-semicircle at a high frequency. It is also obvious from the curve that ZNN1 possessed the lowest internal resistance compared to ZNN2 and ZNN3. Low internal resistance indicates high ionic and electronic conductivity, which ultimately impacts electrochemical performance positively [37-39]. The low internal resistance of ZNN1 may not be unconnected to its uniform morphology and its unique textural properties when compared to ZNN2 and ZNN3.

Table 5.1: Electrochemical performance of the various MOF-based Ni electrode materials.

Electrode material	**Current density**	**Specific capacitance (F/g)**	**Electrolyte**	**Ref.**
$Ni_3(HITP)_2$	0.05 A/g	111	1 M $TEABF_4$/ACN	[40]
Ni-MOF	5 mV/s	309	1M LiOH	[41]
Ni-doped MOF-5	0.05 A/g	380	1M KOH	[42]
MOF-derived NiO	01 A/g	324	6M KOH	[43]
Binder-free Zn-doped Ni-MOF	1 A/g	390	3M KOH	This work

Another key parameter to measure the performance of a supercapacitor is the ability to retain its capacitance over several cycles, which is known as cycling stability. The cycling stability of the samples was evaluated using the GCD method at a current density of 5 A/g for 1000 cycles. As shown in Figure 5.8d, as the cycling number increases, capacitance retention decreases. Again, ZNN1 delivered the highest cycling stability, with about 90% capacitance retention after 1000 cycles. This further confirms that ZNN1 has a high specific capacitance in addition to outstanding cycling stability. The low internal resistance, high surface area and uniform morphology are the essential parameters in this regard, as they help hasten the rapid transfer of ions in the electrolyte solution.

To evaluate the charge storage mechanism in the ZNN1 electrode, the CV curves were used for kinetic analysis of the electrode material. Analysis of the relationship between the peak current and the scan rate helped to determine if the electrode material exhibited battery-type characteristics or pseudocapacitive characteristics during the charge-discharge stage. This is expressed in equations (5.4) and (5.5), which are appropriate for use in evaluating the property of the electrode in this regard [44].

$$i = av^b \qquad (5.4)$$

$$\log i = \log a + b\log v \qquad (5.5)$$

Where: i and v represent the peak current and scan rate; a and b are constants.

Linearization of equation 5.4 produced equation (5.5), from which the value of b could be derived from the slope of logi against log *v*. A b value of approximately 0.5 implies that the electrode material possesses battery characteristics, while a b value close to 1 indicates pseudocapacitive properties. After computation, it was confirmed that the b values are within both limits, which indicates that the material shared both battery-type and capacitive properties. (See Figure 5.9a and 5.9b.) Consequently, further probing was done to distinguish which of the two processes was more prominent. Dunn's equation was used, as shown in equations (5.6) and (5.7) [45].

$$i = k_1 v + k_2 v^{1/2} \quad (5.6)$$

$$i/ v^{1/2} = k_1 v^{1/2} + k_2 \quad (5.7)$$

Where: i is the peak current; *v* is the scan rate; k_1 and k_2 are constants. The contributions from the capacitive and diffusion-controlled processes are denoted by $k_1 v$ and $k_2 v^{1/2}$, respectively.

The plot of $i / v^{1/2}$ vs. $v^{1/2}$ produced a linear curve from which the values of k_1 and k_2 could be determined. (See Figure 5.9c.) It can be seen that the contribution of the diffusion-controlled process increased with an increase in the scan rate, while the capacitive contribution decreased with an increase in the scan rate. The implication of this is that the materials exhibited a predominant pseudocapacitive behavior, i.e. as the scan rate increased, the ions diffuse into the materials faster, and limit the capacitive contribution.

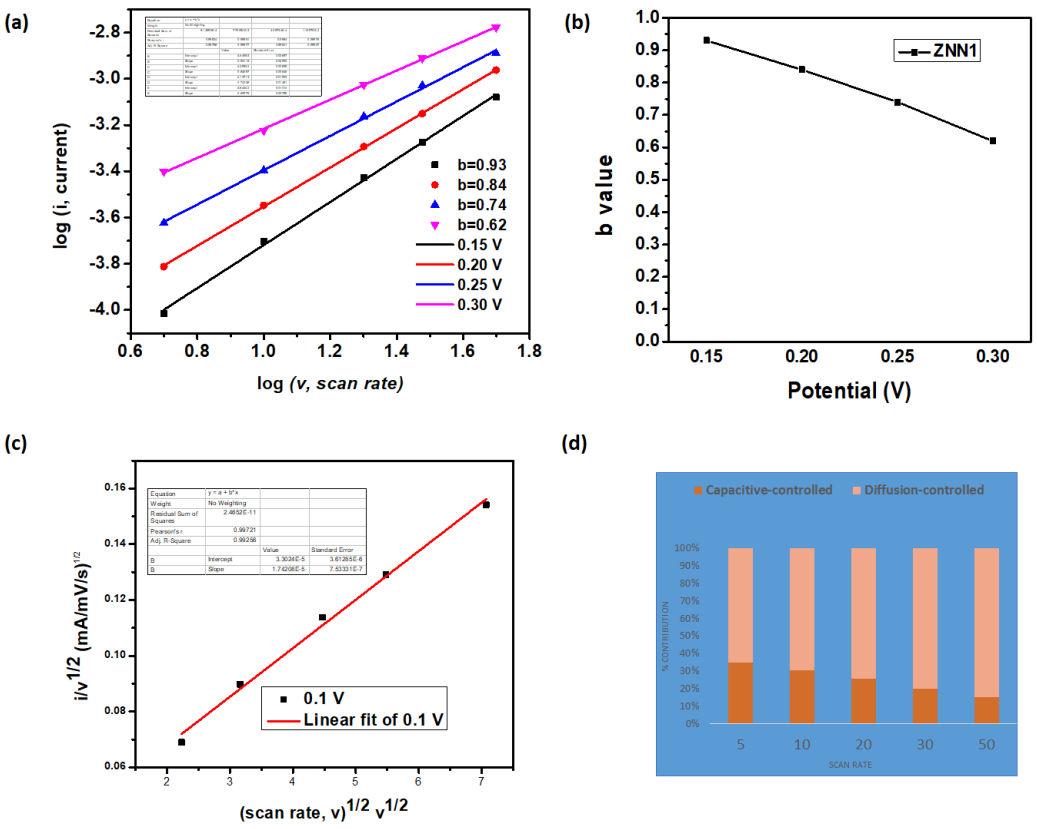

Figure 5.9 Graphs displaying: (a) log of peak current against log of scan rate; (b) value of b at different potential windows; (c) plot of i/v1/2 against the square root of the scan rate, v; (d) scan rate-dependent capacitive and diffusion-controlled contributions.

5.4 Conclusion

In this study, the binder-free Zn-doped Ni-MOFs grown directly on NF were synthesized and used as electrode materials for supercapacitor applications for the first time. By controlling the concentration of Zn ions with respect to the Ni ion, an optimum free-standing electrode was produced. ZNN1 delivered the highest specific capacitance of 391 F/g at 1 A/g, with a good rate capability when the scan rate was increased to 10 A/g. The ZNN1 electrode also exhibited excellent cycling stability of 93% after 1000 cycles. The electrochemical kinetic analysis of ZNN1 revealed that the storage mechanism is predominantly diffusion-controlled at the tested scan rates. The excellent performance could be attributed to the synergistic effects of a high surface area, optimum Zn doping and low internal resistance, which facilitated the rapid transport of ions in the electrolyte solution. The binder-free method employed for doping pristine MOFs in this study could be used

for the rational design of pseudocapacitive electrodes and also as a potential flexible supercapacitor because their of the simple design that requires no binders.

References

1. Abas, N., Kalair, A. and Khan, N., 2015. Review of fossil fuels and future energy technologies. *Futures*, *69*, pp.31-49.
2. Xie, Z., Jin, X., Chen, G., Xu, J., Chen, D. and Shen, G., 2014. Integrated smart electrochromic windows for energy saving and storage applications. *Chemical Communications*, *50*(5), pp.608-610.
3. Zheng, Y., Yang, Y., Chen, S. and Yuan, Q., 2016. Smart, stretchable and wearable supercapacitors: Prospects and challenges. *CrystEngComm*, *18*(23), pp.4218-4235.
4. He, X., Li, R., Liu, J., Liu, Q., Song, D. and Wang, J., 2018. Hierarchical FeCo2O4@ NiCo layered double hydroxide core/shell nanowires for high performance flexible all-solid-state asymmetric supercapacitors. *Chemical Engineering Journal*, *334*, pp.1573-1583.
5. Gopi, C.V.M., Vinodh, R., Sambasivam, S., Obaidat, I.M. and Kim, H.J., 2020. Recent progress of advanced energy storage materials for flexible and wearable supercapacitor: From design and development to applications. *Journal of Energy Storage*, *27*, p.101035.
6. Iro, Z.S., Subramani, C. and Dash, S.S., 2016. A brief review on electrode materials for supercapacitor. *Int. J. Electrochem. Sci*, *11*(12), pp.10628-10643.
7. Zhang, L.L. and Zhao, X.S., 2009. Carbon-based materials as supercapacitor electrodes. *Chemical Society Reviews*, *38*(9), pp.2520-2531.
8. An, C., Zhang, Y., Guo, H. and Wang, Y., 2019. Metal oxide-based supercapacitors: Progress and perspectives. *Nanoscale Advances*, *1*(12), pp.4644-4658.
9. Kesavan, T., Partheeban, T., Vivekanantha, M., Kundu, M., Maduraiveeran, G. and Sasidharan, M., 2019. Hierarchical nanoporous activated carbon as potential electrode materials for high performance electrochemical supercapacitor. *Microporous and Mesoporous Materials*, *274*, pp.236-244.
10. Li, C., Zhang, X., Wang, K., Zhang, H.T., Sun, X.Z. and Ma, Y.W., 2015. Three dimensional graphene networks for supercapacitor electrode materials. *New Carbon Materials*, *30*(3), pp.193-206.

11. Kitagawa, S., 2014. Metal–organic frameworks (MOFs). *Chemical Society Reviews*, *43*(16), pp.5415-5418.
12. Stock, N. and Biswas, S., 2012. Synthesis of metal-organic frameworks (MOFs): Routes to various MOF topologies, morphologies, and composites. *Chemical Reviews*, *112*(2), pp.933-969.
13. Das, R., Pachfule, P., Banerjee, R. and Poddar, P., 2012. Metal and metal oxide nanoparticle synthesis from metal organic frameworks (MOFs): Finding the border of metal and metal oxides. *Nanoscale*, *4*(2), pp.591-599.
14. Salunkhe, R.R., Kaneti, Y.V. and Yamauchi, Y., 2017. Metal–organic framework-derived nanoporous metal oxides toward supercapacitor applications: Progress and prospects. *ACS Nano*, *11*(6), pp.5293-5308.
15. Hosseinian, A., Amjad, A., Hosseinzadeh-Khanmiri, R., Ghorbani-Kalhor, E., Babazadeh, M. and Vessally, E., 2017. Nanocomposite of ZIF-67 metal–organic framework with reduced graphene oxide nanosheets for high-performance supercapacitor applications. *Journal of Materials Science: Materials in Electronics*, *28*(23), pp.18040-18048.
16. Sundriyal, S., Kaur, H., Bhardwaj, S.K., Mishra, S., Kim, K.H. and Deep, A., 2018. Metal-organic frameworks and their composites as efficient electrodes for supercapacitor applications. *Coordination Chemistry Reviews*, *369*, pp.15-38.
17. Rajak, R., Kumar, R., Ansari, S.N., Saraf, M. and Mobin, S.M., 2020. Recent highlights and future prospects on mixed-metal MOFs as emerging supercapacitor candidates. *Dalton Transactions*, *49*(34), pp.11792-11818.
18. Wang, J., Zhong, Q., Xiong, Y., Cheng, D., Zeng, Y. and Bu, Y., 2019. Fabrication of 3D Co-doped Ni-based MOF hierarchical micro-flowers as a high-performance electrode material for supercapacitors. *Applied Surface Science*, *483*, pp.1158-1165.
19. Zhu, Y., Du, W., Zhang, Q., Yang, H., Zong, Q., Wang, Q., Zhou, Z. and Zhan, J., 2020. A metal–organic framework template derived hierarchical Mo-doped LDHs@ MOF-Se core–shell array electrode for supercapacitors. *Chemical Communications*, *56*(89), pp.13848-13851.
20. Qu, C., Zhao, B., Jiao, Y., Chen, D., Dai, S., Deglee, B.M., Chen, Y., Walton, K.S., Zou, R. and Liu, M., 2017. Functionalized bimetallic hydroxides derived from metal–organic

frameworks for high-performance hybrid supercapacitor with exceptional cycling stability. *ACS Energy Letters*, *2*(6), pp.1263-1269.

21. Li, Q., Guo, H., Xue, R., Wang, M., Xu, M., Yang, W., Zhang, J. and Yang, W., 2020. Self-assembled Mo doped Ni-MOF nanosheets based electrode material for high performance battery-supercapacitor hybrid device. *International Journal of Hydrogen Energy*, *45*(41), pp.20820-20831.
22. Chen, Y., Ni, D., Yang, X., Liu, C., Yin, J. and Cai, K., 2018. Microwave-assisted synthesis of honeycomblike hierarchical spherical Zn-doped Ni-MOF as a high-performance battery-type supercapacitor electrode material. *Electrochimica Acta*, *278*, pp.114-123.
23. Chen, H.Y., Huo, Y.Q., Cai, K.Z. and Teng, Y., 2021. Controllable preparation and capacitance performance of bimetal Co/Ni-MOF. *Synthetic Metals*, *276*, p.116761.
24. Sanger, A., Malik, V.K. and Chandra, R., 2018. One step sputtered grown MoS2 nanoworms binder free electrodes for high performance supercapacitor application. *International Journal of Hydrogen Energy*, *43*(24), pp.11141-11149.
25. Shaikh, S. and Rabinal, M.K., 2020. Rapid ambient growth of copper sulfide microstructures: Binder free electrodes for supercapacitor. *Journal of Energy Storage*, *28*, p.101288.
26. Goda, E.S., Hong, S.E. and Yoon, K.R., 2021. Facile synthesis of Cu-PBA nanocubes/graphene oxide composite as binder-free electrodes for supercapacitor. *Journal of Alloys and Compounds*, *859*, p.157868.
27. Meng, S., Mo, Z., Li, Z., Guo, R. and Liu, N., 2019. Binder-free electrodes based on Mn3O4/γ-MnOOH composites on carbon cloth for supercapacitor application. *Journal of Solid State Chemistry*, *274*, pp.134-141.
28. Mariappan, V.K., Krishnamoorthy, K., Pazhamalai, P., Sahoo, S., Nardekar, S.S. and Kim, S.J., 2019. Nanostructured ternary metal chalcogenide-based binder-free electrodes for high energy density asymmetric supercapacitors. *Nano Energy*, *57*, pp.307-316.
29. Come, J., Augustyn, V., Kim, J.W., Rozier, P., Taberna, P.L., Gogotsi, P., Long, J.W., Dunn, B. and Simon, P., 2014. Electrochemical kinetics of nanostructured Nb2O5 electrodes. *Journal of the Electrochemical Society*, *161*(5), p.A718.
30. Wei, T., Zhang, M., Wu, P., Tang, Y.J., Li, S.L., Shen, F.C., Wang, X.L., Zhou, X.P. and Lan, Y.Q., 2017. POM-based metal-organic framework/reduced graphene oxide

nanocomposites with hybrid behavior of battery-supercapacitor for superior lithium storage. *Nano Energy*, *34*, pp.205-214.

31. Raju, K., Venkataiah, G. and Yoon, D.H., 2014. Effect of Zn substitution on the structural and magnetic properties of Ni–Co ferrites. *Ceramics International*, *40*(7), pp.9337-9344.
32. Yang, J., Xiong, P., Zheng, C., Qiu, H. and Wei, M., 2014. Metal–organic frameworks: A new promising class of materials for a high performance supercapacitor electrode. *Journal of Materials Chemistry A*, *2*(39), pp.16640-16644.
33. Iakunkov, A., Skrypnychuk, V., Nordenström, A., Shilayeva, E.A., Korobov, M., Prodana, M., Enachescu, M., Larsson, S.H. and Talyzin, A.V., 2019. Activated graphene as a material for supercapacitor electrodes: Effects of surface area, pore size distribution and hydrophilicity. *Physical Chemistry Chemical Physics*, *21*(32), pp.17901-17912.
34. Yu, H., Yu, J., Cheng, B. and Lin, J., 2007. Synthesis, characterization and photocatalytic activity of mesoporous titania nanorod/titanate nanotube composites. *Journal of Hazardous Materials*, *147*(1-2), pp.581-587.
35. Chen, H., Jiang, J., Zhang, L., Wan, H., Qi, T. and Xia, D., 2013. Highly conductive NiCo 2 S 4 urchin-like nanostructures for high-rate pseudocapacitors. *Nanoscale*, *5*(19), pp.8879-8883.
36. Shrivastav, V., Sundriyal, S., Goel, P., Shrivastav, V., Tiwari, U.K. and Deep, A., 2020. ZIF-67 derived Co3S4 hollow microspheres and WS2 nanorods as a hybrid electrode material for flexible 2V solid-state supercapacitor. *Electrochimica Acta*, *345*, p.136194.
37. Li, Z.J., Yang, B.C., Zhang, S.R. and Zhao, C.M., 2012. Graphene oxide with improved electrical conductivity for supercapacitor electrodes. *Applied Surface Science*, *258*(8), pp.3726-3731.
38. Zhang, S., Shi, X., Wen, X., Chen, X., Chu, P.K., Tang, T. and Mijowska, E., 2019. Interconnected nanoporous carbon structure delivering enhanced mass transport and conductivity toward exceptional performance in supercapacitor. *Journal of Power Sources*, *435*, p.226811.
39. Hwang, H., Kim, C.H., Wee, J.H., Han, J.H. and Yang, C.M., 2019. High-density graphene/single-walled carbon nanohorn composite supercapacitor electrode with high volumetric capacitance. *Applied Surface Science*, *489*, pp.708-716.

40. Sheberla, D., Bachman, J.C., Elias, J.S., Sun, C.J., Shao-Horn, Y. and Dincă, M., 2017. Conductive MOF electrodes for stable supercapacitors with high areal capacitance. *Nature Materials*, *16*(2), pp.220-224.
41. Nirmal, Sharma, K., Poonam and Tripathi, S.K., 2020, November. Synthesis and characterization of Ni-BTC MOF for supercapacitor electrode. In *AIP Conference Proceedings* (Vol. 2265, No. 1, p.030617). AIP Publishing LLC.
42. Banerjee, P.C., Lobo, D.E., Middag, R., Ng, W.K., Shaibani, M.E. and Majumder, M., 2015. Electrochemical capacitance of Ni-doped metal organic framework and reduced graphene oxide composites: More than the sum of its parts. *ACS Applied Materials & Interfaces*, *7*(6), pp.3655-3664.
43. Han, Y., Zhang, S., Shen, N., Li, D. and Li, X., 2017. MOF-derived porous NiO nanoparticle architecture for high performance supercapacitors. *Materials Letters*, *188*, pp.1-4.
44. Zhu, Y., Li, J., Yun, X., Zhao, G., Ge, P., Zou, G., Liu, Y., Hou, H. and Ji, X., 2020. Graphitic carbon quantum dots modified nickel cobalt sulfide as cathode materials for alkaline aqueous batteries. *Nano-Micro Letters*, *12*(1), pp.1-18.
45. Li, J., Yun, X., Hu, Z., Xi, L., Li, N., Tang, H., Lu, P. and Zhu, Y., 2019. Three-dimensional nitrogen and phosphorus co-doped carbon quantum dots/reduced graphene oxide composite aerogels with a hierarchical porous structure as superior electrode materials for supercapacitors. *Journal of Materials Chemistry A*, *7*(46), pp.26311-26325.

Chapter 6: Zeolitic-imidazolate framework-derived ZnO/C decorated functionalized multi-walled carbon nanotubes - a new composite electrode material for hybrid supercapacitors

Abstract

Metal-organic frameworks (MOFs) are difficult to use directly as electrode materials for electrochemical energy storage due to their poor structural stability and low electronic conductivity. The hydroxyl functionalized multi-walled carbon nanotube (f-MWCNT) was employed as a substrate to decorate ZnO/C that was generated by calcining a pristine zeolitic imidazolate framework-8 (ZIF-8) in air. XRD, BET, TGA, BET, SEM/EDX, and TEM were used to investigate the structure of the novel ZnO/C@f-MWCNT electrode. The supercapacitor's performance was measured using cyclic voltammetry (CV), galvanostatic charge-discharge (GCD), and electrochemical impedance spectroscopy in a 3M KOH electrolyte solution (EIS The research concluded that the MOF-derived composite electrode had greater storage capability than conventional electrodes with higher charge transfer resistance, as evidenced by a specific capacitance of 650 F/g at a current density of 1 A/g and a superior energy/power density. The composite electrode also shown high rate cyclability, with 98.5 percent cycling stability after 1000 cycles and 75 percent of its original capacitance preserved at 10 A/g. The synergistic benefits given by MWCNT, which boosted electrical conductivity, and ZnO/C, which supplied adequate redox-active sites and structural stability, were attributable to the outstanding performance of ZnO/C@MWCNT. This research might be used to make improved MOF-based nanocomposites for high-performance energy storage devices.

Keywords: Metal-organic frameworks, ZnO, MWCNT, nanocomposite, ZIF-8

Graphical Abstract

From MOF templates, a novel composite electrode, ZnO/C@MWCNT, was synthesized and used for electrochemical energy storage applications. At a current density of 1 A/g, the ZnO/C@MWCNT composite electrode had a high specific capacitance of 652 F/g. When its electrochemical performance was compared to that of ZnO/C, the latter was found to be better, with a capacitance of 365 F/g at the same current density. Furthermore, the Rs and Rct values of the ZnO/C@MWCNT composite electrode were lower, which explained the quick kinetics of the electrolyte ions aided by the inclusion of MWCNT.

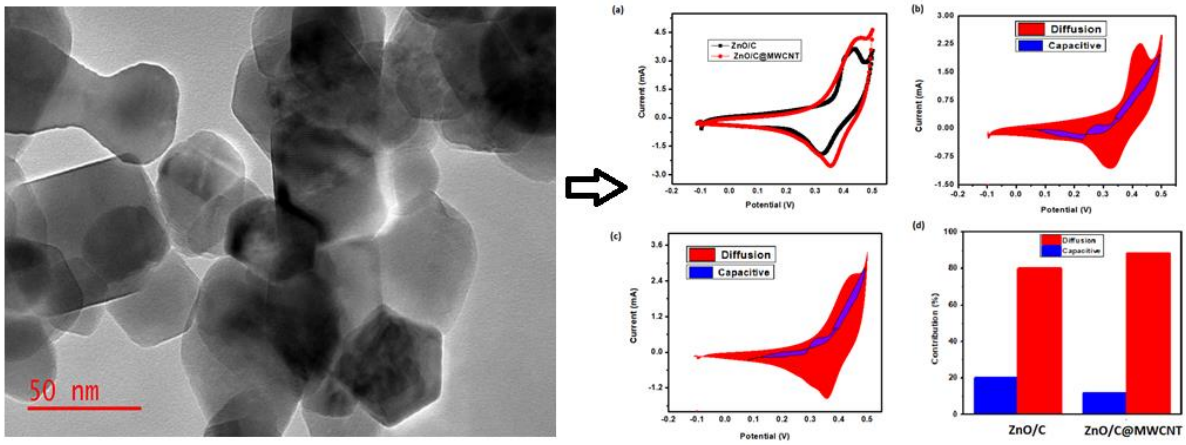

6.1 Introduction

Our fossil-fueled autos and home heating systems will need to transition to electric power in the next decades to prevent the dangers of continuous use of fossil fuels, such as climate change and pollution [1-3]. Despite the fact that electricity is a multi-purpose energy source, its limited capacity to store energy properly might be detrimental [4]. Batteries can hold a lot of energy, but charging them takes a long time [5]. Ordinary capacitors, on the other hand, may be charged relatively fast but only hold a small portion of the energy. Devices that can store and release enormous amounts of energy quickly will likely take the lead in the near future, which will most likely be dominated by electric-powered gadgets [6-7]. Supercapacitors may be able to meet both of these needs [8].

Supercapacitors are a special type of storage device that overcomes the drawbacks of traditional batteries and capacitors by assuring high power density, extended cycle life, and outstanding capacitance [9]. Despite the fact that supercapacitors have a far lower energy density than Li-ion batteries, they can be used as a backup power source [10]. Based on their charge storing method, supercapacitors may now be divided into two kinds [11]. One is the pseudocapacitor, which incorporates the Faradaic storage mechanism and stores charge through redox processes that are both fast and reversible. The electrical double layer capacitor (EDLC) stores energy by the adsorption-desorption of electrolyte ions at the electrode materials' interface. Another option is for the pseudocapacitive material to combine with EDLC to generate a hybrid electrode [12-14].

Pseudocapacitive electrode materials include transition metal oxides (ZnO, NiO, Co_2O_4, MnO_2, and SnO2) [15-16]. ZnO stands out among them because it is both cost-effective and capacitance-rich [17]. Unfortunately, poor conductivity is a problem for ZnO. ZnO can be used with materials that have a high conductivity, such as carbon-based compounds, to offset this disadvantage [18]. MWCNTs (multi-walled carbon nanotubes) are a form of carbon material with high porosity, chemical stability, huge surface area, and (most significantly) high conductivity [19]. As a result, when ZnO is composited with MWCNT, the electrochemical characteristics of ZnO are improved.

Metal-organic frameworks (MOFs) have recently sparked renewed interest as a precursor to metal oxides, such as ZnO [20]. The parent MOFs' features, such as good textural qualities, a large specific surface, high porosity, and effective functionalization, will be passed down to the derived metal oxides [21-22].

Despite the fact that much work has been done on combining MOF-derived metal oxides with carbon materials such as reduced graphene oxide (rGO) and activated carbon (AC) [23-27], the use of ZnO/C that incorporates a functionalized multi-walled carbon nanotube for energy storage applications has not been investigated to our knowledge. The major goals of this research were to look into the impacts of f-MWCNT on MOF-derived ZnO/C on the electrochemical characteristics of composite electrodes, as well as to assess the storage mechanism utilizing electrochemical kinetics.

A zeolitic imidazolate framework (ZIF-8) was used as a sacrificial template to create carbon-modified ZnO linked to functionalized MWCNT in this study. The resulting ZnO/C@f-MWCNT electrode had exceptional electrochemical performance, thanks to its huge surface area compared to a ZnO/C electrode without MWCNT, as well as its high conductivity, which was caused by MWCNT interpenetration, which also helped to support the structural framework. The specific capacitance of ZnO/C@f-MWCNT preserved more than 90% of its initial value after 1000 cycles at a current density of 10 Ag^{-1} based on these properties.

6.2 Materials and methods

6.2.1 Materials

SabiNano (Pty) Ltd in South Africa provided hydroxyl functionalized multi-walled carbon nanotubes (MWCNT, average diameter 30 nm, length 300 m, purity 99 percent). Sigma Aldrich Chemical Co. provided $Zn(NO_3)_2.6H_2O$, 2-Methylimidazolate (2-MeIm, 90%), ethanol, and methanol. Without additional purification, all of the compounds were used.

6.2.2 Synthesis of ZIF-8 MOF-derived ZnO/C

ZIF-8 MOF was originally made by dissolving 1 mmol Zn(NO3)2.6H2O and 2.2 mmol 2-MeIm in 20 mL methanol separately. At room temperature, they were progressively combined. The mixture was agitated for 30 minutes before being kept undisturbed at room temperature for another 24 hours. ZIF-8 precipitated in the bottom of the flask after the reaction and was centrifuged at 6000 rpm/min. To make ZIF-8 powder, the unreacted moieties were washed with water and then ethanol before being dried in a vacuum oven at 60 ^{o}C for 12 hours. The as-prepared ZIF-8 was calcined at 450 ^{o}C for 3 h under air to yield ZnO/C [28].

6.2.3 Synthesis of a new ZnO/C@MWCNT nanocomposite

The identical process as in section 6.2.2 was used to make ZnO/C@MWCNT, with the exception of adding 5mg of f-MWCNT in situ before the calcination stage.

6.2.4 Characterization

Scanning electron microscopy (SEM), transmission electron microscopy (TEM), and energy dispersive X-ray spectroscopy were used to examine the surface morphology and elemental composition of the composite electrode (EDX). X-ray diffraction (XRD) revealed the phase crystallinity and chemical structure, whereas thermogravimetric investigation revealed the thermal behavior (TGA). The Brunauer-Emmett-Teller (BET) technique was used to assess the textural qualities, such as surface area and porosity.

6.2.5 Electrochemical analysis

Using a three-electrode arrangement and a 3M KOH electrolyte solution, electrochemical study of the electrode materials, f-MWCNT, ZnO/C, and ZnO/C@f-MWCNT, was performed. Ag/AgCl and Pt wire were utilized as the reference and counter electrodes, respectively. The working electrode was made by dissolving 80% of the active ingredients, 10% carbon black, and 10% polyvinylidene difluoride (PVDF) in 5 ml N-methyl-2-pyrrolidone (NMP), then coating it on a carefully cleaned 1 x 1 cm^2 nickel foam (NF) and drying it overnight in a vacuum oven.

The electrochemical characteristics were assessed using cyclic voltammetry (CV), galvanostatic charge-discharge (GCD), and electrochemical impedance spectroscopy (EIS). Using equations (6.1), (6.2), and (6.3) [29], the parameters utilized to assess the performance of the electrode materials - such as specific capacitance, energy, and power density in a three-electrode configuration - were determined based on the GCD plots:

$$C = \frac{I \times \Delta t}{m \times \Delta V} \tag{6.1}$$

$$E = \frac{C \times (\Delta V)^2}{7.2} \tag{6.2}$$

$$P = \frac{3600E}{\Delta t} \tag{6.3}$$

Where I(A) represents the discharge current, t (s) represents the discharge period, m(g) represents the active material mass, and V (V) represents the discharge potential window.

6.3 Results and discussion

6.3.1 Thermogravimetric analysis (TGA)

TGA was used to examine the thermal behavior of the as-synthesised samples, as illustrated in Figure 6.1. When the MWCNT was heated to 600 ^{o}C, there was essentially little weight loss, indicating that the hydroxyl functionalized MWCNT had high thermal stability. In the case of ZnO/C, the initial weight loss of around 2% at 150 ^{o}C might be attributed to a loss of water molecules physically adsorbed on the surface of ZnO/C [30]. The breakdown of $Zn(OH)_2$ is responsible for the second weight loss at a higher temperature (550 ^{o}C). Because of the inorganic character of carbon-modified zinc oxide and the added stability provided by the MWCNT, ZnO/C@MWCNT has superior thermal stability than ZnO/C. Functionalized MWCNT was effectively integrated into ZnO/C, according to these findings.

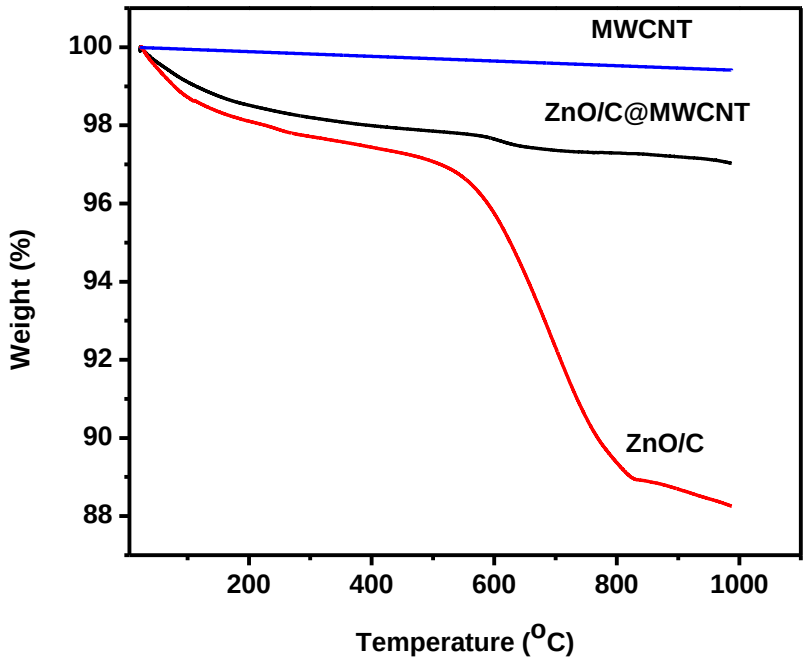

Figure 6.1 TGA curves of functionalized multi-walled carbon nanotube, f-MWCNT; ZnO/C; and ZnO/C@f-MWCNT.

6.3.2 XRD

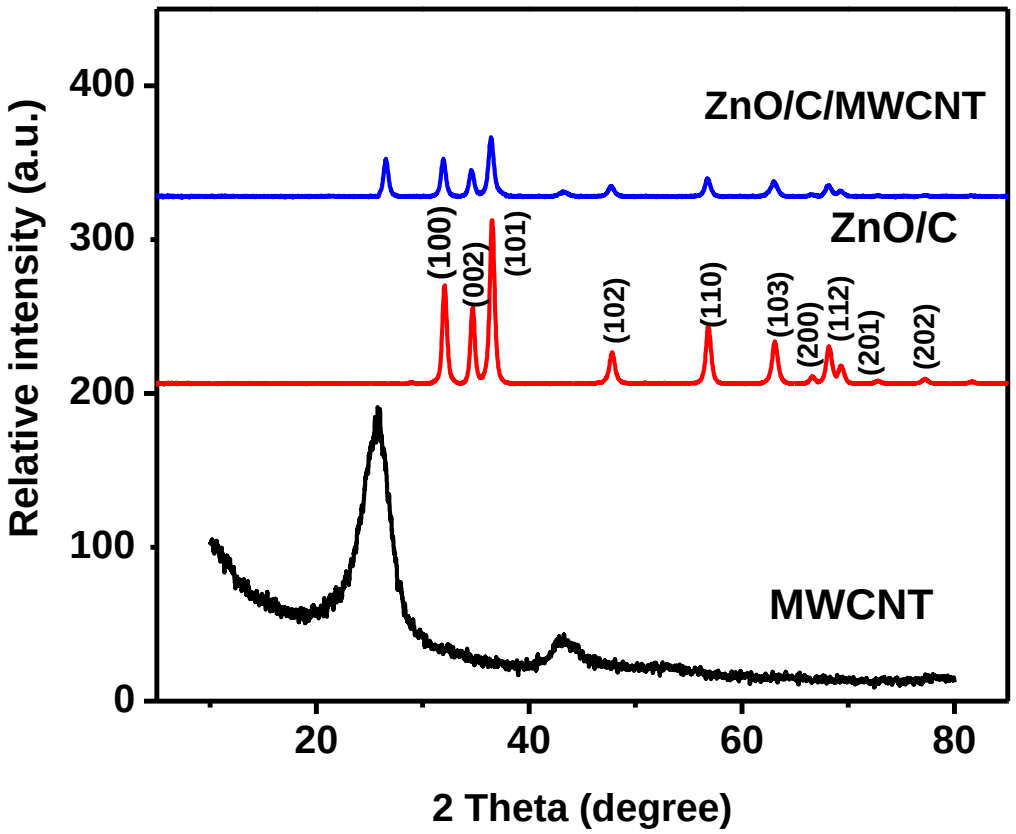

Figure 6.2 XRD patterns of a functionalized multi-walled carbon nanotube, MWCNT, ZnO/C and ZnO/C@MWCNT.

Figure 6.2 shows how the crystalline properties of the nanocomposites were revealed by their diffraction patterns. The peaks of MWCNT are crisp, demonstrating the material's crystallinity, with distinctive peaks at 25.5o and 43.6o. This relates to crystal facets (002) and crystal facets (003), according to JCPDS data card number 03-065-6212. (201). Based on JCPDS file number 04-015-4060 [31], the diffraction patterns of ZnO/C exhibit strong peaks at 2 = 35.5, 37, 39, 45.6, 55.3, 65, and 69, which may be indexed to (100), (002), (101), (102), (110), (103), (200), (112), and (201), respectively. The synthesis of the ZnO/C@MWCNT nanocomposite was effective since it shared the specific peak characteristics of ZnO/C and MWCNT. MWCNT peaks were missing in ZnO/C but evident in ZnO/C@f-MWCNT, indicating that MWCNT was successfully

incorporated. In Figure 6.2, there are no impurity peaks, indicating that the nanocomposite was successfully synthesized.

6.3.3 SEM/EDX and TEM

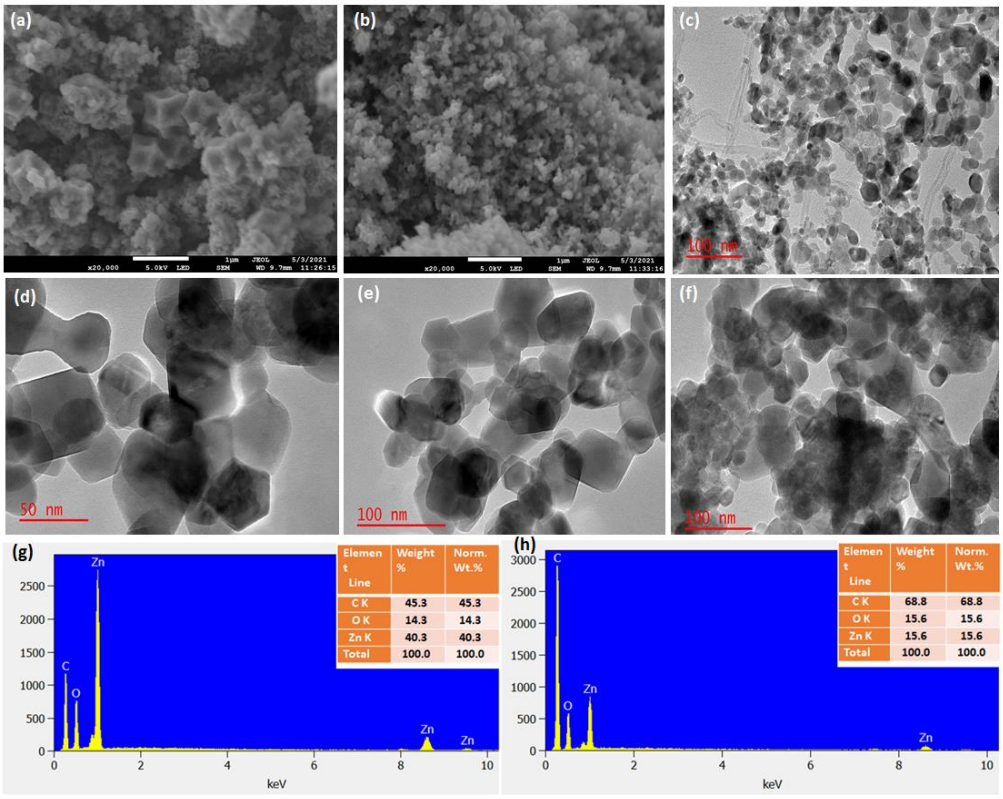

Figure 6.3 SEM images of: (a) ZnO/C; (b) ZnO/C@f-MWCNT. TEM images of: (c) a functionalized multi-walled carbon nanotube, f-MWCNT; (d-e) ZnO/C; (f) ZnO/C@f-MWCNT, EDX spectra of (g) ZnO/C and (h) ZnO/C@f-MWCNT

The morphology of ZnO/C produced by calcination of virgin ZIF-8 preserved the recognized octahedral form of ZIF-8, as shown in Figure 6.3(a) and 6.3(b). MWCNT was included and took on a spherical form that was linked to the MWNCT network. The TEM data in Figure 6.3(c-f), examined at a magnification of 100 nm, likewise verified this form. The TEM pictures clearly show that the as-synthesised materials have a consistent size distribution and a smooth surface. EDX was used to investigate the electrode materials' elemental makeup. They included Zn, O, and C, as predicted. When compared to its ZnO/C counterpart, the ZnO/C@f-MWCNT had a greater carbon contention and a lower Zn concentration. This is because MWCNT has been included into ZnO/C.

6.3.4 BET

The porosity and specific surface areas of the composite electrodes were assessed by BET. The findings are shown in Table 6.1. ZnO/C@f-MWCNT has a surface area of 46.4 m^2/g and a pore size of 0.386 nm, according to the data, whereas ZnO/C has a surface area of 38.5 m^2/g. The presence of MWCNT might explain why ZnO/C@f-MWCNT has a larger surface area than ZnO/C.

Table 6.1: Surface area and pore characteristics of the electrode materials.

Material	Surface area (m^2/g)	Pore volume (cm^3/g)	Pore size (nm)
ZnO/C	38.5	0.17	12.7
ZnO/C@f-MWCNT	46.4	0.38	10.5

6.4 Electrochemical performance

In a three-electrode system arrangement, CV, GCD, and EIS analyses were performed on the composite electrodes ZnO/C and ZnO/C@MWCNT. (For more information, see Figures 6.4 and 6.5.) After testing at various scan rates ranging from 5 to 50 mV/s, the CV curves (Figure 6.4a and Figure 6.4c) were produced. Redox peaks were visible on the curves, which might be attributed to the Faradaic redox process. When the two electrodes were compared (Figure 6.4e), it was discovered that ZnO/C@MWCNT had a higher current than ZnO/C, indicating that it will have greater storage capability.

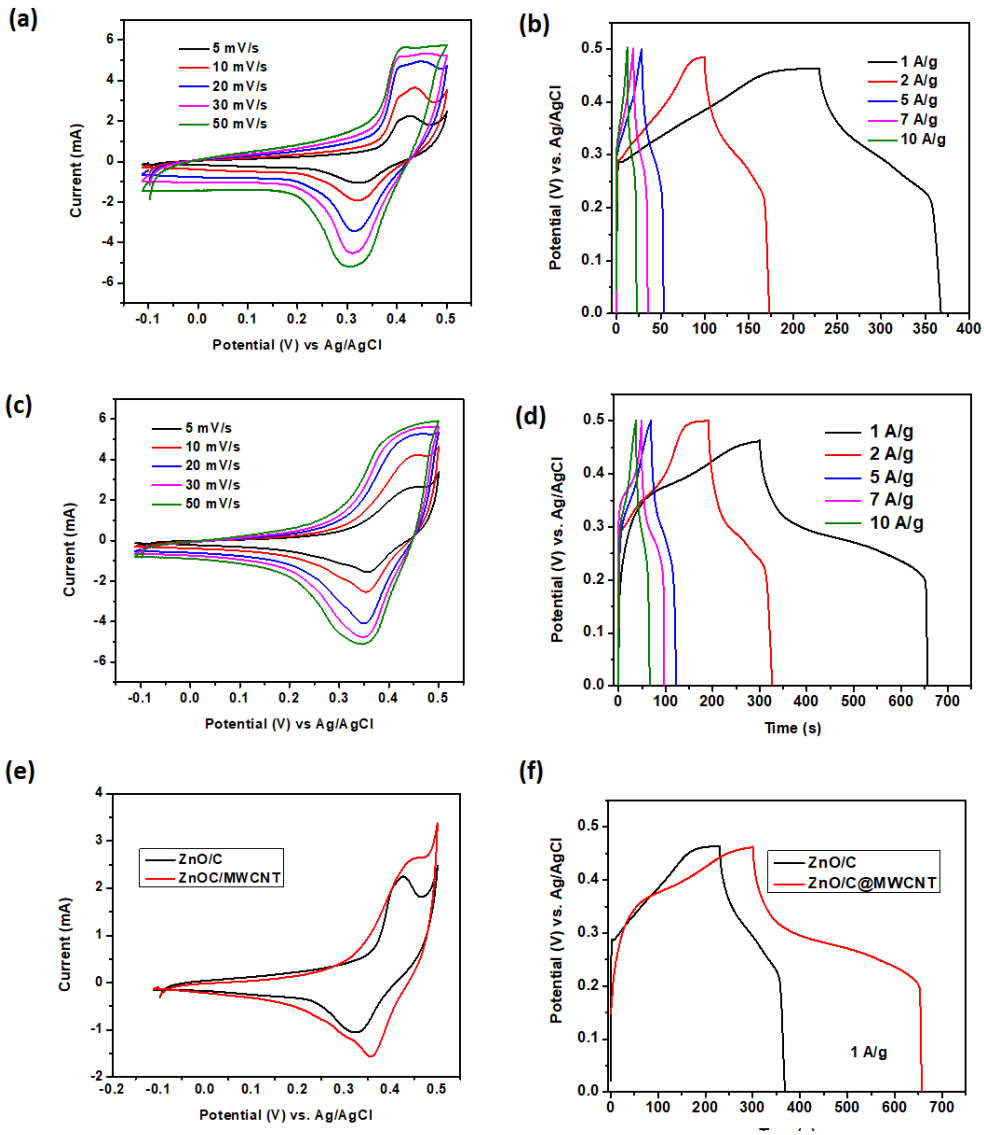

Figure 6.4 Results showing (a) CV and (b) GCD curves of ZnO/C; (c) CV and (d) GCD curves of ZnO/C@MWCNT. Comparison of the (e) CV curves and (f) GCD curves of ZnO/C and ZnO/C@MWCNT.

The performance of the produced electrodes was further tested using GCD analysis. (For further information, see Figures 6.4b, d, and f.) Figure 6.4f reveals that the discharge curves of ZnO/C@MWCNT are the longest, indicating greater performance. The non-linear GCD curves in Figures 6.4b and 6.4d are characteristic of pseudocapacitors. The specific capacitance of each electrode was estimated using equations derived from GCD curves (6.1). The results revealed that ZnO/C@MWCNT had superior performance, with a maximum specific capacitance of 650 F/g at 1 A/g compared to 365 F/g for ZnO/C at the same current density. Furthermore, when compared

to ZnO/C without MWCNT, the ZnO/C@MWCNT preserved around 85% of its original capacitance value, indicating outstanding rate capability. The greater conductivity given by MWCNT, as well as shorter ion diffusion within the electrolyte solution, may explain the enhanced performance of ZnO/C@MWCNT. Table 6.2 compares the electrochemical performance of the synthesized composite electrode to that of comparable materials described in the literature.

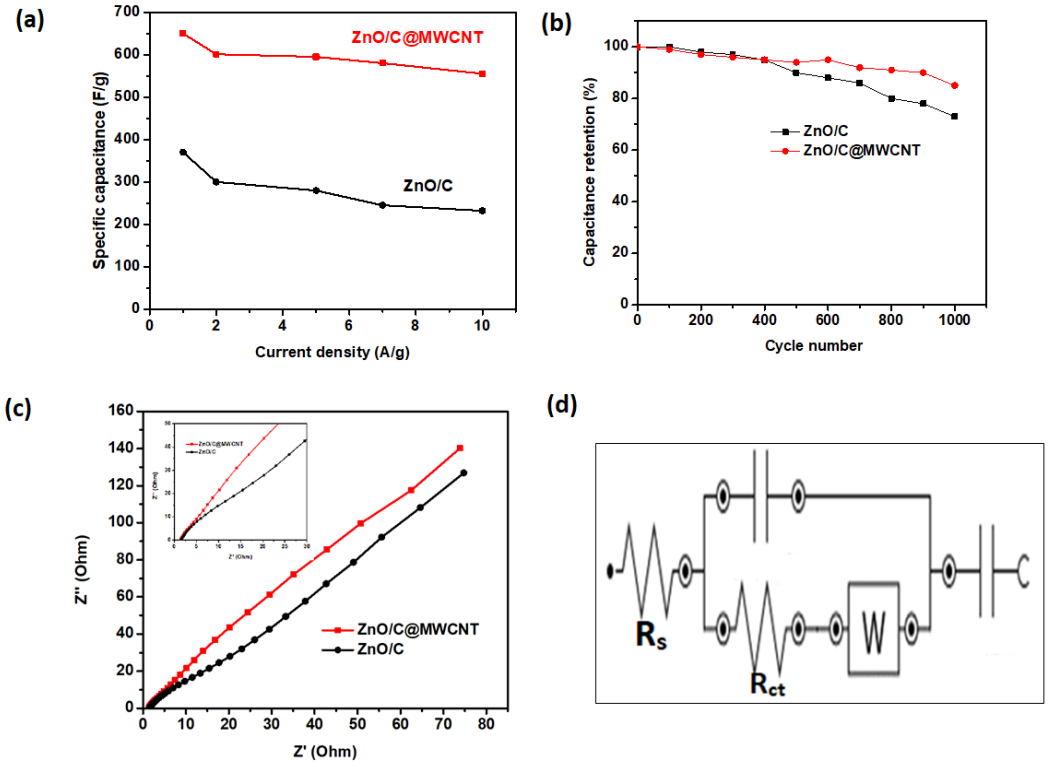

Figure 6.5 (a) Specific capacitance of the electrodes against the current density. (b) Cycling stability of the electrodes. (c) Nyquist plot of the electrodes with the inset showing the curve obtained at a lower frequency. (d) The equivalent electrochemical circuit used to fit the Nyquist plot.

Table 6.2: Comparison of the energy storage performance of the electrode materials.

Electrode	Electrolyte	Specific capacitance (F/g)	Current density/scan rate	Ref.
3DG/ZnO nanorods	1M KOH	554 F/g	5 mV/s	31
ZnO@MOF@PANI	3.0M KCl	340	1 A/g	32
ZnO/rGO	3.5M KOH	203	1 A/g	33
ZnO/AC	1M Na_2SO_4	155	0.5 A/g	34
CuO/ZnO	2M KOH	579	1 A/g	35
ZnO/CNT	1M Na_2SO_4	189	1 mV/s	36
CNT-ZnO	1M KCl	329	-	37
ZnO/C@MWCNT	3M KOH	650	1 A/g	This work

Cycling stability study was performed using GCD curves at a current density of 5A/g/ to further assess the performance of the produced electrodes. (For further information, see Figure 6.5b.) After 1000 cycles, cycling stability was found to be at 85 percent, compared to 72 percent for ZnO/C. This demonstrates that adding MWCNT to the composite electrode improved its stability. To further verify the storage performance and validate the better performance of ZnO/C@MWCNT compared to ZnO/C, an EIS study of the as-synthesised electrodes was performed.

Figure 6.5c depicts the Nyquist plots of ZnO/C and ZnO/C/@MWCNT: a semi-circle and a line angled at roughly 45^o to the x-axis. The solution resistance (Rs) was calculated using the intercept of the plots with respect to the x-axis, while the charge transfer resistance was calculated using the diameter of the semi-circle (R_{ct}). The R_s values for ZnO/C and ZnO/C@MWCNT were 1.07 and 0.24, respectively, whereas the Rct values were 2.57 and 1.32. When compared to ZnO/C, the low

R_s and R_{ct} values found for ZnO/C@MWCNT explain the quick kinetics of the electrolyte ions resulting from the integration of MWCNT, which boosted its performance.

Also, the existence of a prominent Faradaic peak in Figure 6.4 (a), (c), and (e) indicates that the Faradaic reaction is in charge of supercapacitive behavior. Due to the delayed intercalation of ions and electrons to the innermost section of the electrode, the position of the peak current is moved with respect to the potential as the scan rate rises. This might also imply that the Faradaic reaction kinetics are reversible, and that the kinetic hitch causes the Faradaic peaks to be shifted after a short time.

With reference to CV, equations (6.1) and (6.2) were used to distinguish between the contributions produced by capacitive and diffusion-controlled processes:

$$i = k_1 v + k_2 v^{0.5} \quad (6.1)$$

$$i/v^{0.5} = k_1 v^{0.5} + k_2 \quad (6.2)$$

The capacitive contribution is represented by k1v in equation (6.1), whereas the ion-diffusion contribution is represented by $k_2 v^{0.5}$. As a result of equation (6.2), plotting $i/v^{0.5}$ versus $v^{0.5}$ yielded a straight line from which the slope, k_1, and intercept, k_2, could be calculated. The individual percentage contributions were then determined by multiplying the k_1 and k_2 values acquired by the scan rates of interest. The percentage contributions were emphasized in Figure 6.6 and extended in Table 6.3, and the capacitive and ion-diffusion controlled processes were estimated at a scan rate of 5 mV/s for this reason. At a scan rate of 5 mV/s, the diffusion-controlled contribution for ZnO/C and ZnO/C@MWCNT was found to be 80 percent and 88.15 percent, respectively. The capacitive charge storage mechanism of the ZnO/C and ZnO/C@MWCNT electrodes is consistent with the Zn^{2+} charge storage mechanism of the ZnO/C and ZnO/C@MWCNT electrodes.

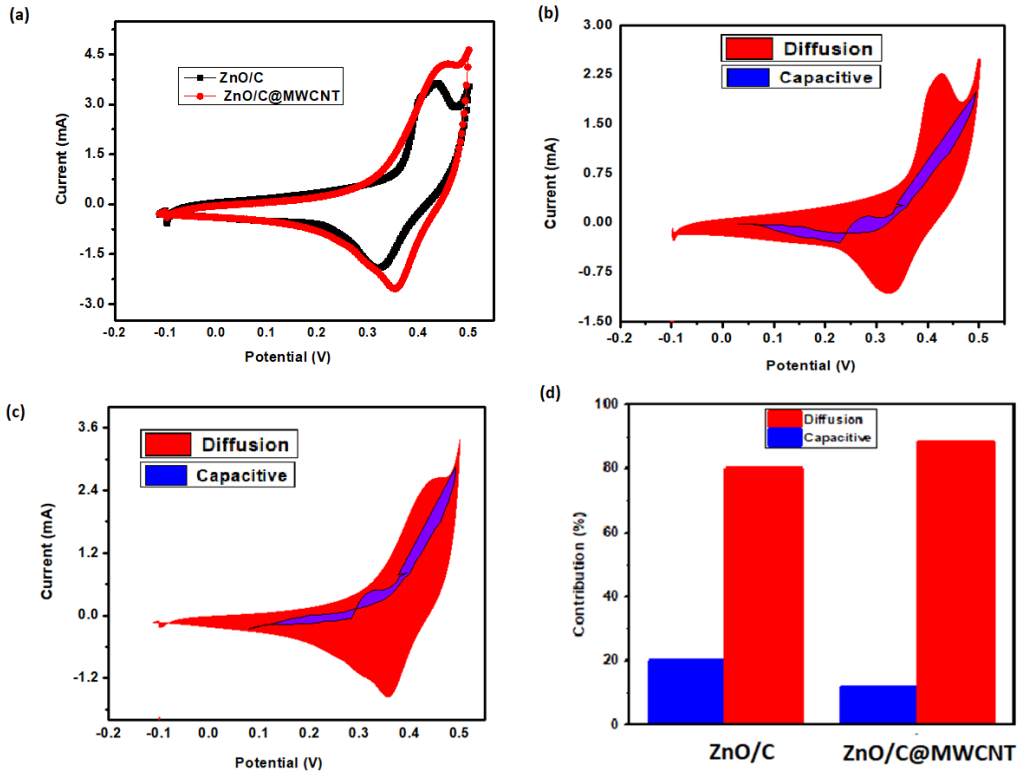

Figure 6.6 Analysis results of (a) Comparative CV curves of ZnO/C and ZnO/C@MWCNT. CV curves with capacitive and diffusion fractions shown in blue and red, respectively, for: (b) ZnO/C; (c) ZnO/C@MWCNT. (d) Bar chart showing the percentage contribution of the capacitive and diffusion-controlled processes at a scan rate of 5mV/s.

Table 6.3: Results of the capacitive and ion-diffusion controlled processes at a scan rate of 5 mV/s.

Electrode materials	Parameters							
	v	$v^{0.5}$	k_1	k_2	k_1/v	$k_2/v^{0.5}$	Capacitive contribution	Ion-diffusion contribution
ZnO/C	5	2.24	1.42	2.53	0.28	1.12	20.0%	80.0%
ZnO/C@MWCNT	5	2.24	1.91	6.32	0.38	2.82	11.9%	88.1%

6.5 Conclusion

The novel MOF-derived ZnO/C@MWCNT composite electrode was effectively synthesized using a pristine zeolitic imidazolate framework, ZIF-8, and simple solvothermal and calcination procedures. In an aqueous 3M KOH solution, the produced composite electrode demonstrated outstanding electrochemical storage performance. At a current density of 1 A/g, the ZnO/C@MWCNT composite electrode had a high specific capacitance of 652 F/g. When comparing electrochemical performance to ZnO/C, the latter has a capacitance value of 365 F/g at the same current density, indicating higher performance. Furthermore, the R_s and R_{ct} values of the ZnO/C@MWCNT composite electrode were lower, which explained the quick kinetics of the electrolyte ions aided by the inclusion of MWCNT. The greater conductivity of MWCNT, as well as shorter ion diffusion within the electrolyte solution, might explain the improved performance of ZnO/C@MWCNT. The findings of this study showed that using a ZnO/C@MWCNT composite electrode to improve energy storage performance is a viable option.

6.6 References

1. Winter, C.J., 2009. Hydrogen energy—Abundant, efficient, clean: A debate over the energy-system-of-change. *International Journal of Hydrogen Energy*, *34*(14), pp.S1-S52.
2. Perez-Sindin, X.S., 2021. Are energy megaprojects socially disruptive? Assessing the impacts of the As Pontes fossil fueled power plant in Spain. *Energy Research & Social Science*, *80*, p.102229.
3. Bartolini, A., Comodi, G., Salvi, D. and Østergaard, P.A., 2020. Renewables self-consumption potential in districts with high penetration of electric vehicles. *Energy*, *213*, p.118653.
4. Gorjian, S., Ebadi, H., Trommsdorff, M., Sharon, H., Demant, M. and Schindele, S., 2021. The advent of modern solar-powered electric agricultural machinery: A solution for sustainable farm operations. *Journal of Cleaner Production*, p.126030.
5. Cho, J., Jeong, S. and Kim, Y., 2015. Commercial and research battery technologies for electrical energy storage applications. *Progress in Energy and Combustion Science*, *48*, pp.84-101.
6. Kötz, R. and Carlen, M.J.E.A., 2000. Principles and applications of electrochemical capacitors. *Electrochimica Acta*, *45*(15-16), pp.2483-2498.

7. Inagaki, M., Konno, H. and Tanaike, O., 2010. Carbon materials for electrochemical capacitors. *Journal of Power Sources*, *195*(24), pp.7880-7903.
8. Raza, W., Ali, F., Raza, N., Luo, Y., Kim, K.H., Yang, J., Kumar, S., Mehmood, A. and Kwon, E.E., 2018. Recent advancements in supercapacitor technology. *Nano Energy*, *52*, pp.441-473.
9. Pan, H., Li, J. and Feng, Y., 2010. Carbon nanotubes for supercapacitor. *Nanoscale Research Letters*, *5*(3), pp.654-668.
10. Niu, J., Shao, R., Liang, J., Dou, M., Li, Z., Huang, Y. and Wang, F., 2017. Biomass-derived mesopore-dominant porous carbons with large specific surface area and high defect density as high performance electrode materials for Li-ion batteries and supercapacitors. *Nano Energy*, *36*, pp.322-330.
11. Ghaemi, M., Ataherian, F., Zolfaghari, A. and Jafari, S.M., 2008. Charge storage mechanism of sonochemically prepared MnO2 as supercapacitor electrode: Effects of physisorbed water and proton conduction. *Electrochimica Acta*, *53*(14), pp.4607-4614.
12. Simon, P. and Gogotsi, Y., 2010. Charge storage mechanism in nanoporous carbons and its consequence for electrical double layer capacitors. *Philosophical Transactions of the Royal Society A: Mathematical, Physical and Engineering Sciences*, *368*(1923), pp.3457-3467.
13. Tiwari, P., Jaiswal, J. and Chandra, R., 2019. Hierarchal growth of MoS2@ CNT heterostructure for all solid state symmetric supercapacitor: Insights into the surface science and storage mechanism. *Electrochimica Acta*, *324*, p.134767.
14. Wang, H., Forse, A.C., Griffin, J.M., Trease, N.M., Trognko, L., Taberna, P.L., Simon, P. and Grey, C.P., 2013. In situ NMR spectroscopy of supercapacitors: Insight into the charge storage mechanism. *Journal of the American Chemical Society*, *135*(50), pp.18968-18980.
15. Nagarani, S., Sasikala, G., Satheesh, K., Yuvaraj, M. and Jayavel, R., 2018. Synthesis and characterization of binary transition metal oxide/reduced graphene oxide nanocomposites and its enhanced electrochemical properties for supercapacitor applications. *Journal of Materials Science: Materials in Electronics*, *29*(14), pp.11738-11748.
16. Low, W.H., Khiew, P.S., Lim, S.S., Siong, C.W. and Ezeigwe, E.R., 2019. Recent development of mixed transition metal oxide and graphene/mixed transition metal oxide based hybrid nanostructures for advanced supercapacitors. *Journal of Alloys and Compounds*, *775*, pp.1324-1356.

17. Purushothaman, K.K., Priya, V.S., Nagamuthu, S., Vijayakumar, S. and Muralidharan, G., 2011. Synthesising of ZnO nanopetals for supercapacitor applications. *Micro & Nano Letters*, *6*(8), pp.668-670.
18. Gao, M., Wang, W.K., Rong, Q., Jiang, J., Zhang, Y.J. and Yu, H.Q., 2018. Porous ZnO-coated Co3O4 nanorod as a high-energy-density supercapacitor material. *ACS Applied Materials & Interfaces*, *10*(27), pp.23163-23173.
19. Sarkar, A., Chakraborty, A.K., Bera, S. and Krishnamurthy, S., 2018. Novel hydrothermal synthesis of CoS2/MWCNT nanohybrid electrode for supercapacitor: A systematic investigation of the influence of MWCNT. *The Journal of Physical Chemistry C*, *122*(32), pp.18237-18246.
20. Xia, H., Zhang, J., Yang, Z., Guo, S., Guo, S. and Xu, Q., 2017. 2D MOF nanoflake-assembled spherical microstructures for enhanced supercapacitor and electrocatalysis performances. *Nano-micro Letters*, *9*(4), pp.1-11.
21. Liu, B., Shioyama, H., Jiang, H., Zhang, X. and Xu, Q., 2010. Metal–organic framework (MOF) as a template for syntheses of nanoporous carbons as electrode materials for supercapacitor. *Carbon*, *48*(2), pp.456-463.
22. Yu, H., Xia, H., Zhang, J., He, J., Guo, S. and Xu, Q., 2018. Fabrication of Fe-doped Co-MOF with mesoporous structure for the optimization of supercapacitor performances. *Chinese Chemical Letters*, *29*(6), pp.834-836.
23. Wu, H.B., Zhang, G., Yu, L. and Lou, X.W.D., 2016. One-dimensional metal oxide–carbon hybrid nanostructures for electrochemical energy storage. *Nanoscale Horizons*, *1*(1), pp.27-40.
24. Zhi, M., Xiang, C., Li, J., Li, M. and Wu, N., 2013. Nanostructured carbon–metal oxide composite electrodes for supercapacitors: A review. *Nanoscale*, *5*(1), pp.72-88.
25. De, B., Banerjee, S., Verma, K.D., Pal, T., Manna, P.K. and Kar, K.K., 2020. Transition metal oxide/carbon nanofiber composites as electrode materials for supercapacitors. In *Handbook of Nanocomposite Supercapacitor Materials II* (pp. 201-227). Springer, Cham.
26. Wang, Y.C., Li, W.B., Zhao, L. and Xu, B.Q., 2016. MOF-derived binary mixed metal/metal oxide@carbon nanoporous materials and their novel supercapacitive performances. *Physical Chemistry Chemical Physics*, *18*(27), pp.17941-17948.

27. Sasirekha, C., Arumugam, S. and Muralidharan, G., 2018. Green synthesis of ZnO/carbon (ZnO/C) as an electrode material for symmetric supercapacitor devices. *Applied Surface Science*, *449*, pp.521-527.
28. Pan, Y., Liu, Y., Zeng, G., Zhao, L. and Lai, Z., 2011. Rapid synthesis of zeolitic imidazolate framework-8 (ZIF-8) nanocrystals in an aqueous system. *Chemical Communications*, *47*(7), pp.2071-2073.
29. Seevakan, K., Manikandan, A., Devendran, P., Slimani, Y., Baykal, A. and Alagesan, T., 2018. Structural, morphological and magneto-optical properties of CuMoO4 electrochemical nanocatalyst as supercapacitor electrode. *Ceramics International*, *44*(16), pp.20075-20083.
30. Samadi, M., Shivaee, H.A., Zanetti, M., Pourjavadi, A. and Moshfegh, A., 2012. Visible light photocatalytic activity of novel MWCNT-doped ZnO electrospun nanofibers. *Journal of Molecular Catalysis A: Chemical*, *359*, pp.42-48.
31. Li, X., Wang, Z., Qiu, Y., Pan, Q. and Hu, P., 2015. 3D graphene/ZnO nanorods composite networks as supercapacitor electrodes. *Journal of Alloys and Compounds*, *620*, pp.31-37.
32. Zhu, C., He, Y., Liu, Y., Kazantseva, N., Saha, P. and Cheng, Q., 2019. ZnO@ MOF@ PANI core-shell nanoarrays on carbon cloth for high-performance supercapacitor electrodes. *Journal of Energy Chemistry*, *35*, pp.124-131.
33. Subramani, K. and Sathish, M., 2019. Facile synthesis of ZnO nanoflowers/reduced graphene oxide nanocomposite using zinc hexacyanoferrate for supercapacitor applications. *Materials Letters*, *236*, pp.424-427.
34. Lee, K.S., Park, C.W. and Kim, J.D., 2018. Synthesis of ZnO/activated carbon with high surface area for supercapacitor electrodes. *Colloids and Surfaces A: Physicochemical and Engineering Aspects*, *555*, pp.482-490.
35. Wu, F., Wang, X., Hu, S., Hao, C., Gao, H. and Zhou, S., 2017. Solid-state preparation of CuO/ZnO nanocomposites for functional supercapacitor electrodes and photocatalysts with enhanced photocatalytic properties. *International Journal of Hydrogen Energy*, *42*(51), pp.30098-30108.
36. Ranjithkumar, R., Arasi, S.E., Sudhahar, S., Nallamuthu, N., Devendran, P., Lakshmanan, P. and Kumar, M.K., 2019. Enhanced electrochemical studies of ZnO/CNT nanocomposite for supercapacitor devices. *Physica B: Condensed Matter*, *568*, pp.51-59.

37. Zhang, Y., Sun, X., Pan, L., Li, H., Sun, Z., Sun, C. and Tay, B.K., 2009. Carbon nanotube–ZnO nanocomposite electrodes for supercapacitors. *Solid State Ionics*, *180*(32-35), pp.1525-1528.

Chapter 7: Conclusion and recommendations

7.1 Conclusion

The primary objective of this research study was to make use of existing experimental findings to advance the knowledge on how to bridge the gap in understanding the deficiencies associated with the utility of MOFs in electrochemical energy storage by: developing a new synthetic route; preparing novel composite electrode materials; probing the storage mechanism of the fabricated electrodes to better understand their performance. The results and discussion were presented in chapters 4, 5 and 6 and the key results emanating from this study are summarized in this chapter.

Significant progress has been made in this study towards enhancing the performance of MOFs for supercapacitor applications. Experimental studies were performed that involved: preparing pristine MOFs; transforming these into new MOF-derived nanocomposites and characterizing them using spectroscopic tools, including XRD, Raman spectroscopy, FTIR, SEM, TEM, EDX, nitrogen adsorption-desorption analysis (BET), EDX and TGA. In other cases, a new synthetic protocol was employed to deliver MOF-derived nanocomposite electrodes. Thereafter, electrochemical evaluation was carried out in a three-electrode system using Autolab PGSTAT 302N. A full analysis was conducted in an aqueous alkaline electrolyte using cyclic voltammetry (CV), galvanostatic charge-discharge (GCD) and electrochemical impedance spectroscopy (EIS) analyses. Useful insight into the storage mechanism of the prepared electrodes was obtained from the electrochemical kinetic analyses.

The experimental work confirmed the possibility of enhancing the performance of MOFs in supercapacitors. The knowledge obtained, either by introducing new functions into the pristine MOFs or by using MOFs as a sacrificial template/precursor to afford MOF-based nanostructures and composites, was tailored towards enhancing the performance of the electrochemical supercapacitor, in terms of specific capacitance, energy and power density, rate capability and cycling stability. Based on the results obtained and reported on in chapters 4, 5 and 6, key conclusions were drawn. These are detailed below.

7.1.1 Double-linker MOF-strategy for the fabrication of NiO and NiO/C composite electrodes

- A double-linker approach was adopted, for the first time, for successful synthesis of NiO and NiO/C supercapacitor electrodes, namely NiO/Ni-400, NiO/Ni-500 and NiO-600.
- The morphology of the parent Ni-MOF was preserved at different annealing temperatures, while the MOF-derived electrodes featured a more porous structure. This confirmed the framework decomposition in Ni-MOF.
- The CV curves showed oxidation-reduction peak pairs, which can be attributed to the Faradaic redox reaction and good reversibility.
- The GCD curves display a non-linear relationship with respect to the current density for all three-electrode materials, which is characteristic of pseudocapacitive behavior.
- The low charge-transfer resistance indicated in the Nyquist plot of the EIS for the NiO/Ni-400 composite electrode suggests high conductivity, which significantly influenced its remarkable specific capacitance.
- The MOF-derived NiO/Ni-400 composite electrode annealed at 400 ^{o}C exhibited superior activity of 753 Fg^{-1} at 1 Ag^{-1}, a maximum energy density of 26 Wh kg^{-1} and a power density of 2393 Wkg^{-1}.
- For the same NO/Ni-400 composite electrode, about 85% of the initial capacitance (753 Fg^{-1}) was retained when the capacitance increased to 10 Ag^{-1}. The reduction in the capacitance value could be ascribed to the active materials leaching from the electrode during the electrochemical reaction.
- The MOF-derived NO/Ni-400 composite electrode exhibited a remarkable cycling performance: 90% after 1000 cycles at 5 Ag^{-1}.
- A linear relationship between the oxidation-reduction peak current and the square root of the scan rates of the tested electrodes showed that the electrode surface reaction was influenced by the diffusion process at all the tested scan rates.

7.1.2 Self-assembled Zn-functionalized Ni-MOFs as binder-free electrodes for electrochemical energy storage applications

- Zinc-functionalized nickel metal-organic framework (Zn/Ni-MOF) composite electrodes were grown directly on nickel foam (NF) and used as binder-free electrodes (ZNN1, ZNN2 and ZNN3) in supercapacitors for the first time.
- The undoped Ni-MOF exhibited a nanosheet structure, which converted to a flower-like nanosphere when the Zn dopant was added.
- The nature of the microspheres and the flowers on them varied as the concentration of the dopant was varied.
- The optimum doping concentration produced a composite electrode (ZNN1) that exhibited the best morphology in terms of smoothness, uniformity and interconnection of its particles.
- The XRD, SEM/EDX and FTIR analyses confirmed the chemical structure and composition of the fabricated electrode materials.
- ZNN1 displayed the largest CV peak current and closed area, with respect to the same area. This was the best performance when compared to ZNN2 and ZNN3.
- The CV curves exhibited two pairs of redox peaks that are typical of pseudocapacitive behavior. An increase in the scan rate did not affect the overall shape of the CV curves, which suggests an outstanding rate capability for storing energy.
- Interestingly, it was obvious that the process of discharging Zn-doped materials required more time than was required by the pristine material, hence showing better performance.
- ZNN1 delivered the highest specific capacitance (391 F/g at 1 A/g) and a good rate capability when the scan rate was increased to 10 A/g. The ZNN1 electrode also exhibited excellent cycling stability of 93% after 1000 cycles.
- The electrochemical kinetic analysis of ZNN1 indicated that the storage mechanism is predominantly a diffusion-controlled process at all tested scan rates.
- The excellent performance was credited to the synergistic effect of the high surface area, optimum Zn doping and low internal resistance, which facilitated the rapid transport of ions in the electrolyte solution.
- The binder-free strategy employed for doping pristine MOFs employed in this study could be used for the rational design of pseudocapacitive electrodes.

7.1.3 New ZnO/C@MWCNT supercapacitor electrode with high performance

- A new ZnO/C that incorporates a functionalized multi-walled carbon nanotube (MWCNT) was successfully synthesized and characterized.
- ZnO/C@MWCNT displayed better thermal stability than ZnO/C, due to the inorganic nature of carbon-modified zinc oxide and the extra stability offered by the MWCNT.
- ZnO/C@MWCNT showed the longest discharge curves, which indicates superior performance compared to ZnO.
- ZnO/C@MWCNT delivered a better performance with a maximum specific capacitance of 650 F/g at a current density of 1 A/g compared to the 365 F/g obtained for ZnO/C at the same current density.
- A comparison of the supercapacitor performance of the new electrode to the data in the related literature showed that it has one of the best specific capacitance values.
- ZnO/C@MWCNT retained about 85% of its initial capacitance value, compared to 76% for ZnO/C without MWCNT. This indicates excellent rate capability.
- The cycling stability of ZnO/C@MWCNT was approximately 85% after 1000 cycles, compared to 72% shown by ZnO/C. This suggests that incorporation of MWCNT gave the composite electrode additional stability.
- The low EIS value of Rs and Rct obtained for ZnO/C@MWCNT compared to those of ZnO/C explained the rapid kinetics of the electrolyte ions from the incorporation of MWCNT, which further improved its performance.
- The high performance of ZnO/C@MWCNT was ascribed to the higher conductivity provided by MWCNT, in addition to shorter diffusion of ions within the electrolyte solution.

7.2 Recommendations

It is hoped that this study will provide incentive for further research. Where the analysis results seem inconclusive, it elicits further thinking for improvement. Nevertheless, this study provides a meaningful contribution to the understanding of the role played by electrode materials in energy storage applications, by investigating MOFs and derived electrodes.

The recommendations for future research are:

- For large-scale applications of the fabricated MOF-derived electrodes, it is recommended that all electrode materials should be tested using a two-electrode system configuration, including LED.

- More kinetic models should be used to determine the storage mechanism of the tested electrodes. This would provide more insight into the enhanced performance of the electrode materials. The new strategies adopted should be extended to other MOFs, in order to improve the prospects of MOFs and their composite electrodes in terms of supercapacitor applications.

Appendix

Chapter 4

Table S4.1. Summary of nitrogen adsorption and desorption analysis of an MOF-derived electrode synthesized at different annealing temperatures.

Material	S_{BET} (m^2 g^{-1})	Average Pore Size (nm)	Total Pore Volume (cm^3 g^{-1})
Ni-MOF	25.2	7.5	0.04
NiO/Ni-400	85.0	13.4	0.15
NiO/Ni-500	46.1	12.5	0.18
NiO-600	33.9	12.1	0.10

S_{BET}: surface area.

Table S4.2. Comparison of specific capacitance and cyclic stability of NiO/Ni-400 with that of other related supercapacitor materials.

Material	Electrolyte	Specific capacitance (Fg^{-1})	Current density Ag^{-1}	% Retention (cycles)	Ref.
NiO/graphene	6 M KOH	555	1	90.8 (2000)	1
*CS@NiO	3 M KOH	825	1	85 (3500)	2
*AC/NiO	1 M KOH	710	1	98 (2000)	3
NiO@Ni-MOF	3 M KOH	144	1	94 (3000)	4
NiO/Ni	3 M KOH	752	1	90 (1000)	This work

***CS: carbon sphere, AC: activated carbon**

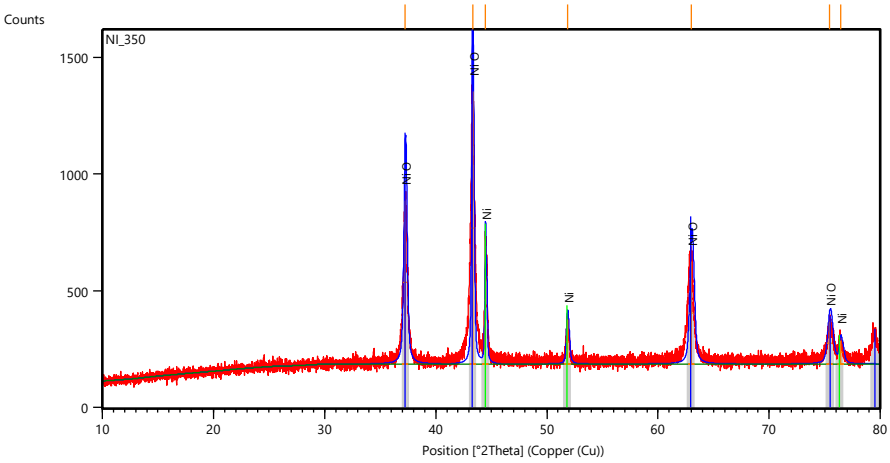

Pos. [°2Th.]	Height [cts]	FWHM Left [°2Th.]	d-spacing [Å]	Rel. Int. [%]
37.2594	699.54	0.3149	2.41332	59.93
43.3163	1167.27	0.1968	2.08888	100.00
44.4810	549.68	0.1378	2.03685	47.09
51.8507	189.00	0.2362	1.76335	16.19
63.0122	439.07	0.3936	1.47522	37.61
75.4487	181.33	0.4723	1.25998	15.53
76.4279	101.05	0.3149	1.24626	8.66

Visible	Ref. Code	Score	Compound Name	Displacement [°2Th.]	Scale Factor	Chemical Formula
*	01-075-0197	87	Nickel Oxide	-0.071	0.890	Ni O
*	00-004-0850	77	Nickel	-0.048	0.370	Ni

Primary reference: *Calculated from ICSD using POWD-12++*, (1997)
Structure: Thomassen, L., *J. Am. Chem. Soc.*, **62**, 1134, (1940)

Peak list

No.	h	k	l	d [A]	2Theta[deg]	I [%]
1	1	1	1	2.40755	37.320	68.8
2	2	0	0	2.08500	43.363	100.0
3	2	2	0	1.47432	62.997	43.7
4	3	1	1	1.25730	75.564	14.3
5	2	2	2	1.20378	79.569	10.4

Stick Pattern

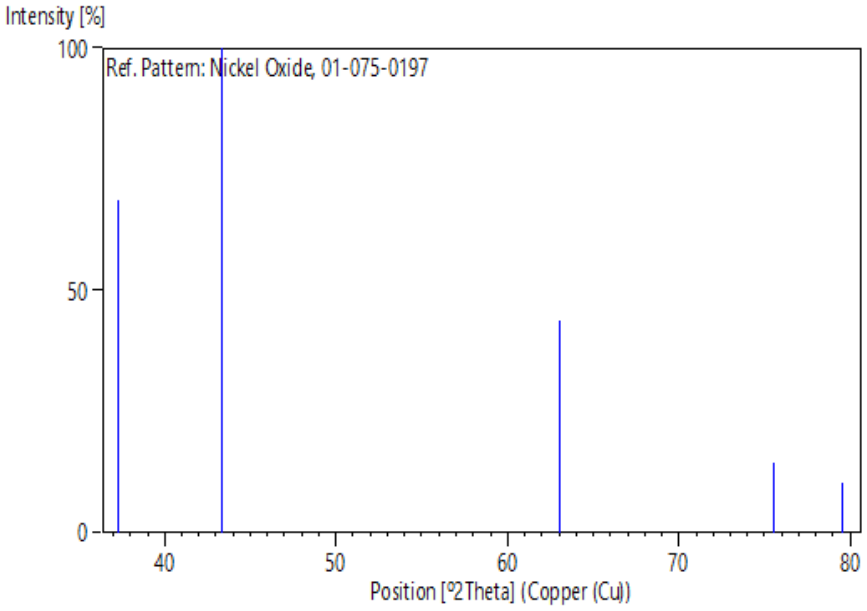

References

1. B. Zhao, H. Zhuang, T. Fang, Z. Jiao, R. Liu, X. Ling, B. Lu, Y. Jiang **Self-assembly of NiO/graphene with three-dimension hierarchical structure as high performance electrode material for supercapacitors** J. Alloys Compd., 597 (2014), pp.291-298.
2. P. Vickraman, B.J. Reddy **Synthesis and characterization of high porous carbon sphere@ nickel oxide core-shell nanocomposite for supercapacitor applications** J. Electroanal. Chem., 823 (2018), pp.342-349.
3. C. Yuan, X. Zhang, L. Su, B. Gao, L. Shen **Facile synthesis and self-assembly of hierarchical porous NiO nano/micro spherical superstructures for high performance supercapacitors** J. Mater. Chem., 19 (2009), pp.5772-5777.

4. S. Xiong, S. Jiang, J. Wang, H. Lin, M. Lin, S. Weng, S. Liu, Y. Jiao, Y. Xu, J. Chen **A high-performance hybrid supercapacitor with NiO derived NiO@ Ni-MOF composite electrodes** Electrochim. Acta, 340 (2020), pp.135956.

5. L. Wang, Y. Jiao, S. Yao, P. Li, R. Wang, G. Chen **MOF-derived NiO/Ni architecture encapsulated into N-doped carbon nanotubes for advanced asymmetric supercapacitors** Inorg. Chem. Front., 6 (2019), pp.1553-1560.

Material/ Current density	**Specific capacitance (Fg^{-1}]**				**Energy density ($Whkg^{-1}$)**				**Power density (Wkg^{-1})**			
	Ni-MOF	ZNN1	ZNN2	ZNN3	Ni-MOF	ZNN1	ZNN2	ZNN3	Ni-MOF	ZNN1	ZNN2	ZNN3
1 Ag^{-1}	164.2	391.5	270	181.2	5.7	13.6	9.4	6.3	250.0	260	250.8	240
2 Ag^{-1}	132.4	327.6	250	145.6	4.6	11.4	8.6	5.1	504	480.4	532.2	609
5 Ag^{-1}	125.5	298	200	144	4.4	10.3	6.9	4.9	1250	1223.4	1412.5	1504
7 Ag^{-1}	117.6	280	190	124.6	4.1	9.7	6.6	4.3	1750	1800	1909.0	2000
10 Ag^{-1}	106.0	272.8	183	116.8	3.7	9.4	6.3	4.0	2500	2600	2650.0	2700

Chapter 5

Table S5.1: Summary of nitrogen adsorption and desorption analysis of doped and undoped samples

Material	S_{BET} (m^2 g^{-1})	Average Pore Size (nm)	Total Pore Volume (cm^3 g^{-1})
Ni-MOF	25.4	7.6	0.05
ZNN1	117.8	8.5	0.25
ZNN2	47.9	12.4	0.15
ZNN3	35.3	13.7	0.12

Table S5.2: Summary of the performance parameters of the doped and undoped samples

	Specific capacitance (Cg^{-1}]				Energy density ($Whkg^{-1}$)				Power density (Wkg^{-1})			
Material/ Current density	Ni-MOF	ZNN1	ZNN2	ZNN3	Ni-MOF	ZNN1	ZNN2	ZNN3	Ni-MOF	ZNN1	ZNN2	ZNN3
1 Ag^{-1}	164.2	391.5	270	181.2	5.7	13.6	9.4	6.3	250.0	260	250.8	240
2 Ag^{-1}	132.4	327.6	250	145.6	4.6	11.4	8.6	5.1	504	480.4	532.2	609
5 Ag^{-1}	125.5	298	200	144	4.4	10.3	6.9	4.9	1250	1223.4	1412.5	1504
7 Ag^{-1}	117.6	280	190	124.6	4.1	9.7	6.6	4.3	1750	1800	1909.0	2000
10 Ag^{-1}	106.0	272.8	183	116.8	3.7	9.4	6.3	4.0	2500	2600	2650.0	2700

Chapter 6

Table S6.1 EIS data on the new ZnO/C@MWCNT composite electrode

Z' (Ω)	-Z" (Ω)	Error Z' (%)	Error Z" (%)	Z (Ω)	-Phase (°)	Frequency (Hz)	Convergence	Number of iterations	χ^2
0.867	0.061		-	0.869	4.026				0.29
482	06	4.03823	75.6164	628	272	1000	true	113	991
0.868	0.076	2.48021		0.872	5.043				
98	693	4	-67.93	358	677	794.33			
0.871	0.096	0.93128	-	0.876	6.302				
304	232	2	59.2816	602	517	630.96			
0.874	0.120		-	0.883	7.846				
89	571	-0.4726	49.9739	159	661	501.19			
0.880	0.150	-	-	0.893	9.716				
388	752	1.90872	40.4146	201	721	398.11			
0.888	0.187	-	-	0.908	11.93				
745	933	3.10956	30.8914	398	983	316.23			
0.901	0.233	-	-	0.931	14.51				
309	323	4.20018	21.8167	02	365	251.19			
0.919	0.288	-	-	0.963	17.38				
922	037	4.85867	13.3762	962	589	199.53			
0.946	0.352	-		1.010	20.43				
988	892	4.61587	-5.5222	603	776	158.49			
0.985	0.428	-	0.78775	1.074	23.48				
406	063	4.01943	8	366	023	125.89			
1.038	0.512	-	5.12439	1.158	26.28				
324	73	2.87256	1	02	043	100			
1.108	0.604	-	7.24698	1.262	28.61				
665	896	1.48097	8	948	723	79.433			
1.198	0.701	1.11826	8.01706	1.388	30.33				
391	368	4	9	546	864	63.096			
1.307	0.798	3.46447	7.52593	1.532	31.40				
845	32	8	1	245	025	50.119			
1.435	0.892	5.40553		1.690	31.86				
45	229	9	5.51197	145	373	39.811			
1.578	0.980	6.86704	2.40106	1.858	31.86				
052	899	3	2	066	46	31.623			
1.731	1.064	7.15698	-	2.032	31.56				
813	099	3	1.30528	605	832	25.119			
1.893	1.143	6.55641	-	2.211	31.13				
248	563	7	4.49488	815	29	19.953			
2.060	1.222	5.04316	-	2.395	30.68				
048	487	9	7.01721	469	602	15.849			
2.231	1.304	3.47489	-	2.584	30.31				
288	769	9	8.65798	776	742	12.589			
2.407	1.394	1.74668	-	2.782	30.08				
34	419	3	9.20182	03	098	10			
2.589	1.495	0.06481	-	2.990	30.00				
696	259	6	8.77243	372	162	7.9433			

2.780	1.610	-	-	3.213	30.08	
498	738	1.12762	7.64763	355	364	6.3096
2.982	1.743	-	-	3.454	30.31	
369	999	1.99218	6.00847	86	78	5.0119
3.198	1.897	-	-	3.719	30.68	
238	981	2.55962	4.07704	013	684	3.9811
3.431	2.075	-	-	4.010	31.16	
272	557	2.76583	1.80886	183	95	3.1623
3.684	2.279	-		4.333	31.74	
855	651	2.76943	0.34096	009	318	2.5119
3.962	2.513		2.50205	4.692	32.38	
581	337	-2.6976	7	432	563	1.9953
4.268	2.780	-	4.58128	5.093	33.07	
398	017	1.92369	2	89	629	1.5849
4.606	3.083	-	6.98381	5.543	33.79	
508	383	1.55537	9	209	651	1.2589
4.981	3.427	-	9.04324	6.046	34.52	
436	484	0.71271	7	681	997	1
5.398	3.817	-	10.5783	6.611	35.26	
346	04	0.16975	9	5	321	0.79433
5.862	4.257	0.98871	12.6378	7.245	35.98	
814	234	1	2	456	497	0.63096
6.381	4.753	1.80915		7.957	36.68	
056	931	4	12.4313	244	637	0.50119
6.959	5.313	3.07169	13.0112	8.756	37.36	
984	733	8	2	548	061	0.39811
7.607	5.944	3.60360	13.3932	9.654	38.00	
314	077	1	2	184	277	0.31623
8.331	6.653	3.11850		10.66	38.60	
655	33	2	15.7955	224	948	0.25119
9.142	7.450	5.01137	19.2582	11.79	39.17	
575	844	3	2	414	87	0.19953
10.05	8.347	4.51335	15.0747	13.06	39.70	
1	357	4	4	526	962	0.15849
11.06	9.354	5.63395		14.49	40.20	
896	717	9	21.8909	25	218	0.12589
12.20	10.48	2.48217	24.4411	16.09	40.65	
968	602	8	8	45	692	0.1